Quantitative MRI in the diagnosis and monitoring of human prion diseases

Thesis submitted for the degree of

Doctor of Philosophy

Dr Harpreet Hyare

MRC Prion Unit

UCL Institute of Neurology

DECLARATION STATEMENT

I, Harpreet Hyare, confirm that the work presented in this thesis is my own. Where information has been derived from other sources, I confirm that this has been indicated in the thesis.

Harpreet Hyare

Quantitative MRI in the diagnosis and monitoring of human prion diseases

Abstract

This thesis examines the application of cerebral diffusion weighted imaging (DWI) and short echo time (TE) proton magnetic resonance spectroscopy (^{1}H-MRS) for the evaluation of patients with different forms of human prion disease. Human prion diseases are progressive, uniformly fatal neurodegenerative diseases and as treatments are developed, early diagnosis is essential. Particularly important is the diagnosis of presymptomatic cases and prediction of disease onset in these individuals.

In this thesis I demonstrate that MRI measures of Apparent Diffusion Coefficient (ADC) at low and high *b*-value and short TE ^{1}H-MRS are potential neuroimaging biomarkers of prion disease activity. I show that *ex-vivo* MRI at high field provides important insights into the microstructural changes underlying the sensitivity of some of these quantitative MRI methods to prion disease pathology. The findings presented here exemplify the potential of quantitative MRI in both increasing our understanding of the pathophysiology of prion diseases and in providing neuroimaging biomarkers which will be of great importance for the future evaluation of treatment efficacy.

Table of contents

Index of Figures

Index of Tables

Abbreviations

AD	**Alzheimer's disease**
ADAS-COG	**Alzheimer's disease assessment scale**
ADC	**Apparent Diffusion Coefficient**
ADL	**Barthel activities of daily living scale**
BET	**Brain Extraction Tool**
BPRS	**brief psychiatric rating scale**
C	**caudate**
CDR	**clinician's dementia rating**
CGIS	**a clinician's global impression of severity scale**
Cho	**Choline**
CNR	**Contrast-to-noise ratio**
Cr	**Creatine**
CSF	**Cerebrospinal Fluid**
Cx	**cortex**
DM	**dorso-medial thalamus**
DWI	**Diffusion Weighted Imaging**
DTI	**Diffusion Tensor Imaging**
EPI	**Echo planar imaging**
FA	**Fractional Anisotropy**
FC	**frontal cortex**
FLAIR	**Fluid Attenuation Inversion Recovery**
FOV	**Field of view**
FSE	**Fast spin echo**
FW	**frontal white matter**
GFAP	**anti-glial fibrillary acid protein**
GM	**Grey matter**
GPC	**glycerol-phosphorocholine**
^{1}H-MRS	**Proton Magnetic Resonance Spectroscopy**
HD	**Huntingdon Disease**
H&E	**haemoxatylin and eosin**
inhPrD	**Inherited Prion Disease**
L	**left**
MD	**Mean Diffusivity**
MI	***myo*-inositol**
MMSE	**mini mental state examination**
MRC	**medical research council**
MREC	**multi-centre research ethics committee**
MRI	**magnetic resonance imaging**
NAA	***N*-acetylcysteine**
NEX	**Number of Excitations**

NBV	**normalized brain volume**
P	**putamen**
P25	**25th percentile**
P50	**50th percentile**
P75	**75th percentile**
PC	**phosphorocholine**
PD	**proton density**
PET	**positron emission tomography**
PH	**peak height**
PL	**peak location**
PRNP	**prion protein gene**
PrP	**prion protein**
PrP^{C}	**normal cellular form of PrP**
PrP^{Sc}	**abnormal β-pleat rich form of PrP**
PRESS	**Point resolved slice selective spectroscopy**
Pu	**pulvinar**
R	**right**
RHC	**Right head of caudate**
ROI	**Region of Interest**
RP	**right putamen**
RPu	**right pulvinar**
RTH	**Right thalamus**
sCJD	**Sporadic Creutzfeldt-Jakob Disease**
SE	**spin echo**
SI	**Signal Intensity**
SNR	**Signal-to-noise ratio**
SP	**superior pons**
SPGE	**Spoiled gradient echo**
T1W	**T1 weighted**
T2W	**T2 weighted**
TE	**Echo time**
TI	**Inversion time**
TR	**Repetition time**
vCJD	**Variant Creutzfeldt-Jakob Disease**
WB	**whole brain**
WM	**white matter**
WHO	**World Health Organisation**

Overview

This thesis evaluates the potential of quantitative MRI measurements in the understanding of the pathophysiological changes underlying human prion diseases and their potential in providing neuroimaging markers of disease activity. As the first therapeutic trials are underway for these disorders, including the recently completed MRC Prion-1 Trial, quantitative MRI techniques offer considerable potential for evaluating treatment efficacy.

The thesis is divided into two parts describing our findings. Part A (chapters 2-4) examines whether *in vivo* ADC and ^{1}H-MRS measurements are able to detect regional and global changes in patients with prion disease as a diagnostic tool and, by correlation with cognitive scales, to monitor disease activity. Part B (chapter 5) describes our *ex vivo* work, where quantitative MRI measurements at high magnetic field strength (9.4T) were performed in order to determine and quantify the microstructural changes that affect the MRI signal in post-mortem brain tissue of patients with prion disease.

The subject of prion diseases and the potential of quantitative MRI as a tool to monitor disease activity are introduced firstly in chapter 1. Chapters 2-4 describe the *in vivo* application of cerebral DWI and ^{1}H-MRS in patients in the MRC Prion-1 trial. Chapter 2 examines the value of basal ganglia regional ADC measurements and the use of whole brain and grey matter ADC histograms in monitoring disease activity in inherited prion diseases (inhPrD). Chapter 3 describes the value of basal ganglia ADC measurements at low and high *b*-values in the diagnosis and differentiation of sporadic CJD (sCJD) and variant CJD (vCJD). Chapter 4 describes a pilot study in a small group of patients with inhPrD, investigating the use of single voxel short echo time (TE) ^{1}H-MRS in two regions of the brain. Longitiudinal data and correlation with clinical scores enabled us to evaluate this technique as a tool to monitor disease activity. Chapter 5 describes *ex vivo* high resolution MRI and quantitative MRI measurements in fixed post-mortem brain tissue at 9.4T in patients with vCJD. Through comparison with histopathology, I discuss how this technique can be used to detect and quantify the microstructural changes that affect the MRI signal in vCJD thus improving our understanding of the pathophysiology of this disease. Finally, in Chapter 6, the findings are summarised, the relative strengths and weaknesses of these techniques are discussed and suggestions for future research directions are given.

Aim

Specifically, this thesis examines whether:

1. Regional differences in cerebral ADC can be detected in variant, sporadic and inherited forms of prion disease when compared to controls.

2. Regional and global cerebral ADC measures in inherited prion disease correlate with clinical disease severity.

3. Regional differences in single voxel short TE ^{1}H-MRS measurements can be detected in inherited prion disease when compared to controls, can be correlated with disease severity and can be demonstrated to evolve in serial MRS examinations.

4. Quantitative MRI measurements of T1- and T2 relaxation times, FA and MD in fixed post-mortem brain tissue at 9.4T can be correlated with histopathological measures to better understand the pathophysiological changes underlying the early disease course.

5. High resolution MRI images of fixed post-mortem tissue at 9.4T can detect the histopathological changes characteristic of human prion diseases.

Hypothesis

Regional and global ADC measures and short TE ^{1}H-MRS measures are potential markers of disease activity in prion diseases.

High field MRI at 9.4T can detect and quantify the histopathological changes characteristic of this disease.

1 Introduction

1.1 Human Prion Diseases

Human prion diseases are a group of progressive, invariably fatal neurodegenerative disorders characterised by accumulated aggregates of an abnormally folded, relatively protease-resistant, beta-sheet rich isoform (PrP^{Sc}) of a normal cellular protein (PrP^{c}). Deposition of PrP^{Sc} in the form of diffuse deposits or plaques of various morphologies is accompanied by a classic histological triad of spongiosis, gliosis and neuronal loss [1]. Most cases occur sporadically but hereditary, iatrogenic and dietary transmission can occur. There has been considerable recent interest in human prion disease following the identification of vCJD and the demonstration through transmission studies in mice and other research that vCJD is caused by the same prion strain as that causing Bovine Spongiform Encephalopathy (BSE)[2]. With recent reports of blood-borne transmission [3], prion diseases remain an important public health issue and attention has focussed on the development of therapeutic agents.

1.1.1 Molecular neurology of prion diseases

The biology of prion diseases is unique because of the transmissible agent or prion (*pro*teinaceous *in*fectious particle). Prions are defined as "small proteinaceous infectious particles which resist inactivation by procedures which modify nucleic acid"[4]. Prions consist principally or entirely of abnormal isoforms of host encoded prion protein. In human prion diseases, the abnormal isoform is designated PrP^{Sc} (denoting the scrapie isoform of the protein) and the normal prion protein is protease sensitive and is termed PrP^{c} (denoting the normal *C*ellular isoform of the protein). PrP^{Sc} is derived from PrP by a post-translational mechanism with no amino acid or covalent differences between PrP^{Sc} and PrP^{c} [4-6].

PrP^{c} is a glycoprotein consisting of an N-terminal region and a C-terminal domain. The N-terminal region contains five repeats of 8 amino-acid sequence (the octapeptide region) and mutations in this region can lead to forms of inherited prion disease[7]. In this region, there are two tight binding sites for Cu ions, suggesting a role for PrP in copper metabolism or transport [8]. Disturbance of this function could be involved in prion related neurotoxicity.

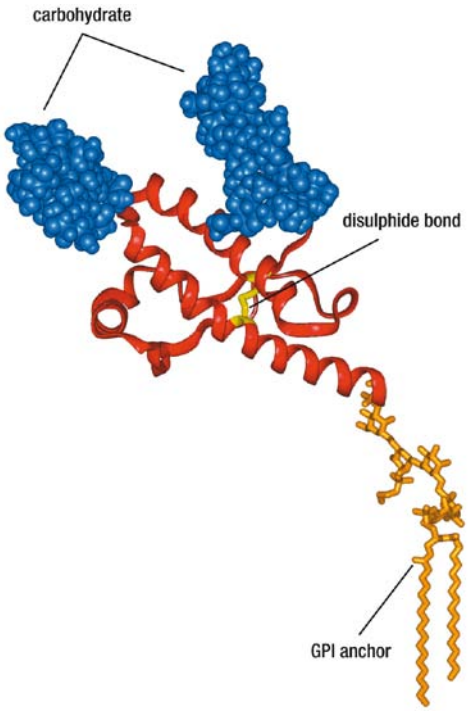

(Courtesy of Ray Young, MRC Prion Unit)

Figure 1.1.1: Model of the C-terminal domain of human prion protein indicating positions of single disulphide bond linking the α-helices, position of the carbohydrate and the GPI anchor which attaches the protein to the outer surface of the cell membrane.

PrP^{Sc} is a highly aggregated, detergent insoluble material that has a high β-sheet content. It is thought that the protein PrP can exist in a dominant native state (PrP^{C}) and several minor conformations, one or a set of which can associate to form a supramolecular structure PrP^{Sc}, composed of misfolded PrP monomers. When a stable "seed" structure of a critical size has been formed, further recruitment of unfolded PrP occurs as an irreversible process driven thermodynamically by intermolecular interactions [7] (Figure 1.1.2).

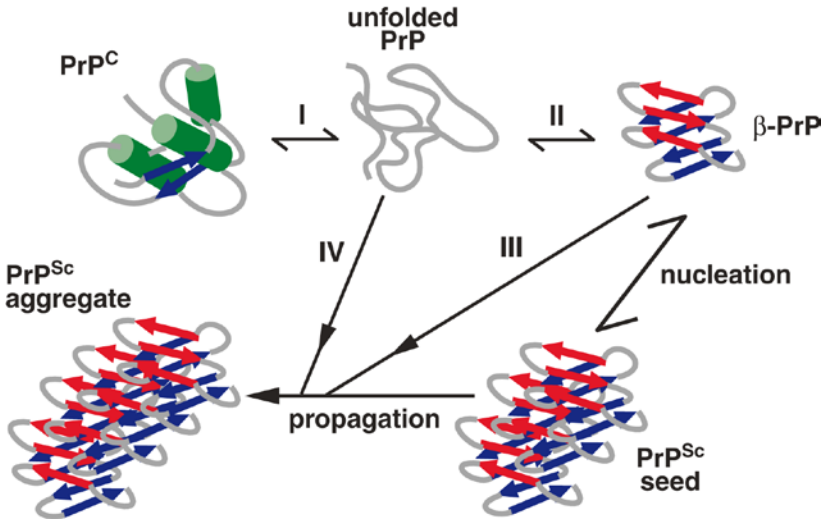

(Courtesy of Ray Young, MRC Prion Unit)

Figure 1.1.2: Scheme demonstrating the hypothesis for prion propagation. Largely α-helical PrP^C proceeds via unfolded state (i) to re-fold into a largely β-sheet form, β-PrP (ii). β-PrP is prone to aggregation in physiological salt concentrations. Prion replication may require a critical "seed" size. Further recruitment of β-PrP monomers (iii) or unfolded PrP (iv) then occurs as an essentially irreversible process driven thermodynamically by intermolecular interactions (red arrows).

1.1.2 **Prion strains**

Distinct naturally occurring isolates or strains of human PrP^{Sc} are observed which are associated with different phenotypes of CJD [9;10]. The different strains are identified on the basis of their different incubation periods and neuropathology, as well as physicochemical properties including differences in fragment size and glycoform ratio (of diglycosylated, monoglycosylated and unglycosylated forms) seen on Western blots following treatment with proteinase K (Figure 1.1.3). Four types of human prion disease have been described using molecular strain typing: sCJD and iatrogenic CJD are associated with strain types 1-3 whilst vCJD is uniquely associated with type 4 PrP^{Sc} and has a distinct glycoform ratio (Figure 1.3). Normally occurring polymorphisms coding for either methionine (M) or valine (V) at codon 129 of the prion gene also influence strain type propagation. Strain types 1 and 4 have only been detected in MM individuals whilst type 3 is seen in MV or VV individuals and type 2 with any codon 129 mutation.

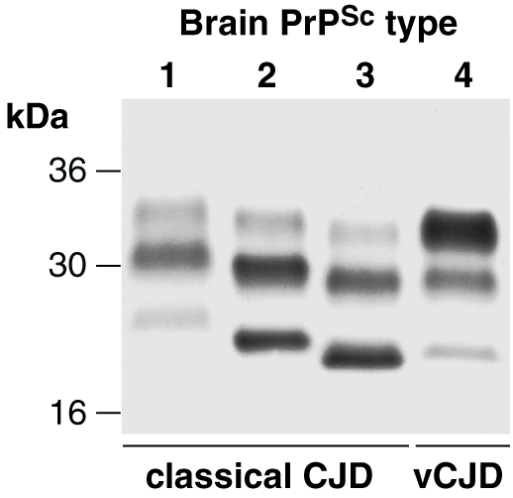

(Courtesy of Ray Young, MRC Prion Unit)

Figure 1.1.3: Molecular strain typing of human prions. Western blot of brain homogenate after treatment with proteinase K shows different apparent molecular mass and glycoform ratios in patients with forms of sporadic or iatrogenic (T1-3) or vCJD (T4).

1.1.3 Pathogenesis

In some animal models, infectivity detected in the spleen precedes neuroinvasion [11]. CNS prion replication then rises to high levels and the clinical phase follows. The route of entry of prions after oral exposure may be through invasion of Peyer's patches and other gut lymphoid tissue. Neuroinvasion may then involve the autonomic nervous system innervating lymphoid tissue, with retrograde invasion via the spinal cord[12]. In human sCJD prion infectivity is largely confined to the CNS, whereas in vCJD, there is involvement of the lymphoreticular tissues and evidence of transmission via blood transfusion [3;13;14].

It has been proposed that prion disease pathogenesis can be explained in terms of the kinetics of prion propagation, as determined by an interplay between prion strain type (the dominant PrP^{Sc} polymer and its ensemble) and the tissue-host environment (including PrP sequence and expression level, modifier genes, and clearance mechanisms). Neurotoxicity is then mediated by a PrP species designated PrP^{L} (lethal), distinct from PrP^{Sc} but catalyzed by it, when PrP^{L} concentrations of this species pass a local toxic threshold. Rapid propagation (with a host-adapted strain and normal or high

levels of host PrP^C expression) results in severe neurotoxicity and death whereas slow propagation (infection across a transmission barrier or with low host PrP^c expression) results in low neurotoxicity, prolonged more variable incubation periods, or a persistent carrier state [15].

1.1.4 Molecular classification of prion diseases

Human prion diseases have been traditionally classified on clinical grounds into Creutzfeldt-Jakob disease (CJD), Gerstmann-Straussler-Scheinker disease (GSS) and Kuru but can also be classified as occurring in inherited, sporadic and acquired forms with sub-classification according to molecular criteria.

Inherited prion diseases (inhPrD) comprise 15% of recognised prion disease and are associated with one of the more than 30 recognised coding mutations in the *PRNP* gene (Collinge, Dementia, London). Kindreds with inhPrD have been described with the phenotypes of classical CJD, GSS and with other clinico-pathological syndromes including familial fatal insomnia (FFI).

sCJD makes up 85% of all recognised human prion disease and occurs in all countries with an apparently random distribution and annual incidence of 1-2 per million. Possible causes are spontaneous production of PrP^{Sc} via rare stochastic events, somatic mutation of *PRNP* or unidentified environmental exposure. There is a marked genetic susceptibility with most cases occurring in homozygotes of methionine (M) or valine (V) at codon 129 of the PRNP gene. MV heterozygotes appear to be relatively protected from developing sCJD [16].

Acquired prion diseases include iatrogenic CJD, Kuru and vCJD. Iatrogenic exposure occurs through accidental exposure to human prions through medical or surgical procedures, most frequently through implantation of dural grafts or through administration of growth hormone derived from the pituitary glands of human cadavers [17]. Kuru arose from exposure to prions during cannibalistic mortuary feasts. vCJD has been shown through strain-typing studies and transmission studies in transgenic mice to be caused by the same prion strain as that causing BSE [9;18].

1.1.5 Clinical features of each type of prion disease

Table 1.1: Diagnosis of different forms of human prion disease.

Diagnosis of prion disease
Sporadic (classical) CJD Rapidly progressive dementia with two or more of myoclonus, cortical blindness, pyramidal signs, akinetic mutism Most cases aged 45-75 Serial EEG shows pseudoperiodic complexes in most cases CSF 14-3-3 protein usually positive *MRI*: T2W hyperintensity in basal ganglia and cortex *PRNP* analysis: no pathogenic mutations Brain biopsy in highly selected cases (to exclude treatable alternative diagnoses): PrP immunocytochemistry or western blot for PrP^{Sc} types 1-3
vCJD (Human BSE) Early features: depression, anxiety, social withdrawal, peripheral sensory symptoms Cerebellar ataxia, chorea, or athetosis often precedes dementia, advanced disease as sCJD Most in young adults: however age at onset 12-74 years seen EEG non-specific slow waves, CSF 14-3-3 may be elevated or normal MRI: most show high T2W signal in the posterior thalamus bilaterally *PRNP* analysis: characteristic PrP immunostaining and PrP^{Sc} on western blot (type 4)
Inherited prion disease Varied clinical syndromes between and within kindreds: should consider in all pre-senile dementias and ataxias irrespective of family history MRI: normal, atrophy or basal ganglia T2W hyperintensity *PRNP* analysis: diagnostic codon 129 genotype may predict age at onset in pre-symptomatic testing

Adapted from Collinge *et al* 2005 [7].

1.1.5.1 Sporadic CJD

sCJD typically presents with a rapidly progressive dementia and additional neurological features including cerebellar ataxia (10%), neuropsychiatric symptoms and myoclonus. Onset usually occurs from 45-75 years of age with a peak age of onset between 60-65 years. Rapid clinical progression usually leads to akinetic mutism and death within weeks or months. The median duration of illness in sCJD is four months with 14% of cases having an illness duration of a year or more and only 5% of cases surviving 2 or more years [19].

There is clinical heterogeneity within sCJD, especially at symptom onset where particular focal deficits may be present: an isolated progressive cerebellar syndrome (10%) [20] or an isolated progressive visual disturbance culminating with cortical blindness may be seen, known as the Heidenhain's variant.

Table 1.2: World Health Organisation Updated Diagnostic criteria for sCJD.

Diagnostic criteria
I. Clinical signs 1. Dementia 2. Cerebellar or visual 3. Pyramidal or extrapyramidal 4. Akinetic mutism, **II. Tests** 1. PSWCs in EEG 2. 14-3-3 detection in CSF (in patients with disease duration of less than 2 year) 3. High signal abnormalities in caudate nucleus or putamen or at least two cortical regions (temporal-parietal-occipital) either in DWI or FLAIR
Probable sCJD Two out I and at least one of II
Possible sCJD Two out of I and duration less than 2 years

As published in Zerr *et al* 2009 [21]

The diagnosis should be considered in any individual with a rapidly progressive dementia where other more common causes have been excluded. Routine haematological and biochemical investigations are normal and no immunological markers or acute phase proteins are elevated. In the CSF, 14-3-3, which is a normal neuronal protein that has no specific connection to CJD and is released following neuronal damage can be a useful adjunct to diagnosis with a reported sensitivity of 94% in the appropriate clinical context [22;23]. CSF 14-3-3 protein is also elevated in cerebral infarction, cerebral haemorrhage or viral encephalitis although these conditions can usually be differentiated from sCJD on clinical grounds.

EEG shows a progressive deterioration in the normal background rhythms with the appearance of periodic sharp wave complexes (PSWCs) with a specificity of 74% [24;25]. Cerebral imaging is important in the exclusion of other diagnoses but more recently imaging features that are characteristic of sCJD have been demonstrated and a combination of cortical and basal ganglia signal change on MRI is reported to have a diagnostic sensitivity of >91% [26] (see chapter 1.1.7).

The different molecular subtypes of sCJD have been associated with particular clinical phenotypes (table 1.3). Clinically the most difficult differential diagnosis for sCJD is rapidly progressive Alzheimer's disease (AD), with cases misdiagnosed as sCJD in several large series [25;27]. The differential diagnosis also includes Dementia with Lewy Bodies, lymphoma and multiple cerebral infarctions [28;29].

Table 1.3: Clinical features, EEG, CSF 14-3-3 and MRI findings in sCJD subtypes.

Subtype of sCJD	**Frequency (% of sCJD cases)**	**Clinical presentation**	**EEG positive**	**14-3-3 positive**	**MRI positive**
MM1/MV1	60-70%	"Classical" form: rapidly progressive dementia and neurological signs including Heidenhain form	75-80%	>96%	Striatum 79% (15/19)
MM2-cortical	1-2%	Slowly progressive dementia, late myoclonus, pyramidal/extrapyramidal signs	50% (2/4	100% (4/4)	Striatum 0% (0/4) Cortex 100% (2/2)
MM2-thalamic	1-2%	Psychiatric symptoms, autonomic failure, ataxia, dementia ("sporadic fatal insomnia")	0% (0/1)-20% (1/5)	20%(1/5)-100% (1/1)	Normal (5/5 MRI)
MV2	10%	Slow cognitive decline, extrapyramidal akinetic-rigid sign, myoclonus	0% (0/10)	30% (3/10) – 57% (4/7)	Striatum 50% (5/10) – 100% (7/7)
VV1	1-2%	Young patients, prolonged duration, personality changes, dementia	0% (0/9)	100% (9/9)	Striatum 28% (2/7) Cortex 100% (7/7)
VV2	10-15%	Dementia, ataxia, myoclonus	0% (0/15)	84%	Striatum 70% (7/10)

Adapted from Tschampa *et al* 2007 [30].

1.1.5.2 Variant CJD

In 1995 reports of suspected sCJD occurring in teenagers [31;32] were considered to be extremely rare and unusual findings. When further cases in young adults were discovered a review of the histology showed a consistent and unique neuropathological appearance and this previously unrecognised disease was termed vCJD. Direct experimental evidence from molecular analysis of prion strain type and transmission studies in transgenic and wild type mice revealed that the disease was caused by the same prion strain as that causing BSE in cattle[18].

In June 2010, a total of 195 vCJD cases had been reported, including 173 cases in the UK, 25 in France, 5 in Spain, 4 in Ireland, 3 in the USA and Netherlands, 2 in Italy and 1 each in Canada, Saudi-Arabia and Japan (for up-to-date numbers please refer to www.eurocjd.ed.ac.uk/vCJD.htm).

Patients typically present with subtle behavioural or psychiatric disturbance and in some cases dysaesthetic or sensory limb symptoms are a prominent early feature [33]. Depression is common but other psychiatric features also occur including anxiety, withdrawal, emotional lability, aggression, insomnia or auditory and visual hallucinations. Will *et al* reported that 17 of 33 early vCJD patients were first seen by a psychiatrist and all but one demonstrated psychiatric symptoms in the early stages of the disease [33].

A prominent feature is dyasthesia or pain in the limbs. Henry *et al* reported sensory symptoms in 42 of the first 50 vCJD cases which included predominantly lower limb pain (63%), paraesthesia (31%), dysaesthesia (28%), numbness (25%) and cold feelings (25%) [34]. In most cases overt neurological signs are not apparent until later in the course of the disease. In most cases cognitive impairment is accompanied by a progressive cerebellar syndrome with gait and limb ataxia. As deterioration continues, limb rigidity and primitive reflexes become evident, eventually with progression to akinetic mutism [33].

The mean age of onset is 29 years and the clinical course is usually prolonged (median 14 months). The EEG is abnormal with generalised slow wave activity but without the pseudoperiodic pattern seen in most sCJD cases. The CSF 14-3-3 may also be elevated, detected with a sensitivity 50-60% and specificity of 94% in vCJD cases.

Table 1.4: World Health Organisation criteria for the diagnosis of vCJD.

Diagnostic criteria
I
A Progressive neuropsychiatric disorder
B Duration of illness >6 months
C Routine investigations do not suggest an alternative diagnosis
D No history of potential iatrogenic exposure
E No evidence of a familial form of TSE
II
A Early psychiatric symptoms
B Persistent painful sensory symptoms
C Ataxia
D Myoclonus or chorea or dystonia
E Dementia
III
A EEG does not show the typical appearance of sCJD (or no EEG performed)
B MRI brain scan shows bilateral symmetrical pulvinar high signal
IV
A Positive tonsil biopsy
DEFINITE: IA and neuropathological confirmation of vCJD
PROBABLE: I and 4/5 of II and IIIA and IIIB
OR
I and IVA
POSSIBLE: I and 4/5 of II and IIIA

As published in Heath *et al* 2010 [35]

In the appropriate clinical setting, the pulvinar sign on MRI is extremely helpful, [36]with a reported sensitivity of 100% on FLAIR imaging [37] and is now included as part of the WHO criteria for the identification of vCJD (Table 1.4).

Polymorphisms at codon 129 appear to be the main genetic risk factor for vCJD [38] with every case genotyped being homozygous for methionine at codon 129 apart from one recent case report of vCJD in an individual heterozygous for *PRNP* codon 129[39]. This case highlights the potential of further clinically silent cases of vCJD in the UK population.

1.1.5.3 Inherited prion disease

10-15% of prion diseases are inherited and occur due to pathogenic mutations in the prion protein gene. Over 30 different mutations have been recognised, due to 3 types of pathogenic *PRNP* mutation: point mutations leading to either an amino acid substitution or a premature stop codon, or insertion of additional octapeptide repeats (Figure 1.1.4).

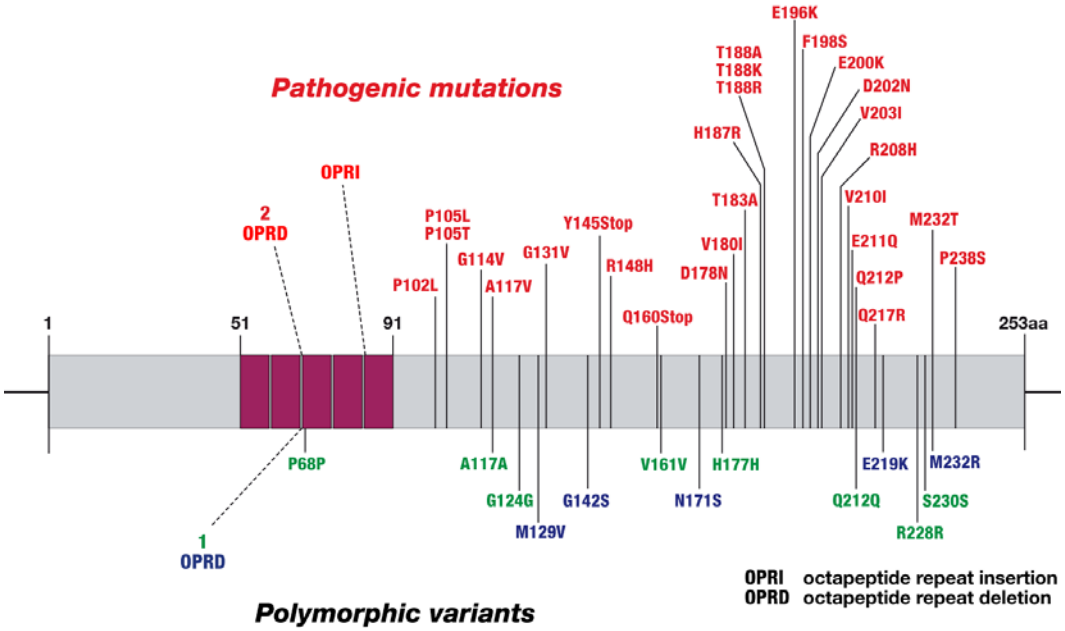

(Courtesy of Ray Young, MRC Prion Unit)

Figure 1.1.4: Scheme demonstrating pathogenic mutations in the *PRNP* gene. Definite or suspected pathogenic mutations are shown above the scheme and neutral or disease susceptibility/modifying polymorphisms are shown below.

Some of the mutations are associated with a particular category of prion disease and others with a spectrum of clinical phenotypes. The clinical phenotypes have historically been divided into Gerstmann-Straussler-Scheinker syndrome (GSS), fatal familial insomnia (FFI) and familial CJD (fCJD). These descriptions preceded the advent of molecular genetic diagnosis. As clinical experience has been gained in the different mutations, the heterogeneity of clinical phenotypes even between individuals with the same family has been striking.

The most common worldwide *PRNP* mutations are P102L, E200K, D178N and OPRI [40]. Several European studies have reviewed the incidence of inherited CJD: in Germany 40 out of 578 suspected prion disease cases had a *PRNP* mutation [41]; in Italy, the most common mutation was the E200K (30 of 38 inherited cases) [42]and in Finland, D178N was the most common mutation (12 of 44 cases) [43]. In the UK, the 6-OPRI mutation is the most frequently detected[40].

The clinical phenotype of inhPrD often overlaps with common causes of dementia such as AD and also with sCJD. However, confirmation of the diagnosis of inhPrDs is easily achieved since a blood test is definitive. Diagnosis may be difficult as often there is no

family history (47% of cases report no family history) [43]. Non-paternity, the absence of a family history and individuals where death occurs prior to disease onset may all make diagnosis difficult and some mutations occur de novo [44] or are not fully penetrant [45].

E200K

The typical presentation is a rapidly progressive dementia with myoclonus and pyramidal, cerebellar or extrapyramidal signs. The presentation of E200K may be highly variable, with disease onset occurring over a wide age range The age of onset is slightly younger than that for sCJD with a median age of onset at 58 and a mean disease duration of 7 months [46;47]. Atypical clinical presentations include peripheral neuropathy, supranuclear gaze palsy and sleep disturbance [40].

Octapeptide repeat insertions

The clinical phenotype is again highly variable with a median age of onset of 35 years (range 21-82) and a disease duration of 7 years (range 3 months – 21 years) [48]. Cortical dementia, often with apraxia, is the main clinical feature but cerebellar ataxia, pyramidal and extrapyramidal signs, myoclonus, chorea and seizures also occur [49].

P102L

The typical clinical phenotype of the P102L mutation is the GSS syndrome, which was later also described with the less common F198S, A117V, P105L and some D178N mutations. Phenotypic variability is a major feature with a median age of onset at 50 years (range 25-70) and median duration of disease of 4 years [50] with earliest clinical onset for MM homozygotes [51]. The traditional GSS phenotype is of a slowly progressive ataxia with later dementia but amyotrophy [52] and a rapid course are also sometimes seen.

D178N

Patients with the D178N mutation may present with the clinicopathological syndrome of FFI, characterised by prominent autonomic dysfunction, untreatable insomnia, and often myoclonus in addition to other features of prion disease. The median age of onset is 50 years (range 20-71) and median duration of disease 11 months (range 5 months – 4 years).

1.1.6 Histopathological findings in prion diseases

A triad of spongiform change, neuronal loss and gliosis involving astrocytes and microglia is the neuropathological hallmark of CJD [53]. Spongiform change is relatively specific to CJD and characterised by diffuse or focally clustered, small, round or oval vacuoles in the neuropil of the cerebral cortex (whole thickness or deep layers), the subcortical grey matter (especially the head of the caudate nucleus), the cerebellar molecular layer, and more rarely the brainstem and spinal cord [54]. The extent of spongiform change varies greatly between patients, disease subtype and from region to region in the brain but the absence of spongiosis is rare. The presence of vacuoles in the nerve cell bodies is uncommon and if ballooning of nerve cells occurs this is usually due to ballooning of neurofilament proteins. The white matter may also be involved, with spongiform change and astrocytosis being prominent pathological features of the pan-encephalopathic form of prion disease described most frequently in Japan [55].

Neuronal loss occurs in the cortical and subcortical regions and seems to correlate with microglial activation and neuronal damage rather than prion protein deposition. This frequently affects the granular layer of the cerebellum and variably affects the basal nucleus of Meynert [56]..

1.1.6.1 Sporadic CJD

In 1996, Parchi *et al*. established a molecular basis for pathologically distinct phenotypes of sCJD [10]. A classification of sCJD according to prion codon 129 genotype and prion strain type (1 or 2) identified six subtypes designated as MM1, MM2, MV1, MV2, VV1 and VV2. The different subtypes of sCJD not only have specific molecular and clinical characteristics but also have specific histological characteristics. The most common subtypes accounting for 70% of all sCJD and associated with PrP^{Sc} strain type 1 (MM1 and MV1) are characterised by a variable degree of spongiform change, gliosis and neuronal loss affecting mainly the cerebral cortex, striatum, medial thalamus and cerebellum, whereas the hippocampus, hypothalamus and brainstem are relatively spared. In the cerebral cortex vacuolization is seen in all layers and is often more prominent in the occipital lobe. Immunohistochemistry demonstrates a synaptic pattern of PrP staining involving most grey matter structures of the cerebrum with relative sparing of the hippocampal formation.

The second most common phenotype, comprising 15% of case, includes patients with strain type 2 (VV2) and is characterised by moderate to severe spongiform change and gliosis with variable neuronal loss in the limbic structures, striatum, thalamus, hypothalamus, cerebellum and brainstem nuclei. Neocortical involvement occurs as the disease progresses, particularly in the occipital lobe which may be spared with a relatively rapid course. The spongiform change is often laminar and mainly involves the deep cortical layers. Immunostaining is characterised by the presence of plaque-like, focal PrP deposits which are present in relatively large amounts throughout the brain other than the neocortex where these are barely detectable [53].

The third most common phenotype described in approximately 8% of cases is the MV2 subtype, characterized by kuru type amyloid plaques in the upper regions of the granular layer of the cerebellum but also in the cerebral cortex, striatum and thalamus. The MM2-cortical subtype shows similar pathology to that of the MM1 subtype except that the cerebellum lacks significant spongiform change, typically consisting of large and coarse vacuoles. The MM2-thalamic variant is indistinguishable from fatal familial insomnia (FFI). Finally, in the rare phenotype VV1, the corticostriatal regions are predominantly affected while other subcortical structures including the cerebellum are relatively spared. There is relative sparing of the occipital lobe in comparison to the frontal and temporal lobes with numerous ballooned neurons in the cerebral cortex [53].

1.1.6.2 Variant CJD

Post-mortem findings in vCJD show the histopathological hallmarks of prion disease: degeneration, astrocytic proliferation and neuronal loss [57]. However in vCJD, this is accompanied by deposition of PrP^{Sc} in the form of multiple rounded amyloid plaques often with a dense eosinophilic core and a pale radiating fibrillary periphery surrounded by a rim or halo of spongiform change (Figure 1.1.5) [53].

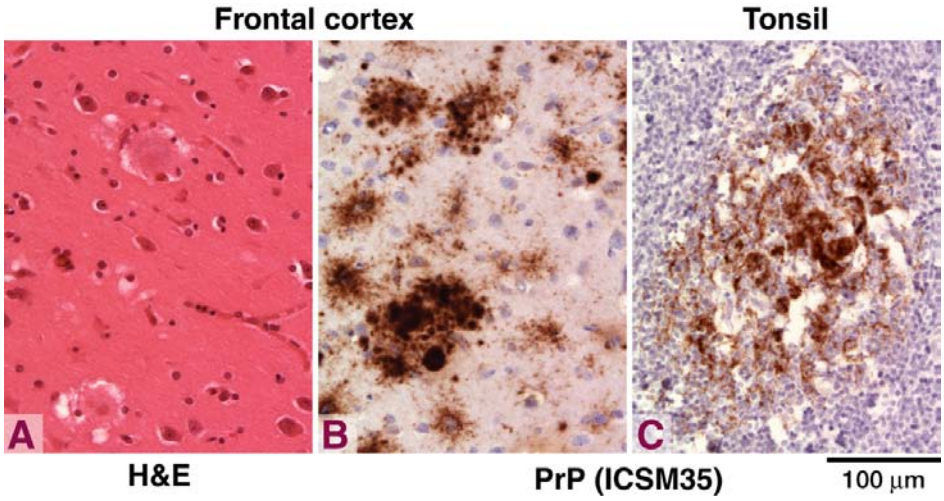

Figure 1.1.5: Histology sections demonstrating large plaques in the frontal cortex and tonsil in vCJD. H&E staining reveals rounded amyloid plaques with a dense eosinophilic core and a halo of spongiform change (A), PrP immunostaining with ICSM35 shows that the plaques are composed of PrP (B), PrP immunostaining also reveals large plaques in the tonsil (C).

These plaques are present in large numbers in the cerebral and cerebellar cortex, particularly in the occipital cortex. Rounded amyloid plaques without spongiform change can be identified in subcortical grey matter structures including the basal ganglia, thalamus and hypothalamus. However, they are not found in the brainstem and spinal cord. Spongiform change is most severe in the basal ganglia, particularly in the caudate nucleus and putamen which contain relatively few amyloid plaques. The thalamus, hypothalamus, brainstem and spinal cord exhibit little spongiform change or amyloid plaque formation. Severe neuronal loss occurs in the posterior thalamic nuclei, periaqueductal grey matter and colliculi with a marked accompanying astrocytosis.

1.1.6.3 Inherited prion diseases

E200K

The histological changes are similar to those of the sCJD MM1 subtype and characterised by the presence of spongiform degeneration, astrogliosis and neuronal loss without amyloid plaques. The cerebral cortex, striatum, medial thalamus and cerebellum are mainly involved and immunostaining consistently shows a synaptic pattern [58].

D178N

The most frequent findings are of spongiform degeneration, associated with a prominent astrogliosis, often in the form of gemistocytic astrocytes and variable degrees of neuronal loss [59]. Frontal and temporal cortices are generally more severely affected than the occipital cortex. The caudate and putamen usually show severe spongiform degeneration. The thalamus is minimally affected and the cerebellum is spared [58]. When associated with the FFI phenotype, there is severe atrophy of the anterior ventral, medial dorsal and thalamic nuclei with 80-90% neuronal loss and a 2-3 fold increase in astrogliosis whilst spongiform change is relatively absent.

P102L

This genotype is characterized by PrP-amyloid plaques and diffuse deposits that are associated with moderate to severe neuronal loss and glial proliferation in the cerebral cortex, deep grey nuclei and cerebellar cortex. The PrP amyloid deposits are birefringent after Congo red staining and strongly fluorescent after thioflavin S treatment. The amyloid is composed of bundles of fibrils radiating out from a central core, each fibril measuring 8-10 nm in diameter.

1.1.7 **MRI findings in prion disease**

Although initially performed to exclude treatable brain diseases, recent advances in MRI technology, including more sensitive and faster sequences, have lead to MRI becoming an extremely important diagnostic tool in human prion diseases. MRI studies are now included in the WHO diagnostic criteria for vCJD and the routine use of DWI has enabled earlier and more accurate diagnosis of sCJD, often with avoidance of brain biopsy. MRI is a very powerful non-invasive technique for imaging soft tissue in vivo with detailed anatomical resolution and has a high sensitivity for the detection of neuropathology which alters T1 and T2 relaxation or the water diffusion properties of affected tissue.

1.1.7.1 *Sporadic CJD*

Increased signal in the striatum, cortex and to a lesser extent in the thalamus are the classical findings in sCJD (Figure 1.1.6). The extent of involvement and the distribution of signal changes varies amongst patients with Young *et al* reporting in 40 patients with sCJD that the combination of signal changes in the cortex and deep grey matter occurred in 68% of subjects whilst involvement of the cortex alone was less common (24%) and high signal in the deep grey matter without cortical signal change was extremely rare (5%) [26]. The cortical signal changes involve all lobes, mainly frontal (89%), limbic (79%), parietal (72%) and temporal (65%), while the precentral and central gyri are usually spared [60]. However, in another study of 55 patients with sCJD, isolated cortical involvement was seen in as many as one third of patients[61].

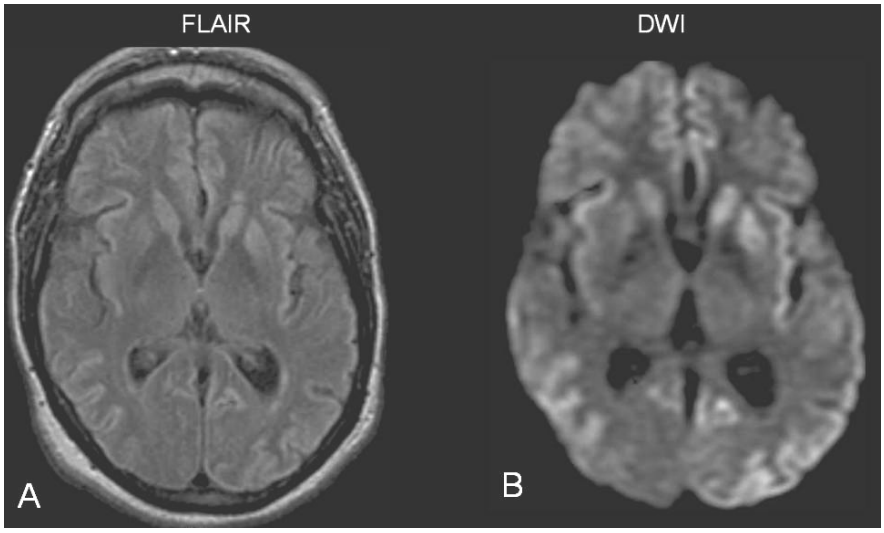

Figure 1.1.6: Axial FLAIR (A) and DWI (b=1000s/mm^2) (B) demonstrating increased signal in the caudate and putamen bilaterally and diffuse cortical hyperintensity

There is now evidence that a characteristic lesion profile may occur with each molecular subtype of sCJD. In a study of 211 patients with histopathologically confirmed sCJD, basal ganglia hyperintensities occurred more frequently with MV2, VV2 and MM1 subtypes and widespread cortical signal most common in VV1, MM2 and MV1 subtypes with thalamic hyperintensities in VV2 and MV2 subtypes [62].

In the majority of cases, the signal changes in the basal ganglia and cortex are symmetrical, although a unilateral predominance does occur [63]. Striate and thalamic high signal is best detected on T2- and PD sequences [64-72]. Recent studies have shown that DWI is the best sequence for detecting signal change in the cortex [26;73-75]. The combined use of DWI and FLAIR sequences to identify abnormal high signal in the cortex and striatum is reported to increase diagnostic sensitivity and specificity for sCJD to greater than 91% [26]. In previous studies without the routine use of DWI to identify cortical signal change the sensitivity of the striate changes alone was reported as 58-78% [65;72].

In many cases, the T2W MRI acquired at an early stage of the disease is normal [76]. Cortical signal changes often precede the basal ganglia signal changes [76]. Murata *et al* reported a defined temporal sequence of events where high signal starts in the anteroinferior putamen and spreads to the posterior part, leading to complete involvement of the putamen. They reported that all putaminal lesions were accompanied by increased signal in the ipsilateral putaminal head. There is one report of expansion of the signal changes and general progression to cerebral atrophy [77] and there are two reports of disappearance of diffusion signal changes [76;78]. In the end stages of disease, there is severe cerebral and cerebellar atrophy, ventricular enlargement, atrophy of the brain stem and midbrain [79].

The panencephalic type of sCJD is defined by the prominent involvement of white matter and has been reported in a series of 8 cases from Asia, and especially in Japan. In this study, prion protein subtypes and codon 129 data were not available and it is not yet clear whether this subtype represents a distinct entity or a non-specific end-stage of sCJD [80]. T1-weighted (T1W) images are usually normal but one publication reported high signal in the globus pallidus [81]. Contrast enhancement does not occur and CT only shows atrophy in advanced cases [82].

The radiological differential diagnosis for the signal change seen in sCJD includes carbon monoxide poisoning, cerebral hypoxia, and Leigh's disease where signal change may be seen in the basal ganglia. Cortical signal changes may also be present in cerebral hypoxia. However, the clinical presentation in these cases is entirely different to that of sCJD.

1.1.7.2 *Variant CJD*

Symmetrical hyperintensity in the pulvinar thalami (relative to the cortex and especially the anterior putamen) is characteristic of vCJD and is known as the pulvinar sign (Figure 1.1.7). The pulvinar sign was initially reported to have a sensitivity of 78-90% and a specificity of 100% for vCJD and was originally described on T2W, PD and FLAIR images [36;37]. The mediodorsal thalamic nucleus is additionally affected in 56% of cases and the combination of this with pulvinar signal change on axial MRI produces an appearance named the "hockey stick" sign. In 86 neuropathologically confirmed cases, the caudate nucleus was involved in 40% of cases, the putamen in 23.3%, and the periaqueductal grey matter in 83.3% [37]. The radiological differential diagnosis for the pulvinar sign includes post-infectious encephalitis, cat-scratch disease, and Alpers syndrome but again, these diseases have a very different clinical presentation to vCJD.

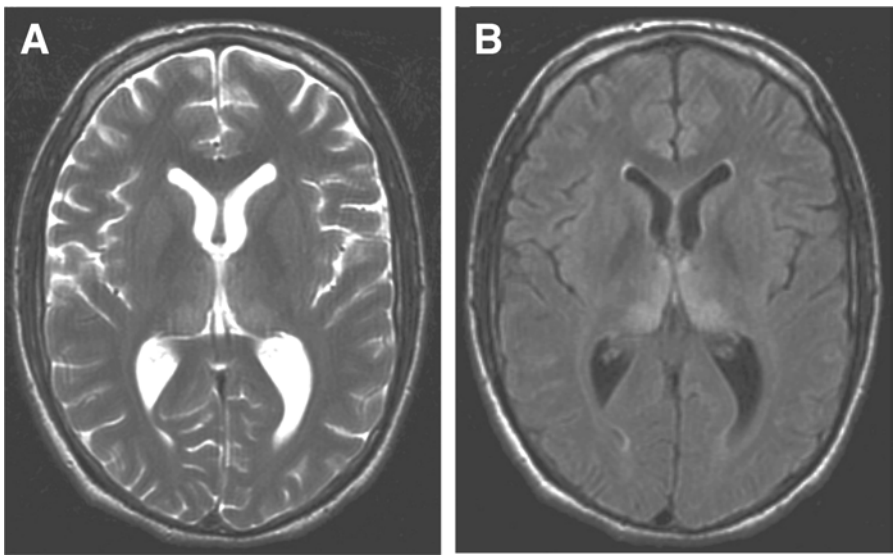

Figure 1.1.7: Axial T2W (A) and FLAIR (B) demonstrating hyperintensity within the pulvinar nuclei and dorsomedial thalamus bilaterally.

Variant CJD has the most consistent changes on MRI of any human prion disease type, perhaps because only one molecular strain is present. As yet, there is no evidence to

support the use of the pulvinar sign in pre-symptomatic testing for vCJD as all reports refer to symptomatic patients. In one report of a blood transfusion acquired case of vCJD, imaging at the time of initial clinical presentation was negative for the pulvinar sign and was only positive when the patient was severely affected, suggesting that the pulvinar sign is a late feature of vCJD [3].

1.1.7.3 Inherited prion diseases

Unlike other forms of prion disease MRI is less important in the diagnosis of inhPrD since a definitive diagnosis can be made with *PRNP* genotyping performed on a blood sample. MRI is still useful to exclude treatable diseases such as subdural collections or vasculitis and can point towards the diagnosis in the early stages, perhaps before an inhPrD has been considered. In a European study of 445 patients with inhPrD, MRI scan data was available in 43% of cases and was positive in 50% of patients with the E200K mutation, 33% of cases with the GSS clinical phenotype and 18% of cases with the FFI clinical phenotype [43]. However, the study did not specify which MRI sequences were available. There are few reports of MRI findings in specific genotypes but a recent reports of a family with the E200K mutation have described increased signal in the caudate, putamen and thalamus bilaterally [83]. On DWI, abnormalities in the cingulate, frontal and occipital cortex were also identified in a pattern similar to that seen in sCJD [84].

1.1.8 Histopathology and MRI

It is not yet known which histopathological changes are responsible for the pathological signal change seen on MRI, with many conflicting reports in the literature. A few studies have reported increased spongiosis in anatomical areas corresponding to DWI signal change [85-88]. However, another study claims that DWI signal change correlates with accumulation of PrP^{Sc}, whereas another study found no correlation between ADC measurements and any histopathological findings [89].

1.1.9 Early diagnosis of human prion disease

Although the current prognosis for human prion disease is poor, it is important to establish an early diagnosis and to exclude potentially treatable alternative diagnoses such as cerebral vasculitis. Early confirmation also excludes uncertainty, allowing a care plan to be established including infection control measures and appropriate counselling. With the advent of the first therapeutic trials in prion disease, there is the need for early diagnosis in order to allow the possibility of therapeutic intervention before significant irreversible neuronal damage has occurred. Currently, diagnosis of human prion disease occurs at a late, clinically-advanced stage on the basis of clinical criteria with the support of diagnostic test such EEG, CSF and neuroimaging.

The identification of the pulvinar sign as highly sensitive for vCJD [37;90] has brought neuroimaging to the forefront in the diagnosis of prion diseases. There is a need for a non-invasive diagnostic test, ideally of blood, which would allow screening of affected or asymptomatically infected individuals. Until this is developed, neuroimaging has the advantage of being non-invasive and potentially a reliable and quantifiable marker of disease activity.

1.2 Quantitative MRI

Over the last few years a number of advanced MRI techniques have been developed with the aim of detecting subtle pathological changes in brain tissue and indirectly reflecting microscopic aspects of tissue damage such as demyelination, microtubule breakdown and axonal loss. The techniques of ^{1}H-MRS, DWI and magnetization transfer imaging have been applied to a variety of diseases with clinical applications particularly for DWI in stroke imaging. In dementia imaging, these techniques have not been shown to be useful in clinical diagnosis but have shown promising results when applied to studies involving groups of patients [91]. In addition, magnetic resonance microscopy (MRM) of post-mortem tissue allows the direct investigation of the relationship between these quantitative MRI measures and tissue microstructure.

1.2.1 DWI and diffusion tensor imaging (DTI)

MRI is naturally sensitive to water self-diffusion, as spins undergoing a random diffusional motion in the presence of a magnetic field gradient accumulate different randomly distributed phase shifts. This results in a loss of phase coherence and therefore in a decrease in signal intensity (SI) which is proportional to the diffusion coefficient. This provides a unique form of MRI contrast that enables the diffusional motion of water molecules to be measured and as a consequence of interactions between tissue water and cellular structures, provides information about the size , shape, orientation and geometry of brain structures [92]

1.2.1.1 MRI sequences

The most commonly applied sequence for producing diffusion-weighted contrast is the pulsed gradient spin echo (PGSE) method. It consists of a 90-180 spin echo pair of radiofrequency pulses with large and equal gradients placed on either side of the 180 pulse (Figure 1.2.1).

Figure 1.2.1: Pulse sequence for DWI

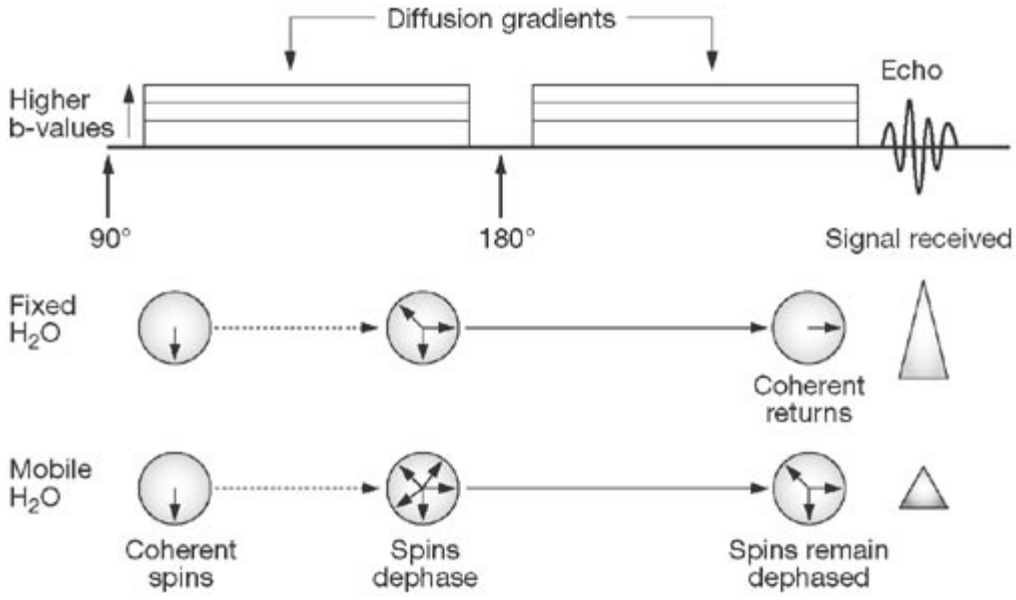

(As published in Patterson et al 2008 [93]).

Manipulating the strength of the gradient amplitude (G) and the timing elements of δ (little delta), the pulse width, and Δ (big delta), the leading edge of separation or centre-to-centre spacing, we can control the degree of weighting or *b-factor*. In the PGSE sequence the value of b is given by

$$b = \gamma^2 G^2 \delta^2 (\Delta - \delta/3)$$

Large gradient amplitudes of up to 30mT m^{-1} are highly advantageous because their use means that the timing parameters can be minimized, thus avoiding very long TE values but even so, DW acquisitions will have some T2 weighting [94].

The signal strength is described by the equation

$$S(b) = S(0)\exp(-bD)$$

Where $S(b)$ is the signal for a particular b value and D is the self-diffusion constant for the tissue. However, in practice, the actual diffusion coefficient may contain contributions from other movement sources such as micro-circulation in pseudo-random capillary systems, bulk flow and movement artefact and also the imaging gradients can

also contribute to diffusion weighting. We therefore usually refer to the ADC which can be calculated from two images using the Stejskal Tanner equation [95]

$$ADC=-\{\ln(S1/S2)/(b1-b2)\}$$

where $S1$ and $S2$ are the signal intensities of DWI with b-factors of 0 ($b1$) and 1000 s/mm^2 ($b2$), respectively. Alternatively, a range of b values can be applied and a "least squares fit" performed which is usually more accurate.

In practice, the echo planar imaging (EPI) is the sequence of choice for DWI with a very rapid acquisition time so that little motion induced artefact is encountered [94].

1.2.1.2 DTI

Pure water is said to have isotropic diffusion properties, in that the direction of movement of the water molecules is equal in all directions. In biological tissues, diffusion is restricted by the presence of cell membranes and there may be a preferential diffusion direction. Such directionally-dependent diffusion behaviour is termed anisotropy, which reflects to some extent the underlying fibre structure. The physical orientation of the tissue, together with the applied gradient direction will determine the SI [96]. The diffusion properties may be described mathematically by a tensor, which is a matrix of nine values corresponding to a gradient orientation and a cell orientation:

$$DT = \begin{Bmatrix} D_{xx} & D_{xy} & D_{xz} \\ D_{xy} & D_{yy} & D_{yz} \\ D_{xz} & D_{yz} & D_{zz} \end{Bmatrix}$$

The first subscript (x, y, z) refers to the "natural" orientation of the cells or tissue and the second refers to the gradient orientation. The orthogonal elements $D_{xx,}$ D_{yy} and D_{zz} correspond to the simple three direction measurements found in commercial scanners. In practice, only seven measurements, six tensor components and an unweighted b=0 image are required. Once the tensor terms have been found, the diffusivity can be described by three eigenvalues that describe the axes of an ellipsoid with direction of the eigenvector associated with the largest eigenvalue coinciding with direction of maximum diffusion (Figure 2.2) [96].

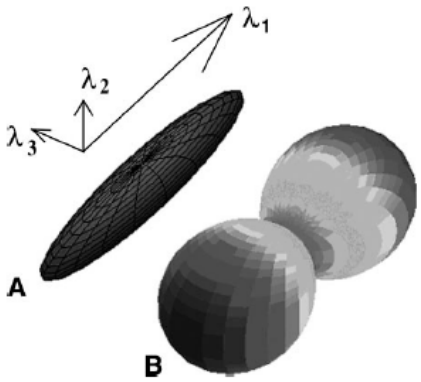

(As published in Beaulieu C, 2002 [96])

Figure 1.2.2: Diagram demonstrating the eigenvalues that describe the diffusion tensor. The ellipsoid representation of the diffusion tensor (A) with λ_1 representing the diffusivity along the longest axis of the ellipsoid, λ_2 represents the diffusivity along the second longest axis and λ_3 represents diffusivity along the shortest axis of the ellipsoid. (A) represents anisotropic diffusion and (B) represents isotropic diffusion.

Diffusion tensor measurements result in a rich data set. Diffusion anisotropy can be measured in different ways by applying mathematical formulae and recalculations using the underlying eigenvectors[97]. A common way to summarise diffusion measurements in DTI is calculation of parameters for overall diffusivity and anisotropy. The ADC or mean diffusivity (MD) serves for overall diffusivity and is derived from the from the trace tensor, while anisotropy is represented by fractional anisotropy (FA) or relative anisotropy (RA).[94].

FA is a measure of the diffusion tensor due to anisotropy. The RA is derived from a ratio between the anisotropic water and isotropic portions of the diffusion tensor. Both FA and RA are 0.0 for a purely isotropic medium. For higher symmetric anisotropic media FA tends towards 1 whilst RA tends towards √2. FA can be respresented as grey-scale maps but by choosing the eigenvector associated with the largest eigenvalue, the principal diffusion direction of the brain structure to be examined can be colour-coded to give directionally encoded colour FA maps[97]

DTI provides some insight into the nature and degree of pathological damage that occurs in central nervous system diseases when cellular structures are damaged or damaged as part of the pathological process. In white matter, where bundles of axons

give healthy tissue a highly ordered structure, diseases that cause axons to degenerate and be replaced by amorphous cells cause a reduction in diffusion anisotropy as a result. [98]. Several studies of diffusion tensor imaging in AD have found a specific pattern of regional abnormalities with reduced FA in the fibre tracts of the corpus callosum, and the white matter of the frontal, temporal and parietal lobes which showed strong correlations with neuropsychological measures [99;100][Bozzali *et al.* 2002;Rose *et al.* 2000]. In addition, whole brain and hippocampal ADCs have shown to be higher in patients with AD compared to controls [101;102]. This increase in diffusivity is thought to be associated with loss of neuron cell bodies, synapses and dendrites which cause an expansion of the extracellular space where water diffusivity is fastest[103].

1.2.1.3 High *b* value DWI

The b values that are applied in clinical diffusion studies are usually of the order of b=1000 s/mm^2. The application of higher *b* values has shown that water diffusion in the brain is bi-exponential and can be described by fast and slow diffusion coefficients. The fast component has a diffusion coefficient on the order of 1.2μm^2/ms with a volume fraction of 70% whereas the slow population has a diffusion coefficient of 0.2μm^2/s with a volume fraction of 30% [104]. The assignment of the slow fraction to a distinct water population is difficult. Although it was previously thought that the fast and slow water populations represent water from the extra- and intracellular spaces respectively[105], there is now evidence that both the fast and slow water diffusion components arise from the intracellular space [104].

The slow diffusion coefficient offers potential as an image contrast or clinical parameter [106]. Recent applications of higher *b* value DWI has increased sensitivity for the detection of signal abnormality in ischaemic stroke [107;108] and the grading of cerebral gliomas as well as being more sensitive to white matter degeneration in AD [109]. Although at higher *b* values, there is a decrease in signal-to-noise ratio (SNR), this is compensated for by an increase in contrast-to noise ratio (CNR)[110;111].

1.2.2 ^{1}H-MRS

^{1}H-MRS has become well established as a non-invasive technique for studies of biological systems *in vivo* and *in vitro* [112]. ^{1}H-MRS is unique among diagnostic imaging modalities in that the signals from several different metabolites are measured within a single examination period and each metabolite is sensitive to a different aspect of in vivo pathological processes at the molecular or the cellular level.

1.2.2.1 Principles of MRS

Over the last 50 years, nuclear magnetic resonance spectroscopy has been the preeminent technique for determining the structure of organic compounds. Proton nuclei in different compounds behave differently in the NMR experiment because of the electrons which surround the protons in covalent compounds and ions. Since electrons are charged particles, they move in response to the external magnetic field and (B_0), generating a secondary field that opposes the much stronger external field. This shielding effect means that the applied field must be increased for the nucleus to absorb at its transition frequency. The difference between the applied magnetic field and that experienced at the nucleus is known as nuclear shielding or chemical shift (σ).

$B=B_0 (1-\sigma)$

The chemical shift is so small compared to the actual field strength that it is referred to in units of parts per million (ppm) and is it is dependent on the strength of the applied field, is often given in reference to a standard compound tetramethylsilane $(CH_3)_4Si$ which as a single proton resonance because it is a completely symmetrical molecule [113].

1.2.2.1 MRI sequences for in vivo ^{1}H-MRS

PRESS or Point-RESolved Spectroscopy is based on a spin-echo (SE) sequence where the 90º pulse is followed by two 180º pulses so that the primary SE is refocused again by the third pulse. Each pulse has a slice selective gradient in order that protons within a voxel are the only ones to experience all three RF pulses (Figure 1.2.3). The SI is intrinsically twice as high as STEAM and therefore spectra with a good SNR can be acquired in a relatively short time [113].

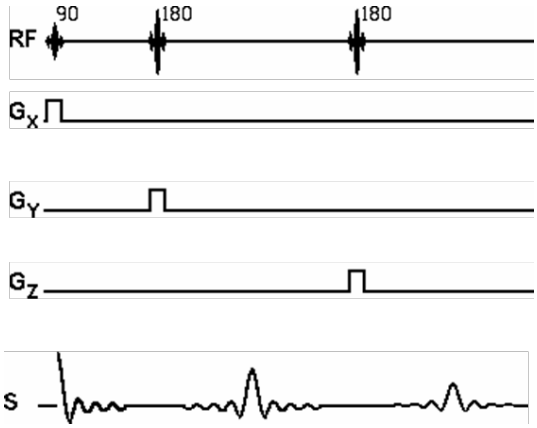

(Courtesy of Ray Young, MRC Prion Unit)

Figure 1.2.3: Pulse sequence for PRESS: 90º pulse is followed by two 180º pulses so that the primary SE is refocused again by the third pulse.

Voxel positioning in the most appropriate anatomical location for the detection of neuropathology is paramount and a good shim over the voxel is essential to produce a good spectrum preferably with a line width of less than 0.08ppm. Voxels in inhomogenous regions of the brain are difficult to shim. In general smaller voxels are easier to shim, but the signal acquired also depends on the voxel size and therefore voxels with 1cm sides are considered the most practical minimum size to achieve a reasonable SNR. Consistent voxel positioning is extremely important for obtaining reliable spectra and short echo times give improved SNR.

1.2.2.4 In vivo ^{1}H-MRS

The most prominent peak of the ^{1}H spectrum belongs to *N*-acetylaspartate (NAA), at 2.0ppm (Figure 1.2.5) which under normal conditions is exclusively synthesized in the mitochondria of neurons [114] and is considered to be a marker of neuronal density and integrity. Other peaks in the ^{1}H spectrum belong to creatine/phosphocreatine (Cr) at 3.0ppm considered to be a marker for energy metabolism as phosphocreatine acts as reservoir for the generation of ATP. As the Cr peak is relatively stable with age and in a variety of diseases, it is commonly used as a concentration reference. However, there are recent reports of decreased levels with tumours and stroke [112].

For MRS studies on tissues, the choline (Cho) signal is observed as a prominent signal at 3.2ppm that includes contributions from free choline, glycerol-phosphorylcholine (GPC) and phosphorylcholine (PC) [115]. These are thought to be markers of membrane activity since phosphocholines are released during myelin breakdown and increased

signal is observed in cancer, ischaemia, head trauma and AD[116]. With shorter echo times at 10-35ms, the peaks of *myo*-inositol (MI) become visible with a peak at 3.6ppm. The function of MI is not well understood but as glia are known to express higher levels of MI than neurons, it has been proposed as a glial marker[112]. Increased levels have been observed in AD and other neurodegenerative conditions [117;118]. However, there are technical challenges in obtaining short TE ^{1}H-MRS such as water suppression, signal contribution from subcutaneous fat and gradient eddy current distortions, all of which reduce the test-retest reproducibility of metabolite measurements.[119]

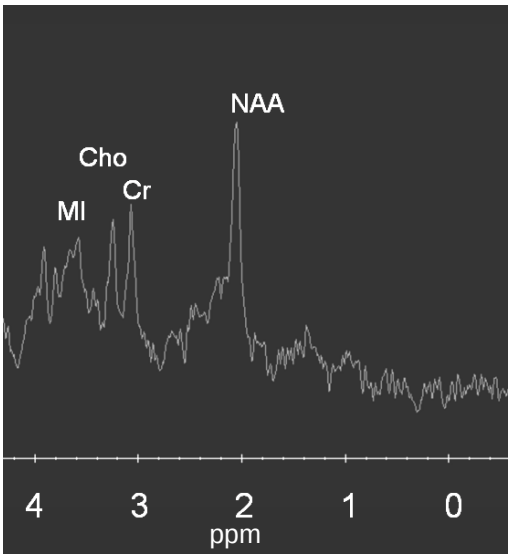

Figure 1.2.4: Example of an in vivo ^{1}H-MRS spectrum of the human brain showing positions of the NAA at 2.0ppm, Cr at 3.0ppm, Cho at 3.2 ppm and MI at 3.6ppm.

1.2.3 Magnetic Resonance Microscopy

MRI has been used to acquire images of the post-mortem brain for a number of years. These images complement the work of the neuropathologist by allowing comparison of these MRI images with the equivalent physical sections prepared for neuropathological assessment. Post-mortem MRI acquisition provides the opportunity to directly investigate the relationship between MRI measures and histology parameters. Post-mortem MRI imaging has been applied to the brains of people with diagnoses of AIDS[120], AD [121] and multiple sclerosis [122;123] focussing on correlating MRI detectable lesions directly with the histological findings.

Magnetic resonance microscopy (MRM) refers to the use of high magnetic field strength magnetic resonance imaging (MRI) to characterise tissue structure at a resolution of less than 100µm. The high spatial resolution and high signal-to-noise ratio (SNR) allows the use of this technique for the mapping of various physical properties of tissue water reflecting different aspects of normal tissue microstructure and pathology [124]. Their measurement, *ex vivo*, may both inform the interpretation of *in vivo* MRI data and provide pathological measures complementary to conventional histology. The high spatial resolution is attained through the use of strong magnetic field gradients (200-800 mT/m) and specialized radiofrequency coils [125;126].

To our knowledge, postmortem MRI of tissue at high magnetic field strengths has not previously been performed in prion diseases. Correlation of post-mortem findings with *antemortem* MRI should be interpreted with caution in the context of such a rapidly progressive disease as prion disease but the use of magnetic resonance microscopy allows an opportunity to directly investigate the relationship between quantitative MRI measures and histopathology.

1.2.4 Methods of image analysis

1.2.4.1 Region of interest (ROI)

ROI analysis is extremely useful when there is a priori hypothesis about the location of pathology and a good knowledge of neuroanatomy. The technique can be very sensitive to small changes and is relatively easy to implement. However, ROI analysis can be time consuming and poorly reproducible. To avoid potential bias, the ROI should be defined on an image where the contrast does not depend on the quantity being measured. For ADC measurements, the ROIs are usually defined on the b0 image which is often of poor contrast and low spatial resolution. In addition, the ROI size is also of importance: a larger ROI is associated with a reduction in the standard error of each measurement due to averaging over more pixels, but also with increased partial volume effect [127]. Finally, when comparing multiple ROIs, a correction for multiple comparisons must be performed.

1.2.4.2 Histograms

Histograms are frequency distributions showing the number of voxels within a particular range of values defined as "bins". Histograms are generally normalized with respect to the total number of voxels considered in order to remove variations due to between-subject differences in head size. Several metrics, the most commonly used being peak height, peak location and the sample mean can be extracted from the histogram and subject to statistical analysis (Figure 1.2.5).

This technique is ideal for studying conditions that affect large regions of the brain, avoids bias in positioning ROIs and therefore observer-dependent bias, and avoiding the need for performing multiple statistical testing. A major issue is the performance of the segmentation procedures to select the voxels to be included in the analysis. Poor segmentation of CSF might result in different degrees of partial volume, with cerebral atrophy therefore providing an undefined contribution to any observed changes. Again, to avoid potential bias, the image data used for segmentation should have the same geometric properties as the quantitative images under investigation but the contrast should not be dependent on the quantity being measured. This technique can also be relatively insensitive to small, highly localised changes.

Figure 1.2.5: Histogram demonstrating the metrics that can be obtained.

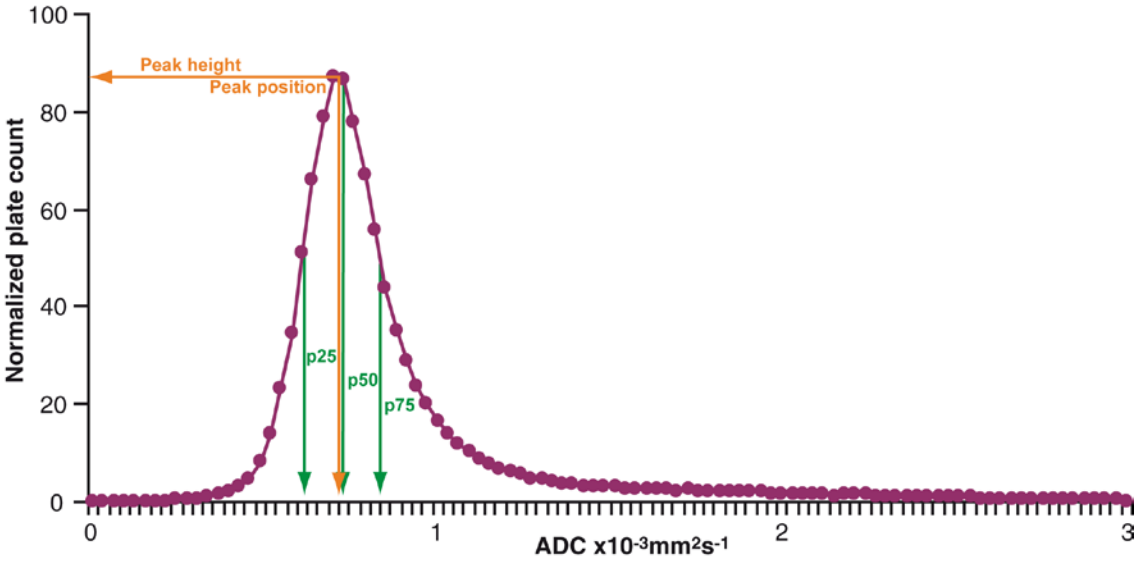

1.2.4.3 Voxel-based analysis

In voxel-by-voxel analysis, the map of interest is registered into a standard space and then voxel-wise statistics are performed to detect regional differences between populations or to find areas that correlate with a covariate of interest. This technique is useful when there is no a priori hypothesis about the location of the neuropathology but can have a low sensitivity. However, there can de difficulties when there is misalignment, after standard normalization algorithms are employed, leading to misinterpretation. Spatial smoothing is a pre-requisite for this technique, but the extent of spatial smoothing can lead to different interpretations [128], such that the optimal extent of spatial smoothing is still a matter of debate.

1.2.4.4 Conclusion

For the purposes of studying this disease, I had a good a priori knowledge as to the location of neuropathology from both histological studies and previous MRI reports, as mentioned previously. Therefore, a combination of ROI analysis for small areas of interest such as the basal ganglia and histogram analysis for large parts of the brain such as the cortical grey matter were used. Voxel-based analysis techniques were considered inappropriate, as the location of neuropathology excluded the white matter and with such small numbers of patients, the technique was expected to have a relatively low sensitivity.

1.3 Therapeutic trials in prion diseases

Therapeutic strategies in prion diseases include targeting normal PrP^{C} to rendering it less available for conversion to pathological PrP^{Sc}. These approaches might include the isolation of small molecule PrP ligands which bind to and stabilise PrP^{C}, antibodies that bind or sequester PrP^{C}, and methods to down-regulate PrP^{C} transcription or translation. The conversion of PrP^{C} to PrP^{Sc} is postulated to proceed through a highly unfolded state that retains little organised native structure, so that compounds which bind to any ordered region of PrP^{C} could inhibit the conversion pathway[129]. High throughput screening of large compound libraries can be applied to detect such ligands and this method has already been used for the proteins p53 and transthyretin where genetic mutations and altered protein conformations result in disease.

Antibodies against several PrP epitopes have been identified which might act by binding cell surface PrP^{C} and reducing its availability for incorporation into propagating prions [130;131]. As antibodies do not cross the blood brain barrier, there was no protective effects in intracerebrally infected mice but humanised anti-PrP monoclonal antibodies may be used for post-exposure prophylaxis of particular risk groups. Active immunisation is limited by immune tolerance to PrP which is a naturally occurring host protein.

Other possible future approaches include the use of small duplex RNA molecules to silence gene expression in a sequence specific manner – RNA interference (RNAi) [132]. Lentiviral mediated RNA silencing of PrP^{C} as a possible therapeutic tool may be possible but would require effective CNS penetration.

At the request of the Government's Chief Medical Officer, a clinical trial protocol to rigorously assess the effect of the drug Quinacrine was developed and also to provide a framework for assessment of new therapies as they are developed. The MRC Prion-1 trial, a partially randomised patient preference trial to evaluate the activity and safety of quinacrine in human prion disease is now completed [133]. This trial showed that Quinacrine at a dose of 300mg does not significantly affect the clinical course of prion diseases.

Therapeutic trials in human prion diseases are beset with a number of issues relating to the rarity of the disease, the rapid progression, and being uniformly fatal which make

randomisation to placebo unacceptable. As the first generation of treatments proposed for prion disease are likely to have only modest effects on disease progression, survival duration as an outcome measure requires studies of a large number of patients in order to determine efficacy. The lack of systematic natural history studies of disease progression and an absence of biological markers of disease activity makes assessment of the effects of treatment extremely difficult.

In clinical trials of neuroprotective drugs, surrogate outcome markers, which are supposed to reflect the number of surviving neurons in a clinically meaningful way, have been used in addition to clinical measures of cognitive impairment and disease severity in AD. Clinical outcome markers may not distinguish between disease modifying effects and purely symptomatic drug effects. In addition, clinical symptoms are usually manifest when the amount the neuron loss/dysfunction is fairly substantial, relatively late in the disease process. Some clinical outcome measures have poor test-retest reliability, usually because they are based on subjective semi-quantitative measures resulting in considerable between-rater and between-site variability.

There is therefore a need to complement clinical outcome markers with objective and quantifiable markers that can detect changes in the preclinical stage of disease, have a high re-test reliability, that are non-invasive and well-tolerated and also relatively inexpensive [134]. Quantitative MRI measures which fulfil the above requirements are increasingly being investigated for replacing clinical measures in outcome trials for neuroprotective drugs.

A IN VIVO

The next three chapters describe the analysis of *in vivo* MRI data obtained from patients diagnosed with prion diseases. The majority of the work focuses on the use of quantitative neuroimaging techniques as measures of disease activity in inhPrDs. I specifically investigated the use of regional and global ADC measures and in a small subgroup of patients and I investigated the use of single voxel ^{1}H-MRS. In addition, I also investigated the use of DWI with higher diffusion factors for improved radiological diagnosis of sCJD and vCJD.

2. Regional and global cerebral diffusion coefficients and disease severity in inherited prion disease

2.1 Introduction

ADC measurements obtained by MRI provide quantitative estimates of regional and whole brain water MD and may provide objective non-invasive markers for early diagnosis, disease progression or monitoring the effects of therapeutic intervention. Although DWI has emerged as a sensitive diagnostic technique in cases of sCJD [26;60;72;135], few studies have quantified cerebral ADC in the various forms of human prion disease [78;136], with even fewer addressing cerebral ADC in inhPrD [83;137].

In this chapter, I measure regional and whole brain cerebral ADCs in patients with inhPrD, and for comparison healthy control subjects. By correlating ADC measures with clinical scores I aimed to find sensitive MRI indices of disease severity as potential objective biomarkers of disease progression.

2.2 Methods

2.2.1 Patients

Twenty five patients with inhPrD (13 female, 12 male, mean age 45.2 years, range 32-58 years) referred to the National Prion Clinic, National Hospital for Neurology and Neurosurgery, London, U.K., were included in this study. All patients were recruited into the MRC Prion-1 trial, a partially randomised patient preference trial to evaluate the activity and safety of quinacrine in human prion disease [133]. Ethical approval for the study was granted by the Eastern Multi-centre Research Ethics Committee (MREC), and informed consent for participation in the study was given by either the patient or patient's next of kin. Seven healthy volunteers were also recruited (4 female, 3 male; mean age 54.1 years; range 42 – 61 years) with no personal or family history of neurological disorders and gave informed consent.

Patients were subject to a structured neurological examination at the time of the MRI scan session by a qualified neurologist blinded to the MRI findings, and the following scores calculated: Mini Mental State Examination (MMSE) [138], Clinician's Dementia Rating Scale (CDR) [139], Rankin scale [140], Alzheimer's Disease Assessment Scale (ADAS-COG) [141], Barthel Activities of Daily Living scale (ADL) [142], A clinician's global impression of disease severity (CGIS) [143], Brief Psychiatric Rating Scale (BPRS) [144]. Please see Appendices A-G.

Fourteen patients were taking a standard clinical dose of Quinacrine 300mg once daily as part of the MRC Prion-1 Trial.

2.2.2 MRI acquisition

All subjects were examined using a GE Signa LX 1.5T MRI system (GE Healthcare, Milwaukee, WI). After scout images were obtained, axial images with slice thickness 5mm, parallel to the bicommisural line from the craniovertebral junction to the vertex, were acquired with T2-weighting (TE 106ms, TR 6000ms, 2 averages, field of view (FOV) 24x18cm, matrix 256x224, slice thickness 5mm), and fluid attenuation inversion recovery (FLAIR) contrast (TE 161ms, inversion time (TI) 2473ms, TR 9897ms, one average, FOV 24 x 24cm, matrix 256 x 224, slice thickness 5mm). DWI was performed using a single-shot echo-planar technique (TE 101ms, TR 10000ms, one average, matrix 96 x 128, FOV 26 x 26cm, slice thickness 5mm) with diffusion-weighting factors ('b values') of 0 and 1000 s/mm^2 applied sequentially along three orthogonal

axes. Three-dimensional T1W image data were acquired from 124 contiguous 1.5mm thick coronal slices (inversion-recovery prepared spoiled gradient-echo sequence; TE 5ms, TR 35ms, flip angle 35º, matrix 256x128, FOV 24x24cm).

2.2.3 MRI analysis

2.2.3.1 Conventional MRI

The T2W, FLAIR and DWI were reviewed independently by 2 consultant neuroradiologists. Pathological signal changes were assessed in the following regions: caudate, putamen, thalamus, frontal, parietal, temporal and occipital cortex. Where a discrepancy was identified, the images were re-reviewed in a consensus reading. A kappa statistic was calculated to assess the level agreement between the two independent observers for pathological signal change.

2.2.3.2 Quantitative MRI

Post-processing was performed at a dedicated work station (Sun Microsystems, Mountain View, CA) by a single neuroradiologist blinded to the clinical and genetic data. Using commercially available software (Jim Version 4.0; Xinapse Systems Ltd, Thorpe Waterville, UK.), pixel-by-pixel ADC maps were generated from the directionally-averaged b=0 and b=1000 s/mm^2 images using the Stejskal Tanner equation [95] for ADC calculation: ADC=-{In($S1/S2$)/($b1$-$b2$)}, where $S1$ and $S2$ are the signal intensities of DWI with b-factors of 0 ($b1$) and 1000 s/mm^2 ($b2$), respectively. Following automatic segmentation of brain from non-brain tissue using the brain extraction tool (BET), a part of the FSL 3.2 software, FAST segmentation [145] was applied to the b=0 images to classify each pixel as either white matter (WM), grey matter (GM), CSF or other tissues. Four classes were selected for segmentation in order that dark non-brain matter was processed correctly. This method uses a prior knowledge of the spatial distribution of tissues in the brain in the form of standard tissue-type probability maps (provided by the Montreal Neurological Institute) to initialise the segmentation and for final segmentation [146]. For each data set a mask was generated with each intracranial pixel classified as either GM or CSF and, the masks were used to extract the appropriate pixels from the ADC map to create a GM ADC map and whole brain (WB) ADC map. To minimise contamination of the measured ADC by values from CSF due to partial volume effects, a single morphological erosion operation was applied to the both the whole brain and grey matter ADC masks. The GM segment was too thin to support more than one erosion.

In order to explore the potential confounding effects of progressive cerebral and cerebellar atrophy upon the ADC measurements, normalized volumes of the entire brain parenchyma (NBV) were estimated from the T1W volumetric image data for each subject using the SIENAX software [147;148], again provided as part of FSL 3.2. Following extraction of separate brain and skull images from the single whole-head input data [145] the brain image is affine-registered to MNI152 space [149;150] (using the skull image to determine the registration scaling); this is primarily in order to obtain the volumetric scaling factor, to be used as a normalisation for head size. Next, tissue-type segmentation with partial volume estimation is carried out [151] in order to calculate total volume of brain tissue.

2.2.3.2.1 Histogram analysis

A histogram generation algorithm was implemented with in-house software to calculate the ADC frequency distribution for each segmented tissue fraction using $3x10^{-5}$ mm^2/s bin widths. To adjust for inter-subject variability in specific tissue volumes the ADC histograms were normalized by dividing the number of counts in each sample bin by the total number of pixels for the respective tissue type. From each normalised histogram, the peak height (PH), peak location (PL), mean ADC and ADC value of the 25^{th}, 50^{th} and 75^{th} percentiles were calculated (Figure 2.1A for examples of WB and GM ADC normalized histograms).

2.2.3.2.2 Region of Interest (ROI) Analysis

As the deep GM structures were difficult to segment with the available software, the mean ADCs in the head of the caudate nucleus, putamen and pulvinar were determined bilaterally by manually drawing around each region on the axial b0 image at the level of the genu of the internal capsule using the DispImage software [152]. The ROIs, ranging in size from 40-70mm^2, were transferred to the inherently co-registered ADC map (Figure 2.2) and mean ADC recorded for each.

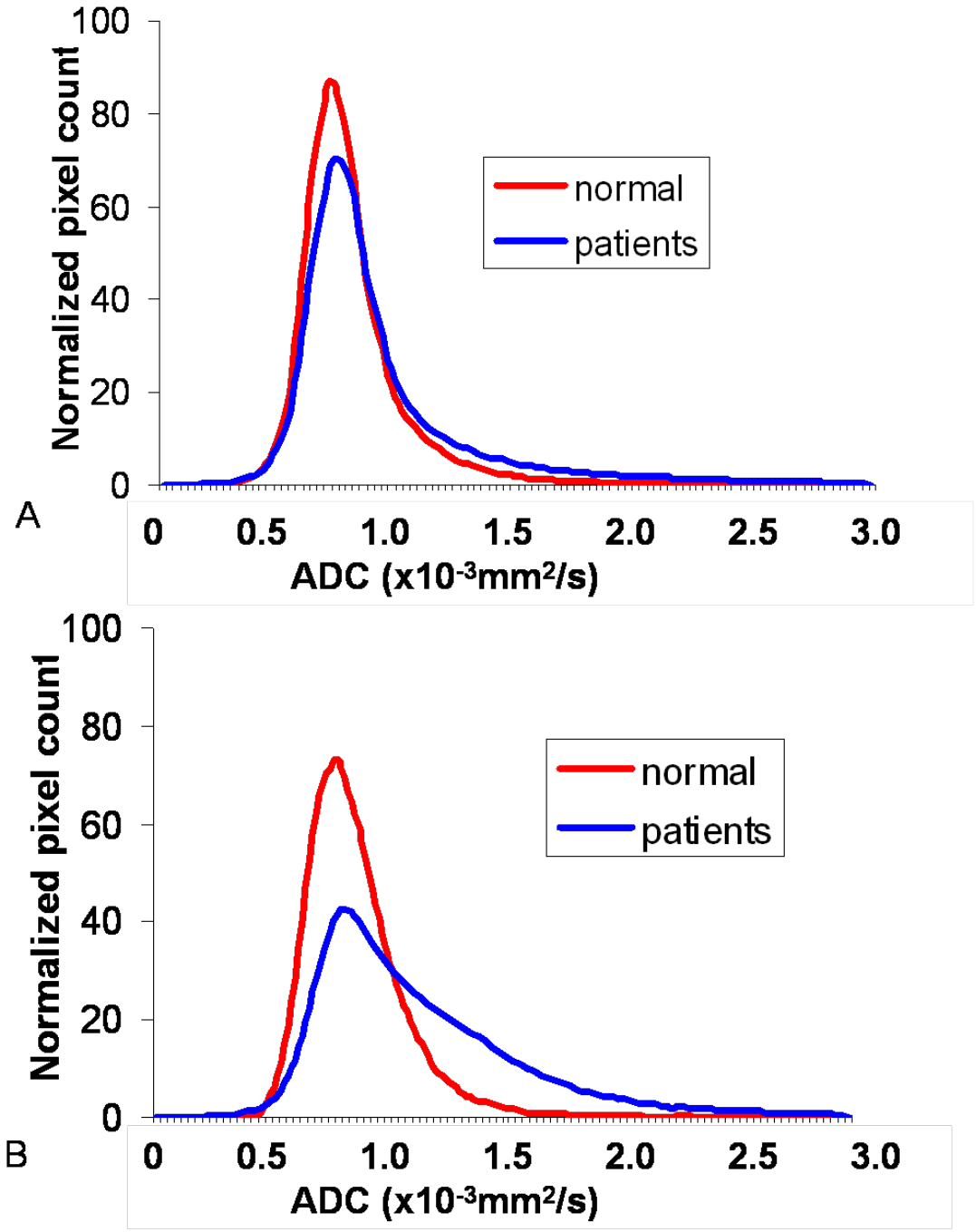

. Fig 2.1: Examples of histograms: (A) Average mean whole brain histograms across all patients (blue) and all controls (red) and (B) average mean grey matter histograms in all symptomatic patients (blue) and controls (red) demonstrating right-ward shift of the histogram.

To assess intraobserver variability, the ROI analysis in all 6 regions was repeated for 4 patient data-sets in 2 sessions separated by 10 days. Bland-Altman analysis demonstrated a mean difference of -5.1 mm^2/s, (95% CI = -13.75 to 3.55), p=0.235. To assess interobserver variability, a second observer placed ROIs on the same four patients and Bland-Altman analysis demonstrated a mean difference of 3.81 mm^2/s, (95% CI = -5.47 to 13.08), p=0.40. See Appendix H.

2.2.4 Statistical analysis

2.2.4.1 Age effects on ADC measures and NBV

I performed a preliminary Spearman rank bivariate correlation analysis across all the subjects (patients and controls) considering age and disease duration versus NBV and all the ADC measures, these comprising for the ROIs: mean right head of caudate (RC) ADC, mean left head of caudate (LC) ADC, mean right putamen (RP) ADC, mean left putamen (LP) ADC, mean right pulvinar (RPu) ADC, mean left pulvinar (LPu) ADC, and for the WB and GM histograms the peak height (PH), peak location (PL), mean ADC and ADC value of the 25^{th}, 50^{th} and 75^{th} percentiles.

2.2.4.2 Comparison of ADC measures between control and patient groups

Differences in the central tendencies of the ADC measures between healthy control subjects, asymptomatic gene positive and symptomatic patients with inhPrD were evaluated with the Kruskal-Wallis test with post-hoc tests.

Patients were considered symptomatic if they or a close informant complained of clinical and neuropsychiatric symptoms. Individuals were considered asymptomatic at risk if tested positive for *PRNP* mutation but they or a close informant did not report any clinical or neuropsychiatric symptoms and a clinician thought that they were not affected on the basis of the clinical examination.

2.2.4.3 Relationships between MRI measures and disease severity

The relationship between MRI measures and clinical scores were assessed across the whole patient group (symptomatic and asymptomatic patients) in 3 stages. Initially, Spearman rank correlation was used to explore the relationship between each clinical score and each MRI variable. To adjust for multiple comparisons, the significance value was set at $p<0.01$ for each test. I then assessed correlations between each clinical score and each MRI variable by fitting standard normal linear regression models, with

outcome the baseline clinical score, considering WB, GM, RC, LC, RP, LP, RPu and LPu mean ADC and NBV one at a time in a univariate analysis. Finally, any factors which reached the significance level of $p<0.05$ were jointly considered in a multivariate model with outcome measure clinical score. The aim of this model was to identify which of the MRI variables were independent predictors of clinical score as opposed to potential confounders. All of the predictor variables in the univariate and multivariate model were rank transformed to avoid violations of the assumption of a linear relationship.

The statistical methods were performed with advice from Dr Sarah Walker, Reader in Statistics and Head of Statistics at the MRC Clinical Trials Unit. With such small numbers, non-parametric test were used for initial exploration of the data, followed by rank transformation to enable the linear regression analyses. Strict corrections were not used for the multiple comparisons as it was felt that clinical scores and many of the ADC histogram parameters were highly related. As a result, a Bonferroni correction would have been too conservative, rather, it was better to present the data showing the effect size in the linear regression analyses.

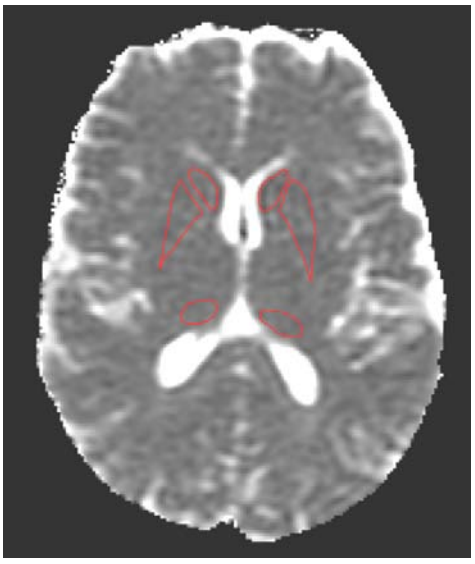

Figure 2.2: ADC map demonstrating positions of the caudate, putamen and pulvinar ROIs bilaterally.

2.3 Results

2.3.1 Clinical Findings

PRNP genotyping revealed the following mutations in the patient group: 6OPRI, n=9; P102L, n=7; D178N, n=2; 5OPRI, n=2; A117V, n=2; Q212P, n=1; E200K, n=1; Y163X; n=1. Nineteen of the patients were symptomatic at baseline with mean disease duration at the time of MRI scan of 43.94 months (range 3-138 months). Six patients with mutations in the *PRNP* gene were asymptomatic at the time of the MRI examination.

2.3.2 MRI findings

Good quality images were obtained in all patients. Motion artefacts or changes in head position between the b0 and b1000 images hindered the segmentation of grey matter in 2 symptomatic patients. However, in these patients, it remained possible to segment the CSF and therefore calculate the WB ADC histograms.

2.3.3 Conventional MRI appearances

On initial assessment, there were discrepancies in 2 patients where one observer noted signal change in the frontal cortex in one patient and another observer noted signal change in the peri-habenular region in another patient (kappa score 0.835). On consensus review of these cases, no evidence of pathological signal change in any of the areas: caudate, putamen, thalamus, frontal parietal, temporal and occipital cortex was demonstrated.

2.3.4 Age effects on ADC parameters and NBV

There was no significant correlation between age or disease duration (for symptomatic patients only) and any of the MRI variables.

2.3.5 Comparison of ADC measures between control and patient groups

Table 1 lists the mean age, MMSE, ADC measures for healthy control subjects and symptomatic patients with inhPrD. Bilateral ROI ADCs were considered as separate parameters, since a Wilcoxon test revealed a significant right ROI versus left ROI difference for the putamen (p=0.002) and pulvinar (p=0.009) ROIs in the patient

Table 2.1: Mean baseline ADC parameters in symptomatic patients, asymptomatic gene positive subjects and healthy control subjects.

Index	A: Healthy control subjects (n=7)	B: Asymptomatic gene-positive (n=6)	C: Symptomatic patients (n=19)	*P* value#
Age (years)	54.14 (6.69)	39.67 (4.84)	43.26 (8.06)	<0.01*
MMSE	29.7 (0.49)	29.5 (0.74)	20.7 (6.60)	<0.01
WB mean ADC x10^{-3} (mm^2/s)	0.89 (0.03)	0.87 (0.02)	0.96 (0.08)	<0.01*
WB PH	0.84 (0.09)	0.88 (0.07)	0.73 (0.13)	0.02
WB PL (x$10^{-3}mm^2$/s)	0.71 (0.02)	0.71 (0.02)	0.73 (0.04)	0.07
WB p25 (x$10^{-3}mm^2$/s)	0.66 (0.02)	0.65 (0.02)	0.69 (0.04)	0.02
WB p50 (x$10^{-3}mm^2$/s)	0.75 (0.02)	0.74 (0.02)	0.81 (0.06)	<0.01*
WB p75 (x$10^{-3}mm^2$/s)	0.89 (0.04)	0.88 (0.03)	0.10 (0.12)	0.01
GM mean ADC (x$10^{-3}mm^2$/s)	0.91 (0.09)	0.87 (0.06)	1.09 (0.26)	<0.01*
GM PH (x$10^{-3}mm^2$/s)	0.78 (0.14)	0.95 (0.15)	0.68 (0.20)	0.29
GM PL (x$10^{-3}mm^2$/s)	0.78 (0.06)	0.78 (0.04)	0.94 (0.26)	0.02
GM p25(x$10^{-3}mm^2$/s)	0.72 (0.06)	0.72 (0.04)	0.86 (0.21)	0.02
GM p50(x$10^{-3}mm^2$/s)	0.83 (0.08)	0.80 (0.06)	0.99 (0.25)	0.03
GM p75(x$10^{-3}mm^2$/s)	0.96 (0.11)	0.90 (0.07)	1.16 (0.31)	0.04
RC mean ADC (x$10^{-3}mm^2$/s)	0.71 (0.05)	0.72 (0.05)	0.74 (0.05)	0.37
LC mean ADC (x$10^{-3}mm^2$/s)	0.74 (0.03)	0.69 (0.04)	0.75 (0.07)	0.06
RP mean ADC (x$10^{-3}mm^2$/s)	0.74 (0.02)	0.73 (0.02)	0.75 (0.04)	0.31
LP mean ADC (x$10^{-3}mm^2$/s)	0.73 (0.05)	0.71 (0.02)	0.73 (0.03)	0.45
RPu mean ADC (x$10^{-3}mm^2$/s)	0.79 (0.05)	0.76 (0.03)	0.83 (0.06)	0.02
LPu mean ADC (x$10^{-3}mm^2$/s)	0.78 (0.04)	0.73 (0.02)	0.80 (0.05)	0.02

Note. All values are mean (standard deviation).

WB = whole brain histogram, GM = grey matter histogram, RC = right caudate ROI, LC = left caudate ROI, RP = right putamen ROI, LP = left putamen ROI, RPu = Right pulvinar ROI, LPu = Left pulvinar ROI, PH = Peak Height, PL = Peak Location, p25 = 25^{th} percentile, p50 = 50^{th} percentile, p75 = 75^{th} percentile.

#Kruskal-Wallis test

*post-hoc tests:
Age: A versus B (p=0.002), A versus C (p=0.004), B versus C (p=0.366)
WB mean: A versus B (p=0.445), A versus C (p=0.006), B versus C (p=0.004)
WB p50: A versus B (p=0.731), A versus C (p=0.008), B versus C (p=0.005)
GM mean: A versus B (p=0.731), A versus C (p=0.024), B versus C (p=0.002)

group. Mean age and MMSE were higher in the healthy control subjects than the symptomatic patients. For the WB and GM tissue fractions, the ADC histograms were shifted towards higher values in the symptomatic patient group compared to the healthy control subjects (Figure 2.1A and B). The most significant differences between groups were for the WB mean ADC (p=0.006) and WB median ADC (p=0.008). There were also significant differences between patient groups for GM mean ADC (p=0.024) and GM p25 ADC (p=0.019). For the ROIs, although there was a trend for higher mean ADCs in the symptomatic patient group compared to the healthy control subjects, differences in the individual ROI mean ADCs did not reach significance.
There were no significant differences in any of the MRI measures comparing the healthy control subjects and the asymptomatic gene positive subjects with inhPrD.

2.3.6 Relationships between MRI measures and disease severity

I found a number of significant associations suggesting increases in ADC, and a decrease in NBV, with increasing disease severity. Table 2.2 provides a synopsis of the correlations observed. All the GM histogram parameters correlated with MMSE, ADL, ADAS-COG, CDR and CGIS. The strongest associations were between GM mean ADC and MMSE ($p<0.0001$) (Fig 2.3A), ADAS-COG ($p<0.0001$), CDR ($p<0.0001$) (Fig 2.3B) and CGIS ($p<0.0001$). All the WB histogram parameters correlated with MMSE and less strongly with ADAS-COG and CDR. The strongest association was between mean WB ADC and MMSE (p=0.006). NBV was strongly associated with MMSE (p=0.001) (Fig 2.3C) and CDR (p=0.001)
For the ROI analysis, mean ADCs also increased with disease severity. The strongest associations were between RPu mean ADC and ADAS-COG ($p<0.0001$), MMSE (p=0.001) and CGIS (p=0.001) but the LPu mean ADC correlated most strongly with CGIS (p=0.003) and less strongly with MMSE (p=0.032). Figure 2.4 demonstrates the association between global severity score and pulvinar mean ADC. The other ROI mean ADCs correlated with some of the clinical scores but only weakly and inconsistently except the left head of caudate mean ROI which correlated with MMSE (p=0.008).

Table 2.2: Synopsis of Spearman Rank Correlations between Clinical Scores and MRI measures.

MRI measures	MMSE	Barthel	ADAS-COG	CDR	CGIS	Rankin	BPRS
WB mean ADC ($x10^{-3}mm^2/s$)	**-0.541**	-0.198	0.433	**0.565**	0.399	0.432	0.151
WB PH	0.511	0.267	-0.415	**-0.582**	-0.408	-0.466	-0.209
WB PL ($x10^{-3}mm^2/s$)	-0.328	-0.059	-0.013	0.322	0.215	0.314	0.042
WB p25 ($x10^{-3}mm^2/s$)	-0.462	-0.156	0.276	**0.517**	0.457	0.424	0.144
WB p50 ($x10^{-3}mm^2/s$)	**-0.539**	-0.274	0.336	**0.587**	0.474	0.516	0.177
WB p75 ($x10^{-3}mm^2/s$)	-0.506	-0.180	0.434	**0.529**	0.353	0.390	0.132
GM mean ADC ($x10^{-3}mm^2/s$)	**-0.767**	**-0.610**	**0.757**	**0.832**	**0.682**	**0.608**	0.149
GM PH	**0.583**	**0.545**	**-0.586**	**-0.751**	**-0.567**	**-0.576**	-0.015
GM PL ($x10^{-3}mm^2/s$)	-0.544	-0.332	0.513	0.526	0.389	0.351	0.063
GM p25($x10^{-3}mm^2/s$)	**-0.654**	-0.483	**0.671**	**0.652**	**0.564**	0.458	0.130
GM p50($x10^{-3}mm^2/s$)	**-0.677**	**-0.570**	**0.679**	**0.765**	**0.642**	**0.576**	0.081
GM p75($x10^{-3}mm^2/s$)	**-0.709**	**-0.584**	**0.717**	**0.804**	**0.660**	**0.615**	0.112
RC mean ADC ($x10^{-3}mm^2/s$)	-0.405	-0.054	0.250	0.157	0.085	0.146	-0.245
LC mean ADC ($x10^{-3}mm^2/s$)	**-0.531**	-0.283	0.420	0.443	0.469	0.260	0.274
RP mean ADC ($x10^{-3}mm^2/s$)	-0.376	-0.155	0.404	0.253	0.244	0.049	-0.037
LP mean ADC ($x10^{-3}mm^2/s$)	-0.026	0.136	-0.006	-0.107	-0.017	0.041	0.021
RPu mean ADC ($x10^{-3}mm^2/s$)	**-0.625**	-0.368	**0.713**	0.504	**0.615**	0.338	0.316
LPu mean ADC ($x10^{-3}mm^2/s$)	-0.439	-0.544	0.421	0.501	**0.575**	**0.526**	**0.527**
NBV (mL)	**0.646**	0.284	-0.480	**-0.622**	-0.488	-0.511	0.316

Note. p<0.01 are in bold. WB = whole brain histogram, GM = grey matter histogram, RC = right caudate ROI, LC = left caudate ROI, RP = right putamen ROI, LP = left putamen ROI, RPu = Right pulvinar ROI, LPu = Left pulvinar ROI, PH = Peak Height, PL = Peak Location, p25 = 25^{th} percentile, p50 = 50^{th} percentile, p75 = 75^{th} percentile, NBV = normalized brain volume, MMSE = Mini Mental State Examination, ADL = Barthel Activities of Daily Living scale, ADAS-COG = Alzheimer's Disease Assessment Scale, CDR = Clinician's Dementia Rating Scale, CGIS = A Clinician's Global Impression of Disease Severity, Rankin = Rankin scale, BPRS = Brief Psychiatric Rating Scale.

A

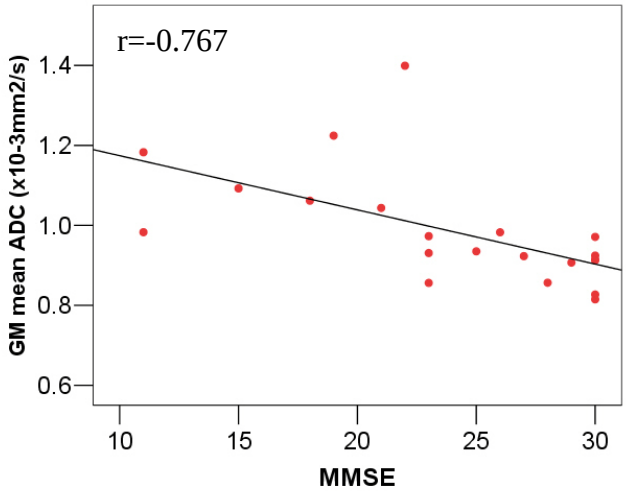

B

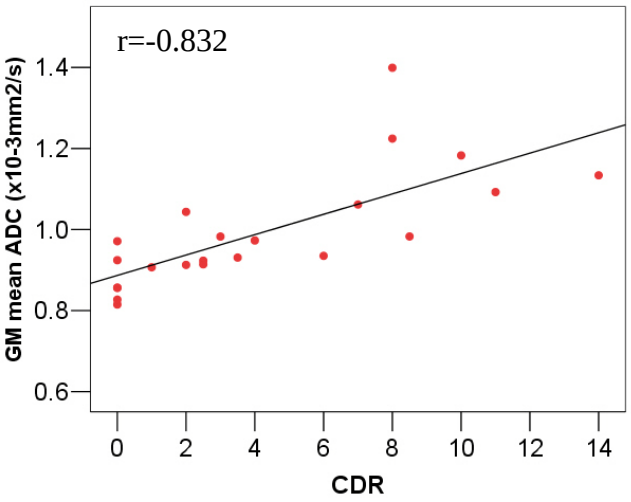

C

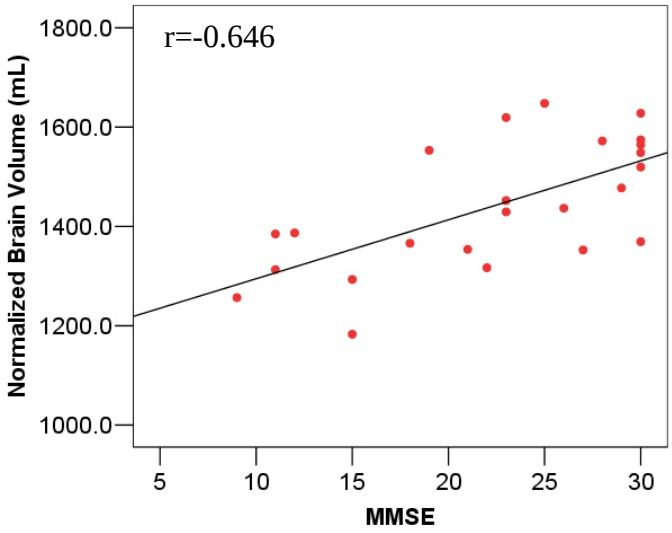

Fig 2.3: Scatter plots of (A) Grey Matter mean ADC and MMSE, (B) Grey Matter mean ADC and CDR, (C) Whole Brain mean ADC and MMSE.

A

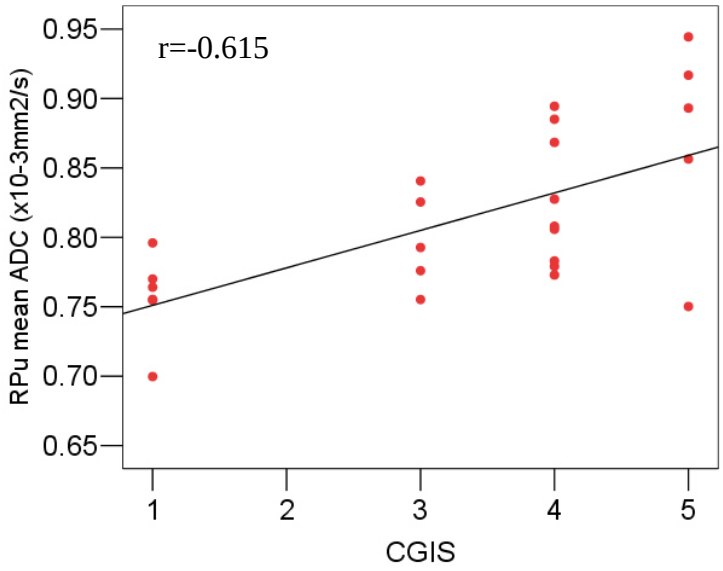

B

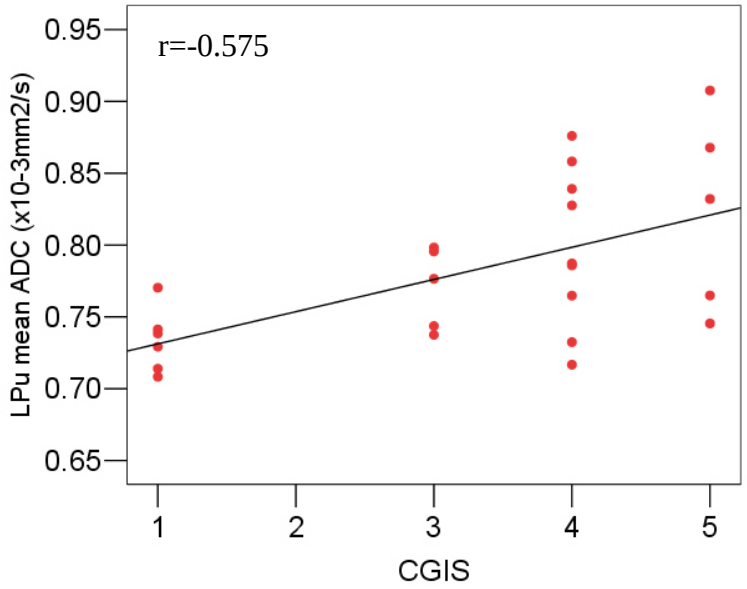

Fig 2.4: Scatter plots of (A) Right and (B) Left pulvinar ROI mean ADC and CGIS.

Using a stepwise multivariate regression procedure with each clinical score as the dependent variable and each of the MRI variables that correlated significantly in the univariate analysis as the independent predictors, GM mean ADC was an independent predictor of CDR (p=0.001), Rankin (p=0.02), ADL (p=0.009). Right pulvinar mean ADC was an independent predictor of ADAS-COG (p=0.001) and CGIS (p=0.001).

2.4 Discussion

This study quantifies cerebral ADC in a cohort of patients with inhPrD. I have demonstrated significantly higher WB and GM mean ADCs in a symptomatic patient population compared to a healthy control group. ADC measures from both the WB and GM tissue fractions, and pulvinar ROIs correlated positively with disease severity and NBV decreased with disease severity. The ADCs obtained in the basal ganglia and WB for our control group are consistent with those reported previously [153-155]. Although no significant differences between asymptomatic patients with inhPrD and the control group were demonstrated for any MRI measure, such changes cannot be excluded given the small number of asymptomatic subjects included in the study and the slightly higher mean age of our control group. Our results suggest that quantitative DWI can detect tissue damage associated with inhPrD as increased mean ADC in the whole brain, grey matter and pulvinar region.

The negative correlation between NBV and disease severity supports the observation that progressive cerebral atrophy is a feature of inhPrD [156;157]. It is known that partial-volume edge-effects can influence segmented brain tissue-fraction diffusion histogram measures [158] and it is a concern that cerebral atrophy may modulate this effect, and thus indirectly contribute to observed changes in the histogram metrics. I attempted to minimize partial-volume effects in this study by applying a single morphological erosion operation to both the whole brain and grey matter ADC masks. However, since in the univariate analysis, the GM ADC measures provided stronger correlations with clinical scores than NBV, and that the stepwise multivariate analysis suggested that NBV did not contribute additional predictive power to the linear model, I believe that cerebral ADC, and in particular GM ADC histogram metrics, provide a highly sensitive index of pathology in inhPrD, essentially independent of, although possibly complementary to, quantifiable changes in brain volume.

Several recent reports have established DWI as the most sensitive sequence for the diagnosis of prion diseases, particularly sCJD [26;30;72;135]. However, thus far few studies have addressed quantitative cerebral ADC measurement in prion diseases. Only three studies have attempted to quantify cerebral ADCs in inhPrD, two of which have been in patients with the E200K mutation which is pathologically similar to classical MM1 sCJD. In one study, values in the basal ganglia in 4 symptomatic patients with the E200K mutation were lower in the putamen and caudate compared to controls [83].

However, voxel-wise SPM analysis demonstrated increased ADC in multiple cortical and cerebellar regions where no SI changes could be detected on DWI. In a larger study including asymptomatic gene positive subjects and symptomatic patients with the E200K mutation, decreased ADC was seen in thalamo-striatal regions before symptom onset [159]. However, in another study *increased* ADC values were noted in the thalamus, in a patient with the D178N mutation, corresponding to increased thalamic gliosis on pathological examination [137]. These findings suggest that cerebral water diffusivity changes may vary according to anatomical location, perhaps reflecting anatomical patterns in the severity of histopathological changes.

In other neurodegenerative disorders, whole brain or regional ADC values are usually increased in association with clinical or subclinical disease, consistent with our findings. Whole brain and caudate ADCs in patients with Huntingdon disease are increased and rise with disease progression [160]. In patients with amnestic mild cognitive impairment or AD whole brain and hippocampal ADCs have been shown to be higher than in controls [118] and higher hippocampal baseline diffusivity is associated with a greater risk of progression from mild cognitive impairment to AD [102].

It has been reported that DWI derived ADC measurements inversely correlate with histopathological assessment of cellular density in tumours [161;162]. Increase in ADC measurements can be seen in in tumours after treatment [163], thought to reflect a decrease in tumour cellularity after necrosis, cell death and microcyst formation. Similarly, the increase in diffusivity in neurodegenerative diseases is thought to be associated with loss of neuron cell bodies, synapses and dendrites which cause an expansion of the extracellular space [102].

The hallmark of all forms of inhPrD is spongiform degeneration of neurones and their processes, neuronal loss and intense reactive astrocytosis [164]. Histopathological changes are found in the cerebral neocortex, the subiculum of the hippocampus, putamen, caudate nucleus, thalamus and the molecular layer of the cerebral cortex [164]. The stronger association of the global ADC measures, particularly the grey matter mean ADC with disease severity reflect the diffuse nature and anatomical distribution of histopathological change seen in prion disease.

There is considerable variability of pathological appearance within a patient, between patients with the same genotype and between different genotypes in inhPrD. The histopathology also changes with the stage of the disease. In an animal model of scrapie, complete loss of neurons in the terminal stages of disease also resulted in a reduction in spongiosis due to loss of the cells exhibiting vacuoles [165]. Our findings of increased ADC measurements with disease severity may reflect these histopathological changes at the terminal stages of the disease: a combination of decreased spongiosis, increased neuronal loss and increased gliosis.

Quantitative MRI studies are susceptible to a number of potential sources of error and measurement limitations. Although masks for the white matter were obtained, these were not used to calculate white matter histograms. Using the essentially T2W b0 image to segment the CSF and grey matter, some of the basal ganglia structures were consistently mis-classified into the white matter mask. The recent development of more sophisticated segmentation approaches may allow the future unambiguous interrogation of the cerebral WM tissue fraction in this disease. In addition, delineation of small ROIs manually may increase measurement error and could account for our failure to correlate ADC signal change in the caudate and putamen with disease severity.

It is also possible that the changes in ADC observed were influenced to an unknown extent by the effects of the drug Quinacrine. Although I demonstrated clear associations between disease severity and ADC measures, it is possible that an as yet unspecified interaction of the drug Quinacrine with water diffusivity may have influenced our results. It will be necessary to confirm in a larger cohort of affected patients who are not undergoing treatment that cerebral ADC changes detected do indeed reflect the disease process. Full reports regarding the safety and therapeutic efficacy of Quinacrine in inhPrD will be the subject of future communications.

Conventional MRI findings in inhPrD report cortical atrophy, cerebellar atrophy or increased T2 signal in the basal ganglia [156;166;167]. Some inhPrD cases show hyperintensity in the basal ganglia and fronto-parietal cortices, similar to sCJD [168]. In the EUROCJD experience with data on 23 specified *PRNP* mutations, MRI scans were only positive in 50% of E200K mutations, 30% of GSS and 18% of FFI cases [43]. In our study, conventional MRI, including visual assessment of DWI, was relatively insensitive to cerebral pathology in this patient group. Despite this, I have shown that

quantification of cerebral ADC provides both regional and global measures that correlate with clinical neurological status.

The advent of potential treatments for a number of neurodegenerative diseases has increased the need to develop non-invasive and objective biomarkers of disease progression. These should be quantitative with a high test re-test reliability [134]. The demonstration that cerebral ADC values correlate with clinical measures of disease severity suggests that these techniques will be useful surrogate markers in future therapeutic trials in patients with inhPrD.

2.5 Conclusion

Whole brain and cortical grey matter mean ADCs are significantly higher in symptomatic patients with inhPrD compared to controls. Both global and regional ADC metrics correlated with disease severity and were more sensitive predictors of disease status than brain volume measurements. Global and regional ADC measures, particularly GM mean ADC correlate with clinical neurological status and show promise as quantitative pathological biomarkers in inhPrD.

3 High b-value diffusion MR imaging and basal nuclei ADC measurements in Variant and Sporadic Creutzfeldt-Jakob disease

3.1 Introduction

The diffusion-weighting factors ("*b* values") that are used in routine clinical DWI studies are usually in the order of b=1000s/mm^2. Recently higher *b* value DWI has shown increased sensitivity for detection of signal abnormality in ischaemic stroke [107;108], the grading of cerebral gliomas [169] and has been shown to improve sensitivity to white matter degeneration in AD [109]. Higher *b* values lead to a decrease in SNR but the disease detection may be facilitated by an increase in CNR [110;111]. This is partially due to the increased diffusion weighting *per se*, and additionally, high *b* value DWI offers increased sensitivity to any slower diffusion component water compartment present within the tissue.

The purpose of this chapter was to investigate whether DWI at high *b* value (b=3000s/mm^2) and ADC measurements in the basal nuclei improve the diagnosis of vCJD and sCJD compared to visual assessment of than DWI at standard *b* value (b=1000s/mm^2).

3.2 Methods

3.2.1 Patients

Eight patients with vCJD (5 male, mean age 36.1 years, range 19-76) and 9 patients with sCJD (6 male, mean age59.2, range 54-72) referred to the National Prion Clinic, National Hospital for Neurology and Neurosurgery, London, U.K. were included in this study. All patients were recruited into the MRC Prion-1 trial [133] and ethical approval for the study was given by the Eastern MREC and informed consent for participation in the study was given by either the patient or patient's next of kin. Five healthy volunteers (2 male, mean age 41.2 years, range 33 – 52) with no personal or family history of neurological disorders were also recruited and gave informed consent.

3.2.2 MRI acquisition

All subjects were examined using a clinical 1.5T MRI system (GE Healthcare, Milwaukee, WI). After scout images were obtained, axial images with slice thickness 5mm parallel to the bicommisural line from the craniovertebral junction to the vertex were acquired for T2W (TE 106ms, TR 6000ms, 2 averages, FOV 24x18cm, matrix 256x224), FLAIR (TE 161ms, TI 2473ms, TR 9897ms, one average, FOV 24 x 24cm, matrix 256 x 224) and DWI. DWI was performed using a single-shot echo-planar technique (TR 10000ms, one average, matrix 96 x 128, FOV 26x26) with diffusion-weighting factors ('b values') of 0 and 1000 s/mm^2 (TE 101ms, 1 average) and of 0 and 3000 s/mm^2 (TE 136ms, 3 averages) applied sequentially along three orthogonal axes.

Ten patients (5 with vCJD, 4 with sCJD, and 1 growth hormone-related CJD) had additional DWI with *b* values of 0 and 3000 s/mm^2 (TE 136ms, 3 averages). The DWI images obtained for each orthogonal direction were averaged to yield diffusion trace-weighted images for each slice.

3.2.3 MRI analysis

3.2.3.1 Qualitative analysis by visual inspection

Two independent consultant neuroradiologists (JS and RJ) with experience in DWI imaging performed qualitative analysis of the diffusion trace images in a non-blinded fashion.

3.2.3.1.1 Assessment of signal intensity changes on b=1000 and FLAIR images

Basal ganglia and cortical signal intensities were compared with normal grey matter and classified and hyper, iso or hypointense to grey matter.

3.2.3.1.2 Comparison of b=1000 and b=3000 DWI images

Each of the b = 1000 and b = 3000 trace-weighted images were assessed for pathological signal changes. The observers then compared the b = 1000 with the b = 3000 images side by side, and using a scoring system concluded whether the b = 3000 images were better (+1), the same as (0), or worse (-1) than the b = 1000 images for signal conspicuity. Where a discrepancy was identified, the images were re-reviewed in a consensus reading. A kappa statistic was calculated to assess the level agreement between the two independent observers for pathological signal change.

3.2.3.2 Quantitative MRI

Post-processing was performed at a dedicated work station (Sun Microsystems, Mountain View, Calif) by a single neuroradiologist. Using commercially available software (Jim Version 4.0; Xinapse Systems Ltd, Thorpe Waterville, UK.), pixel-by-pixel ADC maps were generated, from the b=0 and b=1000 trace-weighted images using the Stejskal Tanner equation [95] for ADC calculation: $ADC=-\{\ln(S1/S2)/(b1-b2)\}$, where $S1$ and $S2$ are the signal intensities of DWI with b-factors of 0 ($b1$) and 1000 ($b2$), respectively. This process was repeated for the b=0 and b=3000 trace-weighted images.

3.2.3.2.1 Measurement of signal intensity ratios on diffusion-weighted trace images

The ROIs as described above were also used to measure the MR SI of the caudate, putamen, dorsomedial thalamus and white matter from the trace-weighted images obtained with both *b* values of 1000 and b 3000 s/mm^2. Right versus left asymmetry was assessed for ADC and SI measurements in the caudate, putamen, pulvinar and dorsomedial thalamus using the paired t-test. As no significant asymmetry was detected, mean SI of the caudate (C), putamen (P), dorsomedial thalamus (DM) and pulvinar (Pu) ROIs were calculated. From these SI measurements, the SI ratios of each ROI to WM ROI were calculated.

3.2.3.2.2 Regional ADC measurements

Mean ADC in the head of the caudate nuclei, putamen and dorsomedial thalamus were determined bilaterally by manually defining regions of interest (ROIs) enclosing each anatomical region on the axial b0 image from the b=1000 dataset at the level of the genu of the internal capsule. For the vCJD cases, the ADC values in the pulvinar nucleus of the thalamus were also determined. Two control ROIs were selected in the right frontal white matter (FWM) and the superior pons (SP). The ROIs, ranging in size from 40-70mm^2, were transferred to the corresponding b=1000 ADC map (see Fig 3.1) and then to the b=3000 ADC map, and the mean ADC for each ROI was recorded. To assess intraobserver variability, the ROI analysis in all six regions was repeated for 4 patient data-sets in 2 sessions separated by 10 days. Bland-Altman analysis demonstrated a mean difference of -5.1 mm^2/s, (95% CI = -13.75 to 3.55), p=0.235. To assess interobserver variability, a second observer placed ROIs on the same four patients and Bland-Altman analysis demonstrated a mean difference of 3.81 mm^2/s, (95% CI = -5.47 to 13.08), p=0.40.

3.2.4 Statistical analysis

The paired sample *t*-test was used to compare ADC and SI ratios between the b=1000 and b=3000 images. Comparison of mean ADC in each ROI between the vCJD patients, sCJD patients and healthy volunteers were determined using a one-way ANOVA and ad-hoc multiple comparison tests with Bonferroni correction for each *b* value.

Figure 3.1: Demonstrates position of the key ROIs on (A) b0, (B) b1000 ADC map and (C) b3000 ADC map.

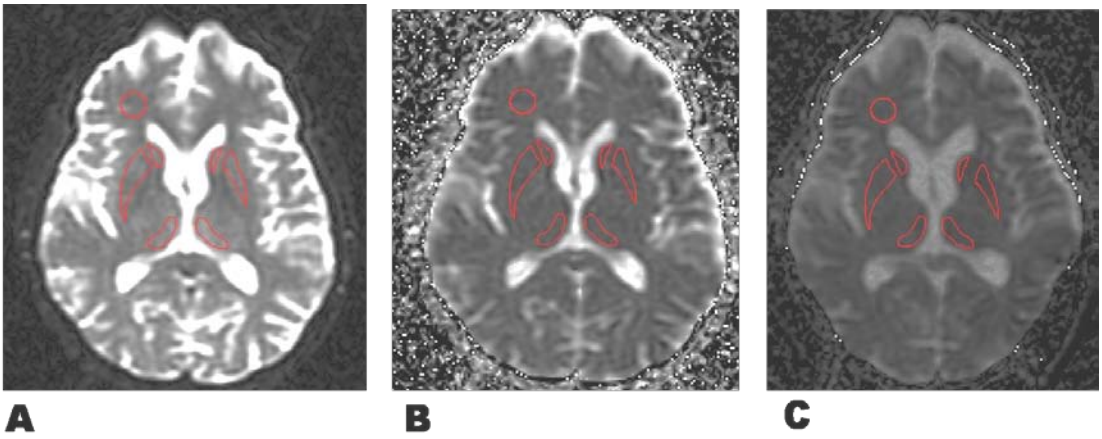

3.3 Results

3.3.1 Clinical findings

The 8 patients with vCJD (3 female, 5 male, mean age 36.1 years, range 19-76) were all confirmed by either tonsil biopsy or post-mortem examination. The mean disease duration at the time of MRI was 6.2 weeks (range 2 – 16 weeks). The 9 patients with sCJD (3 female, 6 male, mean age 59.2, range 54-72) were included in the study. The diagnosis was confirmed in all patients by post-mortem examination in eight patients and brain biopsy in one patient. The mean disease duration at the time of onset was 16.7 weeks (range 3 – 24 weeks).

3.3.2 MRI findings

3.3.2.1 Qualitative assessment

3.3.2.1.1 Visual inspection of trace –weighted and FLAIR images

All 8 vCJD patients demonstrated bilateral dorsomedial thalamic signal hyperintensity, but only 6/8 demonstrated caudate hyperintensity and 4/8 demonstrated putamen hyperintensity on FLAIR and DWI (b=1000s/mm^2). No cortical hyperintensity was visualized. See Table 3.1 for a summary of SI at b=1000s/mm^2 in vCJD and sCJD. All 9 patients with sCJD demonstrated cortical signal hyperintensity, predominantly in the cingulate cortex and occipital cortex. All 9 patients demonstrated hyperintensity in the head of caudate bilaterally but only 8/9 demonstrated hyperintensity in the putamen and 6/9 demonstrated hyperintensity in the thalami (see Table 3.1).

3.3.2.1.2 Comparison of b=1000 and b=3000 images

In the 10 patients that had both b=1000 and b=3000 sequences, I found complete agreement between the two observers that in all cases (kappa score 1.0). In 9 out of the 10 cases, signal change was more conspicuous on the higher *b* value images and in one case the higher *b* value image did not aid in assessment, possibly because there was some movement artefact. In all cases, no new areas of signal change were identified on the higher *b* value images, but increased confidence was obtained, particularly for areas which were equivocal on the b=1000 images (Fig 3.2). In particular, cortical and thalamic signal changes were more conspicuous at the higher *b* value.

Table 3.1: Visual assessment of signal intensity findings in vCJD and sCJD on FLAIR and DWI (b=1000s/mm^2).

vCJD	C	P	DM	Pu	Cx	SP	FWM
1	+	+	+	+	-	-	-
2	+	+	+	+	-	-	-
3	-	-	+	+	-	-	-
4	+	-	+	+	-	-	-
5	-	-	+	+	-	-	-
6	+	+	+	+	-	-	-
7	+	-	+	+	-	-	-
8	+	+	+	+	-	-	-

sCJD	C	P	DM	Pu	Cx	SP	FWM
1	+	+	+	+	+	-	-
2	+	+	-	-	+	-	-
3	+	+	+	+	+	-	-
4	+	+	+	+	+	-	-
5	+	+	+	+	+	-	-
6	+	+	-	-	+	-	-
7	+	-	-	-	+	-	-
8	+	+	+	+	+	-	-
9	+	+	+	+	+	-	-

Note. SP = superior-pons, C = caudate, P = putamen, DM = dorso-medial thalamus, Pu = pulvinar, FWM = right frontal white matter, Cx = cortex, + hyperintense to grey matter, - isointense to grey matter

Figure 3.2: Differences in signal intensities in the basal ganglia in sCJD at (A) b1000 and (B) b3000 and in vCJD at (C) b1000 and (D) b3000

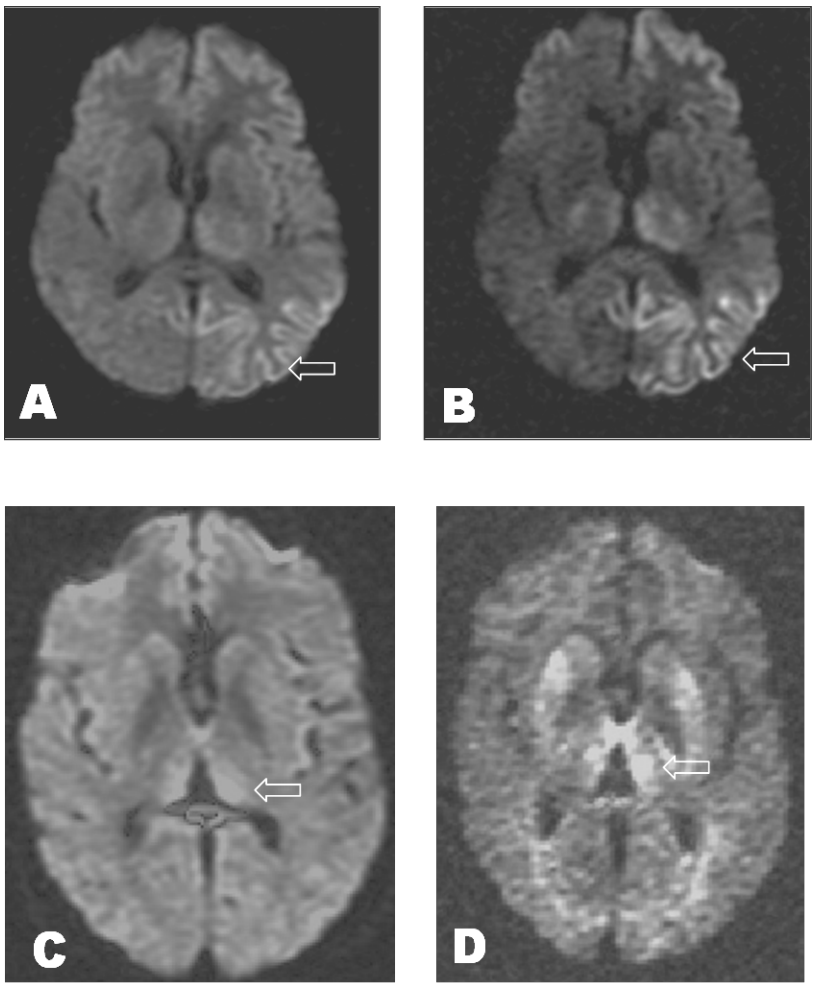

3.3.2.2 Quantitative assessment

3.3.2.2.1 Measurement of SI ratios on trace-weighted images

The SI ratios were higher in the b=3000 images when compared to b=1000, particularly in the DM ROI (1.93 ± 0.72 on b=3000 versus 1.39 ± 0.19 on b=1000, p=0.028). See Table 3.2.

Table 3.2: Summary of SI, values between the b=1000 and b=3000 images in the patients (n=10).

	SI ratio		
	b1000	b3000	*p* value
C	1.51(0.33)	1.99(1.12)	0.124
P	1.41(0.47)	2.10(1.73)	0.133
DM	1.39(0.19)	1.92(0.71)	**0.028**

Note. All data is expressed in mean values with standard deviations in brackets.

SP = superior-pons ROI, C = mean caudate ROI, P = mean putamen ROI, DM = mean dorso-medial thalamus ROI, Pu = mean pulvinar ROI, FWM = right frontal white matter ROI

3.3.2.2.2 ADC measurements

3.3.2.2.2.1 ADC measurement in vCJD

At b=1000, I found significantly higher mean ADC values in the pulvinar ROIs bilaterally in the vCJD patients when compared to healthy volunteers (mean Pu ADC = 837.6±33.0 mm^2/s in vCJD patients compared with 748.0±17.3 mm^2/s in controls, p=<0.001; Table 3.3a). The mean ADC in the dorsomedial thalamic ROIs were higher in vCJD patients when compared to controls but did not reach significance. There were no significant differences in mean ADC in the caudate, putamen and dorsomedial thalamic ROIs and there were no significant differences in the mean ADC values for the control ROIs. At b=3000, no significant differences were found for mean ADC values in any of the ROIs between vCJD patients and controls.

3.3.2.2.2.2 ADC measurements in sCJD

At b=1000, I found significantly lower mean ADC values in the caudate and putamen ROIs in sCJD patients when compared to controls (mean C ADC = 587.3 ± 84.7 mm^2/s in sCJD versus 722.7 ± 16.6 mm^2/s in controls, p=0.007; mean P ADC = 603.3 ± 98.7 mm^2/s in sCJD versus 727.8 ± 24.4 mm^2/s, p = 0.018; Table 3.3A and Fig 3.3A). There were no significant differences in ADC in the DM ROIs between sCJD compared to controls. At b=3000s/mm^2, I found significantly lower mean ADC values in the caudate and putamen but also in the DM ROIs (mean DM ADC = 485.7 ± 87.4 mm^2/s in sCJD versus 627.3 ± 13.1 mm^2/s in controls, p=0.001) (Fig 3.3B).

Figure 3.3: Bar charts demonstrating difference in ADC values between sCJD and controls at (A) b=1000s/mm^2 and (B) b=3000s/mm^2

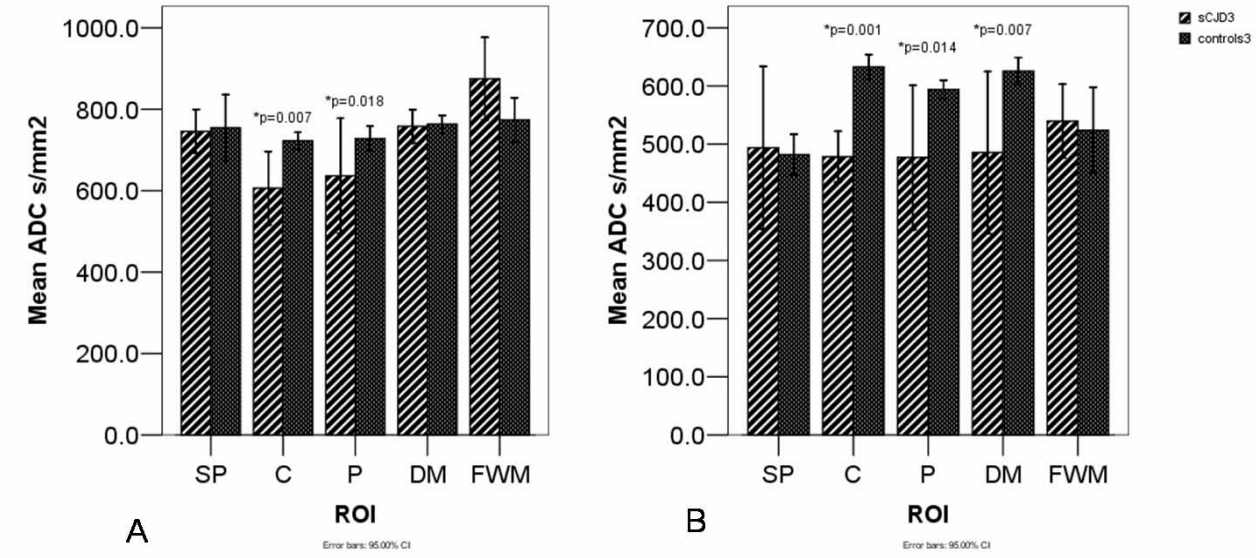

Table 3.3: Summary of mean diffusivity values (in mm^2/s) measured in vCJD patients, sCJD patients and controls for each ROI at (a) b=1000 s/mm^2 and (b) b=3000 s/mm^2 with *P*-values from *post hoc* comparisons.

(a) b = 1000 s/mm^2 (group averages for 8 vCJD and 9 sCJD patients)

Group	*SP*	*C*	*P*	*DM*	*Pu*	*FWM*
(A)vCJD	741.6(104.0)	687.9(70.6)	670.9(56.2)	834.1(51.3)	837.6(33.0)	820.7(44.6)
(B)sCJD	753.8(44.3)	587.3(84.6)	603.3(98.7)	691.8(85.7)	-	830.9(89.1)
(C)control	754.8(64.9)	722.7(16.6)	727.8(24.4)	763.7(17.1)	748.0(17.4)	773.7(43.7)
A versus C	P=0.949	P=0.655	P=0.382	P=0.159	**P<0.001**	P=0.450
A versus B	P=0.941	P=0.021	P=0.167	**P=0.001**	-	P=0.947
B versus C	P=1.000	**P=0.007**	**P=0.018**	P=0.137	-	P=0.299

(b) b = 3000 s/mm^2(group averages for 4 vCJD and 5 sCJD patients)

Group	*SP*	*C*	*P*	*DM*	*Pu*	*FWM*
(A)vCJD	524.5(87.7)	554.8(69.4)	530.3(49.7)	584.7(48.1)	603.2(59.0)	556.6(23.7)
(B)sCJD	493.9(87.9)	478.4(27.5)	477.1(77.8)	485.8(87.4)	-	539.5(39.9)
(C)control	484.1(19.9)	628.3(15.4)	594.8(8.8)	627.3(13.1)	625.4(10.6)	528.3(41.4)
A versus C	P=0.652	P=0.063	P=0.156	P=0.460	P=0.432	P=0.444
A versus B	P=0.800	P=0.068	P=0.302	P=0.050	-	P=0.759
B versus C	P=0.977	**P=0.001**	**P=0.014**	**P=0.007**	-	P=0.885

Note. All data is expressed in mean values with standard deviations in brackets.

SP = superior-pons ROI, C = mean caudate ROI, P = mean putamen ROI, DM = mean dorso-medial thalamus ROI, Pu = mean pulvinar ROI, FWM = right frontal white matter ROI

3.4 Discussion

This is, to our knowledge, the first study to investigate high *b* value DWI in prion diseases. In addition, I have compared regional ADC measurements in patients with sCJD and vCJD to those in 5 healthy volunteers and was able to show distinct patterns of the ADC changes in the two forms of prion disease.

Several recent reports have established DWI as the most sensitive sequence for the diagnosis of sCJD [26;60;72;135]. Visual inspection of the DW trace image demonstrates typically increased SI in the cerebral cortex with up to 95 per cent of cases showing hyperintensity affecting the insula, cingulate and superior frontal cortex independently of deep grey matter involvement [60]. DWI is superior to FLAIR in detecting MRI cortical signal change and this has been shown to correlate with lateralised clinical and EEG abnormalities [170]. It is suggested that the anatomical distribution of abnormal hyperintensity affecting the basal ganglia is influenced by *PRNP* genotype and PrP^{Sc} strain type [171;172]. However, using conventional *b* values, DWI signal change is not seen in all patients with sCJD [173]. I have shown that at high *b* value DWI, both cortical and basal ganglia signal changes are better detected in sCJD, thereby improving confidence in the radiological diagnosis.

Due to the reported high sensitivity of the pulvinar sign on conventional MRI for the diagnosis of vCJD [36], very few studies have investigated DWI in vCJD. DWI is less motion sensitive due to their rapid acquisition time, and pulvinar signal change may be more easily detected on DWI images in a restless patient [174]. In vCJD, I also found pathological signal change to be more conspicuous on high *b* value images. Using frontal white matter as reference, I found higher SI ratios at the higher *b* values, particularly in the thalamus. This is likely to have contributed to the improved detection of signal change by our observers.

High *b* value diffusion-weighted imaging could be very useful for the radiological diagnosis of sCJD and vCJD where SI changes are equivocal on the low *b* value DWI images. As therapies are being developed, the early identification of vCJD and sCJD cases is important and DWI at high *b* value may be helpful. As the pulvinar sign has also been shown to be a late feature in a blood-transfusion acquired case of vCJD [3], it remains to be seen whether high *b* value DWI would allows earlier detection of this sign in patients at risk from this disease.

There have been a small number of reports on ADC measurements in sCJD [78;89;136] and there have been only two case reports describing ADC measurements in vCJD [174;175]. Although abnormal areas appear bright on trace-weighted images in both sCJD and vCJD, I found distinct differences in the ADC values of the affected areas: the ADC was reduced in sCJD but elevated in the thalamus in vCJD, when compared to normal volunteers. Reduced ADC measurements in the caudate, putamen and thalamus in sCJD are in concordance with previous reports [78;135]. Tschampa *et al* found decreased ADC measurements before signal change was detected in the thalamus in sCJD, suggesting that ADC measurements could be more sensitive than visual DWI inspection to pathology in this disease [78]. Two studies addressed longitudinal measurements of ADC in sCJD [78;135]: whereas Murata *et al* found persistence of reduced ADC values in the corpus striatum for over two weeks, Tschampa *et al* detected an increase in ADC values with time and suggested that ADC may vary according to the stage of disease [78].

The precise histopathological correlates for the decreased ADC are not yet known. The histological hallmarks of CJD are spongiosis, neuronal loss and gliosis. It is likely that the proportion of these histological changes that are present in the target tissue determines the ADC. Severe spongiform change with areas of confluent vacuolation, restricting the extracellular space, has been advocated as potential cause of decreased ADC [85;88;135;176]. In a single case report, Russman *et al* found a reduction of ADC in all regions with spongiform alterations but no correlation between the histological degree of spongiform alterations and the decrease in the ADC [89]. Another study claimed that DWI signal change correlated with accumulation of the abnormal prion protein PrP^{Sc} [177] and in a further study of 10 patients, decreases in ADC correlated with increased spongiosis, gliosis and abnormal prion protein deposition in the cortex but not deep grey nuclei of patients with sCJD [88].

In our eight patients with vCJD I found increased ADC in the pulvinar which is in concordance with the two previous case reports using ADC measurements [174;175]. As in these case reports I also found a slightly decreased ADC in the caudate and putamen, compared to volunteers, but this did not reach statistical significance.

In some cases the clinical presentation and radiological findings are very similar in vCJD and sCJD. In our study, the thalamus was the only anatomical region where I found a significant difference in ADC between sCJD and vCJD. It is possible that

thalamic ADC measurements may be used to differentiate vCJD from sCJD in cases where the radiological findings are similar.

From our ADC measurements I conclude that the pulvinar high SI seen on DWI trace images in vCJD is due to T2 prolongation rather than restricted diffusion. The T2 prolongation of the tissue appears to be made more conspicuous by the longer echo time at the higher *b* value. It is believed that the histopathological substrate of the pulvinar sign is astrocytosis [37]. It is therefore likely that the increased T2 and increased diffusivity noted in the pulvinar is due to reactive astrocytosis. Spongiform change is also seen in the pulvinar but the changes are much less pronounced as in the caudate and putamen [37].

At higher *b* values the changes in ADC measurements were more pronounced for sCJD and less pronounced for vCJD. Compared to normal brains I found more significant ADC differences, in sCJD at b =3000, but not in vCJD. As the *b* value increases, a progressive change in visual contrast between brain regions is noticed with reversal of the grey-white matter and an overall decrease in ADC [109;111;178]. At high *b* values, the decrease in ADC cannot be adequately explained by monoexponential diffusion in tissues and it has been suggested that there are fast and slow components of diffusion in the random motion of water molecules in brain tissues [105;179]. Niendorf *et al* suggest that at low *b* value, DWI signal is dominated by the fast component and at high *b* value the DWI signal is dominated by the slow component. Our results demonstrate that heavier weighting on the slow component at higher *b* value is more sensitive to pathology in sCJD. Measurements of ADC based on high *b* value imaging appear to be more specific to the histopathological changes that occur in vCJD and sCJD.

3.5 Conclusion

I have shown that at high *b* values, signal change is better detected, improving confidence in the radiological diagnosis of human prion disease. I have demonstrated anatomically specific ADC changes in human prion disease compared to the normal brain and have demonstrated different patterns in the ADC measurements between sCJD and vCJD, reflecting the regional variation in the underlying pathology.

4. Short TE ^{1}H-MRS as a biomarker in prion disease

4.1 Introduction

Single and multi-voxel ^{1}H-MRS at short and long TEs has previously been performed in patients with all forms of human prion disease at single time points. The findings are that of a decrease in the NAA/Cr peak area ratio, a marker of neuronal loss, in diseased patients when compared to healthy volunteers at various anatomical locations, including the basal ganglia, thalami, and cerebellar vermis [83;180-186]. ^{1}H-MRS at short TE permits detection of cerebral MI, postulated to be a glial marker [112], in addition to other metabolites In all three studies, an elevation of MI was observed: in the pulvinar in a case of vCJD [180]and in the caudate, thalamus and frontal white matter in both asymptomatic and symptomatic cases of inhPrD with the P102L mutation [186] and in the thalamus in sCJD [187].

The purpose of the work described in this chapter was to i) determine short TE ^{1}H-MRS cerebral metabolite concentrations and metabolite ratios in inhPrD and to correlate these with clinical scores to investigate cross-sectional relationships with disease severity and ii) to investigate longitudinal changes in these metabolites which may provide potential biomarkers of disease progression.

4.2 Methods

4.2.1 Subjects

Seven patients (3 male, 4 female, range 32- 58 years, mean 43.1 years) were included in the study. All patients were being followed in the MRC Prion-1 trial [133] and ethical approval for the study was given by the Eastern MREC and informed consent for inclusion in the study and ^{1}H-MRS under general anaesthesia (GA) was given by either the patient or the patient's next of kin. Five healthy volunteers (3 female, 2 male; mean age 42.6 years; range 33 – 52 years), with no personal or family history of neurological disorders underwent scanning without GA after giving informed consent.

Patients were subjected to a structured neurological examination at 3 month intervals by a qualified neurologist. At each time point, cognitive impairment was assessed using MMSE [138], ADAS-COG) [141] and CDR [139]; functional ability was assessed using the Rankin scale [140] and ADL [142]; psychiatric impairment was assessed with the BPRS [144] ; and overall disease severity using CGIS [143]. See Appendices for A – G for examples of the score sheets used.

All patients had inhPrD as identified by *PRNP* genotyping. Five patients had a 6-octapeptide repeat insertion (6-OPRI), one a P102L mutation, and one a Y163X mutation. Mean disease duration at the time of first measurement was 65.2 months (range 24 – 146 months). Six of the patients were assessed at 3 month intervals with a mean follow up of 8.0 months (range 3-18 months). Patients 1, 2 and 4 were not taking quinacrine. Patients 3, 5, 6 and 7 were being treated with quinacrine at 300mg daily as part of the MRC PRION-1 Trial.

4.2.2 MRI and ^{1}H-MRS acquisition

Short TE, single-voxel ^{1}H-MRS was performed using an automated PRESS localisation technique with TE 35ms, TR 3000ms, number of excitations (NEX) 8, at 1.5T (GE Medical Systems, Milwaukee, WI) under GA (see Appendix I for MRI patient information sheet and Appendix J for Standard Operating Procedures under GA). A standard transmit-receive birdcage head coil was used. In all sessions, axial T2W (TE 105ms, TR 4000ms, 3 NEX) fast spin-echo (FSE) MRI images through the basal ganglia with 1.7mm slice thickness were acquired in order to plan voxel position with a neuroradiologist supervising. In all subjects a 13x15x18mm voxel (volume 3.51ml) was centred on the right head of caudate (RHC) to include the right anterior putamen

(Figure 4.1a) and a second 13x13x20mm voxel (volume 3.38ml) was centred on the right thalamus (RTH) (Fig. 4.1b).

Figure 4.1: Axial T2W fast spin-echo images demonstrating the positions of: (a) RHC voxel, (b) RTH voxel and representative spectra from (c) the RHC voxel (d) and RTH voxel in a patient with inherited prion disease (patient 6).

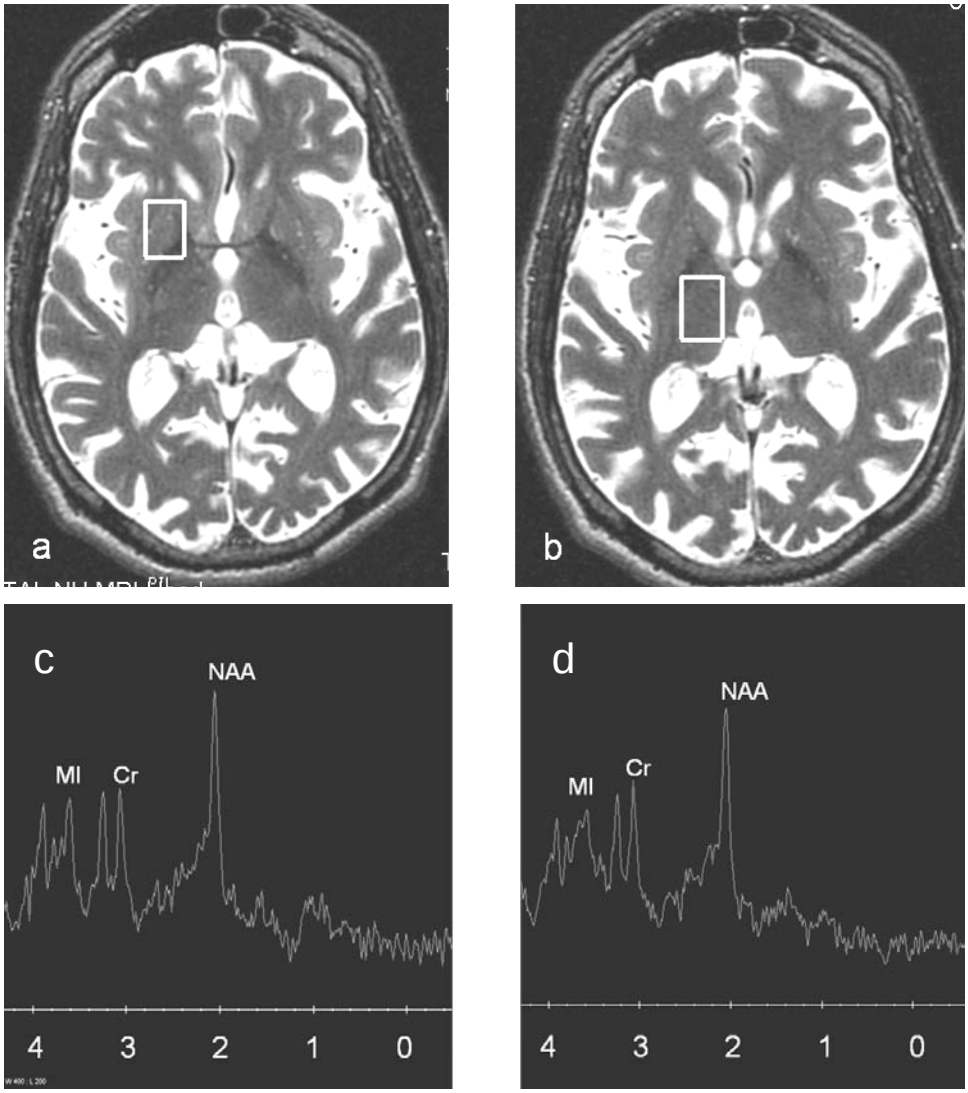

Water suppression was achieved before localization by a chemical shift selective excitation. T2W FSE (TE 110ms, TR 6000ms, 2 NEX) and FLAIR (TI 2500ms, TE 160ms, TR 10000ms, 1 NEX) images were also acquired and directionally-averaged DWI images were acquired using a single-shot echo-planar technique (diffusion-weighting (b) = 1000 s/mm^2; TE = 100ms, TR 10000ms, 3 NEX). All patients were studied under general anaesthetic to enable tolerance of the MRI protocol and were anaesthetized by administration of 50-100mg intravenous propofol. In 6/7 patients where serial examinations were performed, spectra were obtained using the same

protocol at each visit, care being taken to ensure consistency in voxel placement on follow-up scanning. For healthy volunteers spectra were acquired using the same protocol at one time point only without GA.

4.2.3 MRI analysis

4.2.3.1 Qualitative

The T2W, FLAIR and DWI images were reviewed by 2 independent consultant neuroradiologists. Pathological signal changes were assessed in the following regions: caudate, putamen, thalamus, frontal, parietal, temporal and occipital cortex. Where a discrepancy was identified, the images were re-reviewed in a consensus reading.

4.2.3.2 Quantitative

LCModel software [188] was used to estimate relative metabolite peak-areas for NAA, Cr, Cho, and MI using an LCModel basis set obtained for the TE 35ms GE PRESS sequence. As metabolite relaxation times were not measured, absolute quantification was not possible and therefore T2W metabolite levels relative to tissue-water were estimated and expressed in institutional units (IU) rather than as millimolar concentrations. The metabolite peak-area ratios NAA/Cr, Cho/Cr, MI/Cr and NAA/MI were also calculated for each voxel at each time point. All spectra were visually assessed by an independent observer and metabolite data excluded if the standard deviation for the model fit in each case were less than 15%, or the spectrum demonstrated inadequate signal-to-noise ratio or water line width. Please see Figure 4.2 for example of LCModel output.

Figure 4.2: Example of LCModel output

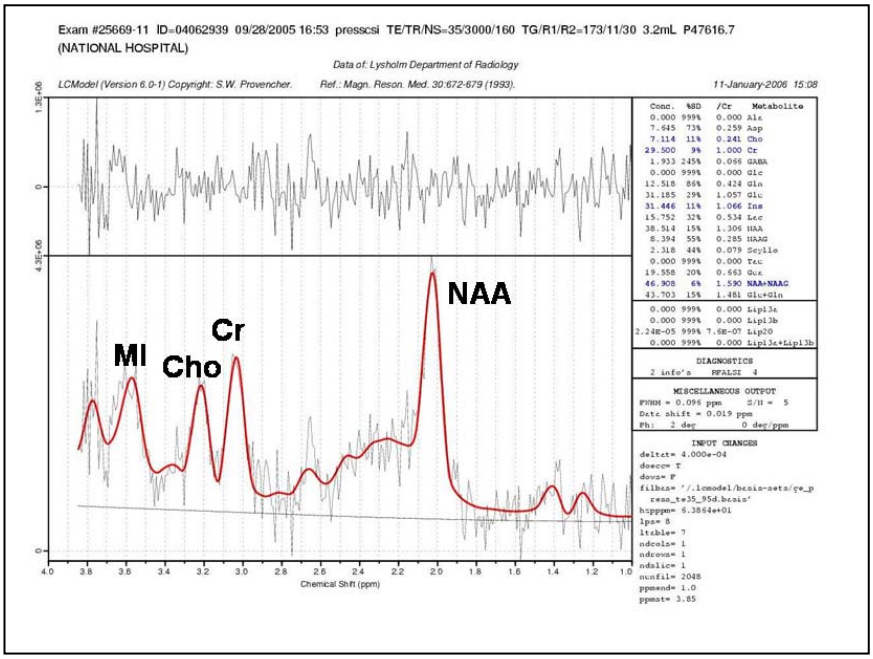

4.2.4 Statistical Analysis

Differences in the central tendencies of metabolite concentrations and metabolite ratios between the patient and healthy volunteer groups were assessed for each voxel location after logarithmic transformation using the independent *t* test. The relationship between MRS measures and disease severity at baseline were assessed using linear regression, incorporating subject age as a potential confound. Pair-wise comparisons of the metabolite concentrations and metabolite ratios at baseline, 3 months, 6 months and 9 months were performed using the paired *t* test. To account for multiple comparisons, a *p* value of 0.01 was considered significant. Finally a kappa statistic was calculated to assess the level of agreement between the two independent observers for pathological signal change on the structural MRI sequences.

4.3 Results

4.3.1 Clinical findings

The mean patient MMSE of 17.83 ± 4.02 was lower compared to a mean of 30 in the healthy volunteers (p=0.004). There was no significant difference in age between the patients (41.71 ± 10.09 years) and healthy volunteers (mean age 42.6 ± 7.861 years). All patients were symptomatic at the time of baseline MRS, although estimated disease durations at this time point ranged from 24 months (patient 5) to 146 months (patient 6). They exhibited differing severities of illness at baseline and differing clinical courses. Table 4.1 provides a summary of the patient characteristics and clinical scores at baseline.

Table 4.1: Patient characteristics and neurological scores obtained at baseline

Patient	Mutation	Disease duration (months)	ADAS-COG (75)	MMSE (30)	BPRS (168)	BARTEL (20)	CDR (18)	RANKIN (5)	CGIS (7)
1	P102L	63	13	23	35	13	5	4	4
2	6OPRI	43	-	-	-	9		3	5
3	6OPRI	93	33	13	-	14	8	3	4
4	6OPRI	33	24	19	35	20	7	3	4
5	Y163X	24	20	19	42	17	3.5	2	4
6	6OPRI	146	23	13	31	15	8	3	4
7	6OPRI	52	13	20	-	18	7	4	3

Note. Scores expected from healthy individuals are indicated in brackets. – indicates that patient was not able to compete the assessment. ADAS-COG = Alzheimer's Disease Assessment Scale, MMSE = Mini-Mental State Examination, BART = Barthel Activities of daily living scale: these measures *decrease* with disease severity. BPRS = Brief Psychiatric Rating Scale, CDR = Clinician's dementia rating, RANKIN = Rankin scale and CGIS = clinician's impression of global severity: these measures *increase* with disease severity.

All patients demonstrated clinical deterioration over time. Patient 1 was moderately ill with a baseline MMSE score of 23 at baseline but had a rapid progression in disease severity following the last assessment resulting in death within 2 months. Patient 2 was markedly ill with global dysphasia and disorientation in time and place preventing assessment by MMSE, ADAS-COG, BPRS and CDR clinical scores. Patient 3 was moderately ill with marked dyspraxia and disorientation in time and place. Patients 4 and 5 were moderately ill at baseline with MMSE scores of 19 each and progressed slowly. Patient 6 was followed up over the longest period (18 months) and progressed slowly from moderately ill at baseline to markedly ill. Patient 7 was mildly ill with symptoms of depression and apathy.

4.3.2 Qualitative image assessment

On initial assessment, there were discrepancies in 2 patients where one observer noted signal change in the frontal cortex in one patient and another observer noted signal change in the peri-habenular region in another patient (kappa score 0.835). On consensus review of these cases, no evidence of pathological signal change in any of the areas: caudate, putamen, thalamus, frontal parietal, temporal and occipital cortex was demonstrated.

4.3.3 Quantitative results

4.3.3.1 Baseline findings

Representative spectra from the RHC voxel in patient 6 can be seen in Figure 4.1c and from the RTH voxel in Figure 4.1d. A spectrum at 3 months from the RHC voxel in patient 2 was excluded from the analysis as the standard deviations for model fitting were greater than 15% for all metabolites. For the same patient, the MI at 6 and 9 months was excluded from the analysis as the model-fitting standard deviation for this metabolite was greater than 15%, possibly due to poor shim and inaccurate water suppression.

In the RHC voxel, I found a significantly lower [NAA] in patients than in the healthy volunteers (6.59IU ± 1.27 in patients versus 9.20IU ± 1.55, p=0.01; Figure 4.3a). [Cr] was borderline lower in the patients than in controls (Figure 4.2b). No significant difference in mean metabolite concentration was noted for [MI]. The mean MI/Cr was higher and the mean NAA/MI was lower in the patients than in the healthy volunteers but did not reach significance. The standard deviations for each metabolite concentration and metabolite ratio were higher in the patient group than in the controls, particularly for MI, reflecting the clinical heterogeneity of the former (see Table 4.2). In the RTH voxel, [Cr] was borderline lower and [MI] was borderline higher in patients than controls (Figure 4.3 d-e). There were no further significant differences in the other metabolites and metabolite ratios between patients and controls in this voxel.

Table 4.2: Baseline metabolite concentration estimates and metabolite peak-area ratios for patients and controls in the RHC voxel.

Parameter	Patients	Controls	Significance*
Cr	5.86(1.46)	7.72(0.81)	0.03
Cho	4.28(1.34)	4.43(0.80)	0.69
MI	3.96(1.38)	4.01(1.75)	0.90
NAA	6.59(1.27)	9.20(1.55)	**0.01**
Cho/Cr	0.74(0.19)	0.61(0.05)	0.26
MI/Cr	0.69(0.25)	0.53(0.24)	0.24
NAA/Cr	1.17(0.34)	1.19(0.09)	0.73
NAA/MI	1.79(0.52)	3.09(2.55)	0.21

Note. Values are mean (sd) institutional units or ratios

*independent *t* test on log values, patients vs. controls

Cr = total creatine, MI = *myo*inositol, Cho = choline containing compounds, NAA = N-acetylaspartate

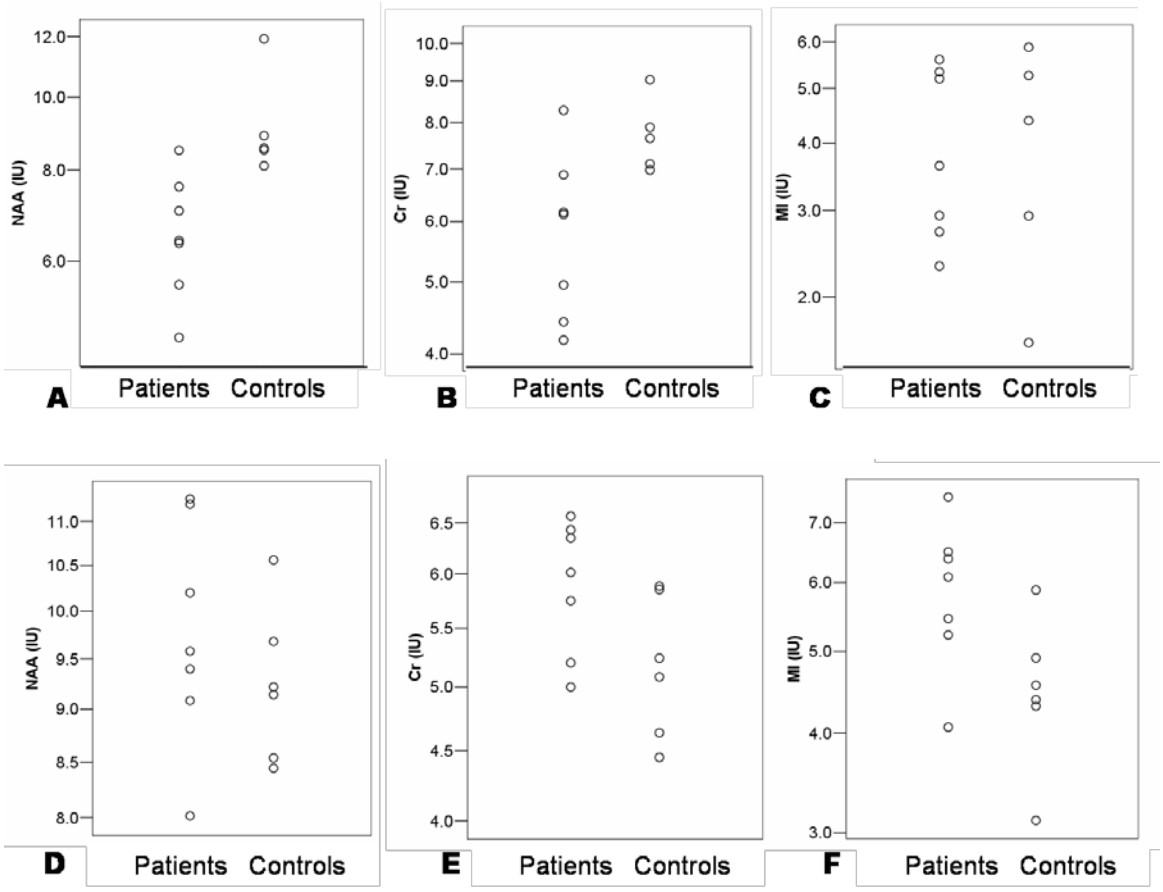

Fig 4.3: Metabolite concentration estimates (institutional units) in patients and healthy volunteers at baseline: in right head of caudate and putamen voxel (A) [NAA], p=0.01; (B) [Cr], p=0.03, (C) [MI], p=0.90; in thalamus voxel (D) [NAA], p=0.18; (E) [Cr], p=0.04, [MI], p=0.04. p-values refer to unpaired t test performed on log transformed values, patients versus controls

Linear regression revealed no dependence of either metabolite concentrations or peak-area ratios upon the age of the patient. In the RHC voxel, I found a significant association between higher [MI] and increased CDR (p=0.005; Figure 4.4A). MI/Cr demonstrated weaker association with disease duration at initial scan (p=0.021) and also with CDR (p=0.029), increasing with disease severity (Figure 4.4B and C). There were no significant correlations between baseline clinical scores and MRS-measures in the RTH voxel.

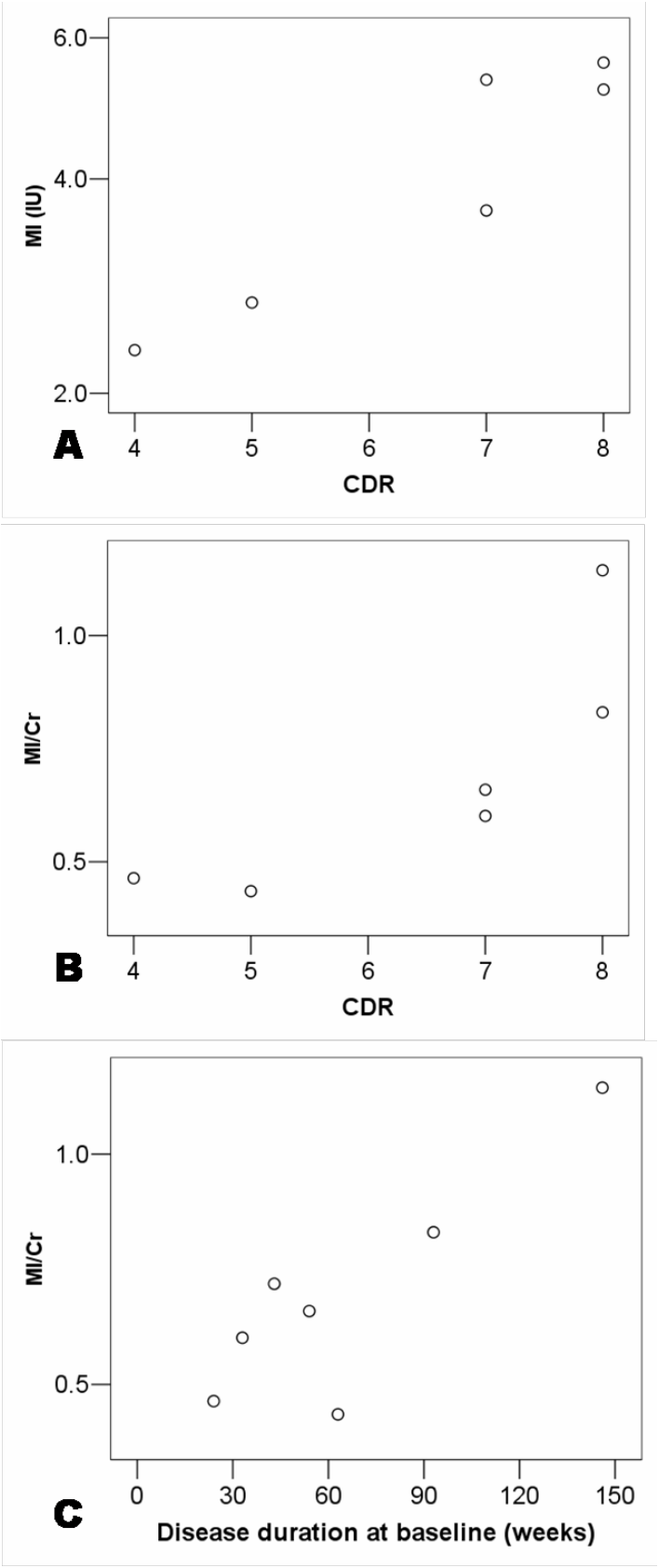

Figure 4.4: Associations between baseline metabolite right head of caudate concentration estimates and peak-area ratios, with clinical scores: (A) [MI] versus CDR, r=0.943, p=<0.01; (B) MI/Cr versus CDR r=0.857; p=0.03, (C) MI/Cr versus disease duration at baseline, r=0.830 p=0.02

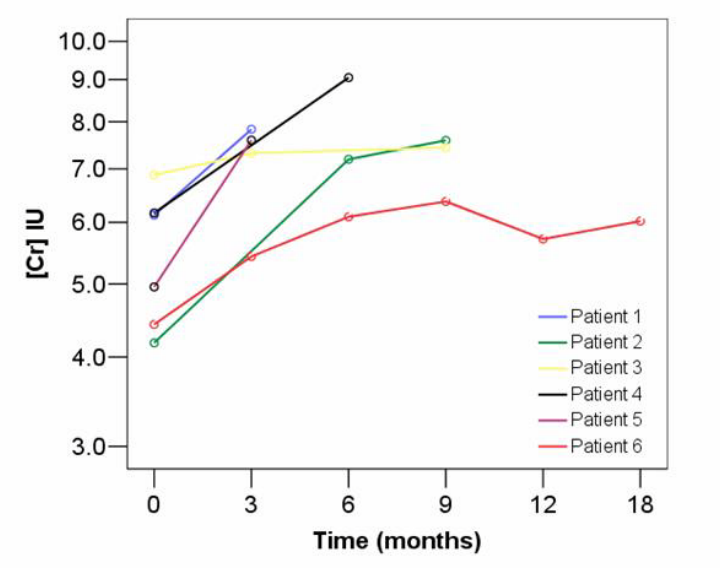

A

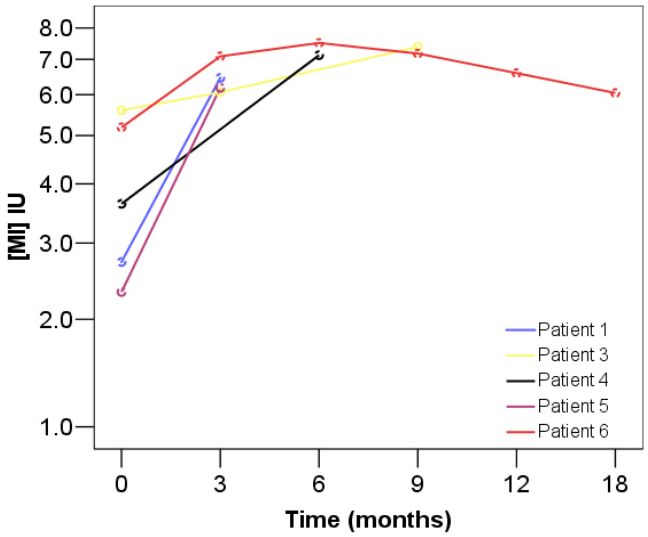

B

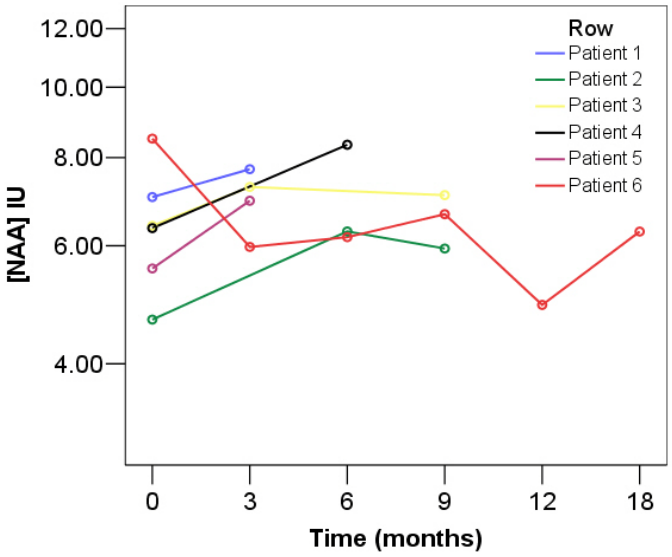

C

Fig 4.5: Changes in estimated right head of caudate metabolite concentrations with time: (A) Cr, (B) MI, (C) NAA

4.3.3.2 Longitudinal findings

Longitudinal data was obtained in 6 of the patients with a mean follow-up interval of 8.0 months (range 3-18). Longitudinal MI estimates in the RHC voxel were available in only 5 patients due to the necessary exclusion of poor quality data as detailed above. For all patients, [Cr] and [MI] increased with time (Figure 4.5A and B). Patient 6 was followed up for the longest and [MI] initially increased from baseline to 6 months before subsequently slightly declining. [NAA] remained stable except for patient 6 where [NAA] decreased with time (Figure 4.5C).

Using pair-wise comparisons, I found significant increases in mean [MI] between baseline and 3 months (3.96IU ± 1.38 versus 6.44IU ± 0.46, p=0.004), baseline and six months (3.96IU ± 1.38 versus 7.32IU ± 0.27, p=0.001) and baseline and 9 months (3.96IU ± 1.38 in patients versus 7.27IU ± 0.15, p=0.001). There were no significant differences in the other mean metabolite and metabolite ratios in the RHC voxel or any time points in the RTH voxel.

4.4 Discussion

I have quantified cerebral metabolites and metabolite-ratios in a small group of patients with inhPrD. I have shown significantly lower NAA concentrations in symptomatic patients compared to healthy volunteers in the caudate and putamen but not in the thalamus. Although no significant differences in MI concentrations were observed between patients and controls in the RHC voxel I found borderline higher MI in the RTH voxel. I also found, in the RHC voxel, a significant association of MI with disease severity at baseline, and significant increases in MI concentrations with time. These results are preliminary in a small number of patients and need to be confirmed in a larger cohort.

Our results are supported by the literature where a number of ^{1}H-MRS studies performed with long TEs have reported a decrease in NAA/Cr in inhPrD in multiple anatomical regions, including the caudate, putamen, cingulate gyrus and corpus callosum at single time points [84;181;184;186]. NAA is exclusively synthesized in the mitochondria of neurons and is widely considered to be a marker of neuronal density and integrity [114]. In our study, using a short TE, there was no significant change in [NAA] with time. It is possible that our follow-up interval of on average 8 months, was too short to allow the evolution of sufficiently large changes in NAA to allow detection. Certainly, in an animal model of this disease, reduced NAA/Cr in the posterior fossa was noted at an advanced symptomatic stage (180 days post infection) [189].

In contrast, very few studies in this disease have investigated cerebral metabolite abnormalities at short TE, which enables quantification of MI. An increase in MI was observed in the thalamus and frontal white matter in 2 symptomatic patients with the P102L mutation [186] and MI was the only metabolite that was elevated in 2 asymptomatic carriers of the mutation: in the thalamus, caudate and frontal white matter in one patient and in the frontal white matter in the other. In an animal model, an increase in MI was observed in the cerebral cortex of hamsters infected with CJD prions [190] and an increase in MI/Cr has been observed in the posterior fossa of BSE prion-infected mice [189]. In the latter study, the increase in MI/Cr preceded clinical signs by 20 days. The detected changes coincided with subtle alterations in behaviour suggesting that not only is MI/Cr a more sensitive marker of disease progression but that MI may be an indicator of functional impairments that precede the development of overt motor symptoms.

In our study mean [MI] and MI/Cr, although elevated in the RHC voxel, were not significantly different between patients and controls in the caudate and only borderline elevation was noted in the thalamus. One possible explanation is the rather wide spread of [MI] in our control group compared to that reported in previous studies [186;187]. I found accurate quantification of [MI] challenging in our control subjects compared with the inhPrD group; this may be partially a result of greater motion artefact in the awake controls, compared with the patients under GA, compromising data quality in the spectral region closer to the water resonance. Nevertheless in the RHC voxel in the inhPrD group I found a strong association of [MI] with disease severity and significant changes in mean [MI] with time, suggesting that [MI] could indeed prove a sensitive index of disease progression.

The function of MI is not well understood but as glia are known to express higher levels of MI than neurons, it has been proposed as a glial marker [112]. The triad of spongiform change, neuronal loss and gliosis involving astrocytes and microglia are the neuropathological hallmarks of prion disease, together with abnormal PrP immunoreactivity, and although neuronal loss and gliosis are not specific to prion diseases, it is generally accepted that the degree of reactive astrocytosis is more intense than would be predicted by the degree of nerve cell loss [164].

The severity of the histopathological changes can vary between different forms of prion disease with spongiform degeneration found in the cerebral neocortex, the subiculum of the hippocampus, putamen, caudate nucleus, thalamus and the molecular layer of the cerebral cortex [164]. I observed changes in cerebral metabolite ratios in the right head of caudate and putamen voxel but not in the right thalamus voxel. Although elevated [MI] was noted in the thalamus voxel an increase in [MI] with time or correlations between [MI] and clinical scores were perhaps not observed due to a saturation effect of the greater histological changes.

In our study, the Cr level apparently increased with time in all patients in the RHC voxel. The Cr peak is often presumed stable and is commonly used as a concentration reference but decreased levels are observed with tumours and stroke and increased levels with myotonic dystrophy [112]. The concentration of Cr is highest in oligodendrocytes and astrocytes compared to other cell types [191] and therefore the

elevation in Cr could reflect the reactive astrocytosis that is a histological feature of this disease. However, since our measurements were limited to a single TE it cannot be discounted that disease-related changes in the concentration or T2 of tissue water in the interrogated voxel may also have contributed to the observed changes.

Stability and homogeneity of the main magnetic field are important factors that directly impact the accuracy of MRS experiments. Major sources of frequency drifts include air-conditioning cycles and normal drift in the main magnetic field that fall within the magnet's specifications. Whilst it is possible that magnetic drift may have influenced our findings, a standard GE NAA phantom was used to check reproducibility and stability of our MRS measurements at each month throughout the time course of the MRS study.

The degree of change in the cerebral metabolite ratios differs between the various patients studied, with the largest change observed in Patient 1 who died shortly after the last assessment. Patient 6 was followed up for the longest time and showed a plateau in the cerebral metabolite ratios. This large inter-patient variability is possibly due to the clinical heterogeneity of our patient group where I observed a wide range of clinical scores at baseline. Our patients also had different mutations in the *PRNP* gene: 5 patients with 6OPRI, one patient with Y163X, one patient with P102L mutations. There is heterogeneity of clinical phenotype between the different mutations. Within the 6OPRI mutation, the disease course can vary between an aggressive course similar to sCJD to a more indolent course over several decades [192].

A potential confound in our study is the use of general anaesthetic in patients but not in controls during MRS examinations, which could contribute some of the observed between-group differences in metabolite ratios. However, one study in the literature which measured metabolite concentrations in both anaesthetized and awake monkeys found that the only difference in the spectra acquired under GA were a decreased line width and therefore improved spectral separation and higher sensitivities for the detection of metabolite concentrations [193]. It is also possible that changes in cerebral metabolites observed were modulated to an unknown extent by the effects of the drug Quinacrine. Pharmacokinetic studies of Quinacrine in mice demonstrate a concentration of up to1500ng/g in brain tissue [194] which is several orders of magnitude below the concentration of cerebral metabolites that can be detected by MRS. Although

I demonstrated clear associations between clinical presentation and ^{1}H-MRS measures, it is possible that an as yet unspecified interaction of the drug Quinacrine with the metabolism of NAA and MI may have influenced our results and therefore it is necessary to establish in a larger cohort of affected patients who are not undergoing treatment, that the MRS changes detected do indeed reflect the disease process. Full reports regarding the safety and therapeutic efficacy of Quinacrine in inhPrD will be the subject of future communications.

For the assessment of therapeutic efficacy of neuroprotective drugs, there is an increasing need to complement clinical outcome markers with objective and quantifiable outcome measures that are non-invasive, relatively inexpensive and have a high test re-test reliability [134]. Although MRI fulfils many of the above criteria, 1H-MRS may be particularly useful as changes in cerebral metabolite ratios can be detected before the onset of clinical symptoms in prion [186] and other neurodegenerative diseases [117;118;195] Proton-MRS thus offers promise as a biomarker in detecting neuronal dysfunction prior to the onset of neurodegeneration.

4.5 Conclusion

In this pilot study, anatomically specific changes in MI and NAA were observed with a strong association of MI with disease severity at baseline and increases in time that were concomitant with clinical deterioration. In contrast to conventional MRI, longitudinal short-TE ^{1}H-MRS metabolite-measures show significant promise as surrogate markers of disease progression in inhPrD.

B EX VIVO

The previous chapters (2-4) have demonstrated the potential of *in vivo* quantitative MRI in the assessment of prion disease activity in the brain. As the histopathology of this disease is distinctive, MRI examination of post-mortem specimens may inform our understanding of the microstructural changes underlying these quantitative MRI changes. The following chapter describes a number of experiments that were performed on formalin-fixed brain tissue samples from patients who had died from vCJD. I focus on vCJD because of its importance as a public health issue and the aim of the experiments was to determine whether post-mortem MRI at high field (9.4T) can detect and quantify the microstructural changes that affect the MRI signal in vCJD.

5 Imaging microstructural changes in post mortem brain in vCJD using MRI at 9.4T

5.1 Introduction

The precise histopathological correlates for the MRI signal changes in prion diseases are not yet known with conflicting reports in the literature. Severe spongiform change with confluent vacuolation, restricting the extracellular space, has been advocated as a potential cause of decreased cerebral ADC *seen in vivo* [85;87;88;135]. However, another study claims that DWI signal change correlates with accumulation of the abnormal prion protein PrP^{Sc} [88;177]. Due to the inevitable time delays between investigations, correlation of post-mortem histopathological findings with antemortem MRI should be interpreted with caution in such a rapidly progressive disease. Magnetic resonance microscopy (MRM) of post-mortem tissue, therefore, provides an opportunity to directly investigate the relationship between MRI and histopathology by providing high resolution structural and quantitative MRI data concurrently with histopathology.

In the work described in this chapter by performing MRI at 9.4T on fixed human tissue samples, I aimed to (i) detect structural differences between excised formalin-fixed specimens from patients who died from vCJD and a non-CJD control group, comparing the results with histological findings and (ii) systematically explore the association of quantitative histopathological measures with two important diffusion measures derived from DTI: MD and FA, in addition to T1 and T2 relaxometry.

5.2 Methods

5.2.1 Subjects

This study was approved by the Joint Ethics Committees of The National Hospital for Neurology and Neurosurgery and the Institute of Neurology, University College London, London WC1N 3BG, UK. Pulvinar and frontal lobe samples were excised from post-mortem formalin-fixed cerebral hemispheres from 6 patients who had died from vCJD (4 male, 2 female, mean age 41.6 years, range 19-76 years. Six non-prion disease controls (1 male, 5 female, mean age 68.6 years, range 47-86 years) were also obtained. Prior consent had been given by patients or their families to the National Prion Clinic, The National Hospital for Neurology and Neurosurgery, and the Division of Neuropathology, Institute of Neurology, University College London, London WC1N 3BG, UK. The course of the disease was assessed retrospectively from the case notes and the mean length of disease duration at presentation was 16.6 weeks (range 4 – 20 weeks) and the mean MMSE at presentation was 20.5 (range 18-23). The control specimens were obtained from patients that had died of a number of conditions which included AD, Lewy body dementia and vascular dementia. The mean age was 68.5 years ± 17.8 and the mean length of fixation was 46.5 weeks ± 14.7.

All the vCJD patients had *in vivo* MRI imaging performed before death. 4/6 patients had antemortem imaging performed at our institution where all subjects were examined using a GE Signa LX 1.5T MRI system (GE Healthcare, Milwaukee, WI). After scout images were obtained, axial images with slice thickness 5mm parallel to the bicommisural line from the craniovertebral junction to the vertex were acquired for T2W (TE 106ms, TR 6000ms, 2 averages, FOV 24x18cm, matrix 256x224, slice thickness 5mm), and FLAIR (TE 161ms, TI 2473ms, TR 9897ms, one average, FOV 24 x 24cm, matrix 256 x 224, slice thickness 5mm). DWI was performed using a single-shot echo-planar technique (TE 101ms, TR 10000ms, 1 average, matrix 96 x 128, FOV 26 x 26cm, slice thickness 5mm) with diffusion-weighting factors (‘b values’) of 0 and 1000 s/mm^2 applied sequentially along three orthogonal axes.

5.2.2 Specimens

Post-mortem specimens were obtained 24 hours - 7 days after death. The specimens (right cerebral hemisphere) were stored in plastic containers bathed in formalin at room temperature, approximately (22°C), until immediately prior to scanning. The mean duration of formalin-fixation for both control and patient specimens was 46.25 weeks

(range 4-88 weeks). Two tissue blocks were excised per specimen: from the pulvinar nucleus of the thalamus (the region of specific interest in this study) and the frontal cortex (control region).

5.2.3 Specimen preparation

Excised frontal cortex and pulvinar samples of approximately 20 x 20 x 7mm were held in a standard histopathology cassette (Figure 5.1) which was positioned tightly in a 50ml Vycon tube filled Fomblin Perfluorosolv PFS-1 (Solvay Solexis, Milan, Italy) to minimize sample motion (see Appendix K). Fomblin® is a perfluoropolyether which has no MRI visible protons and acts as an embedding and wetting agent, minimizing magnetic susceptibility-induced edge artefacts and I have shown that it has no significant effect on either quantitative MRI measures or subsequent histopathology (see Appendix L). All samples were transported to the Biological Imaging Centre at Imperial College London following appropriate risk assessment, optimisation of transport procedures and using a specimen trail document (see Appendix K and M)

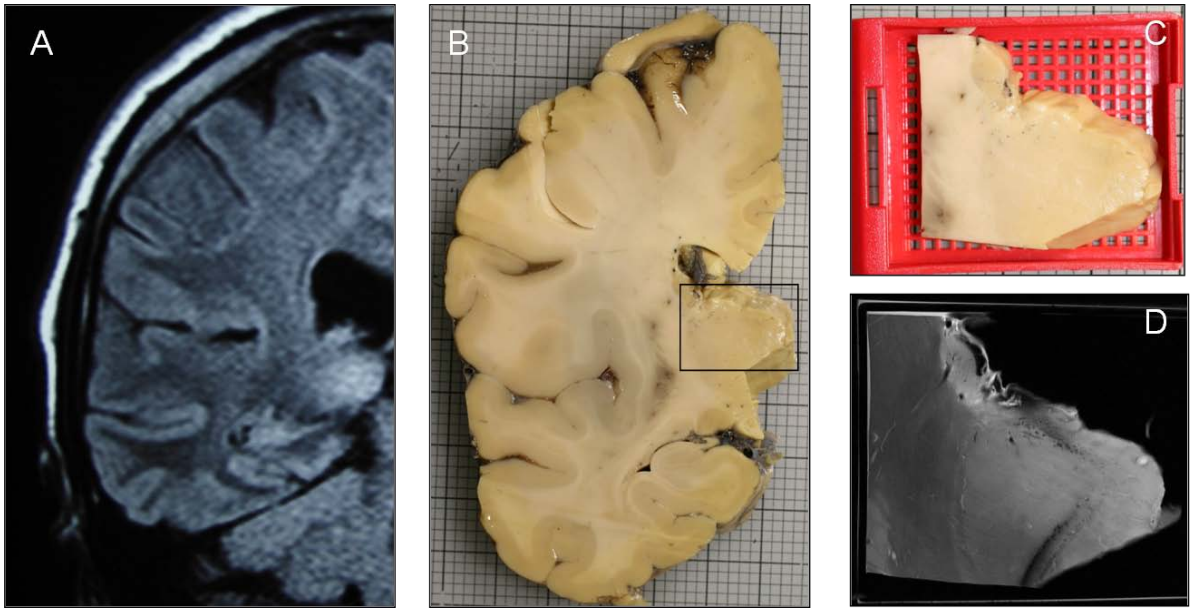

Figure 5.1: Protocol for *ex-vivo* sectioning of the brain and tissue block selection. (A) Coronal FLAIR MRI study demonstrating the pulvinar sign in a patient with v CJD, (B) 10mm thickness coronal section of the brain *ex-vivo* of the same patient matched to the MRI slice, (C) 20x20x7mm tissue block of the pulvinar nucleus cut from the coronal brain slice in image (B)in standard histopathology cassette, (D) T2W image of the same tissue block at 9.4T (TE = 24ms, TR = 2400ms, FOV=40x40mm, matrix=512x512, number of averages = 24, slice thickness =1mm).

5.2.4 MRI sequence optimisation

MRI was performed with a horizontal bore 9.4T/21cm Varian Inova MRI system (Varian Inc, Palo Alto, CA) located within the Biological Imaging Centre at Imperial College London using a 43 mm internal diameter quadrature transmit-receive volume RF coil (Magnetic Resonance Laboratories, Oxford) at room temperature (bore temperature was approximately 22 ºC). To determine the optimal imaging parameters for measurement of MD, FA T1, T2 and for high resolution T2W imaging, a number of pilot experiments were performed on a single control specimen. This was necessary to establish preliminary estimates of the MRI properties of these specimens at 9.4T: the fact that formalin-fixation may affect quantitative MRI parameters is well known with several studies reporting a decrease in T1 and T2 at 1.5T in both grey and white matter compared to in vivo values [196-198]. A further complication is that T1 relaxation times are prolonged at high magnetic field strengths [199].

5.2.4.1 T2 pilot experiment

For T2 measurement, a single SE sequence with 4 repeat SE acquisitions with TEs 24, 36, 48 and 60ms and TR of 2000ms (Figure 5.2). A single exponential model was fitted using the equation $S(TE) = \rho(\exp(-TE/T2))$ where $S(TE)$ is the SI obtained at each TE. All image processing was performed off-line, on a dedicated workstation (Sun Microsystems, Mountain View, CA, USA), using commercially available software (JIM Version 4.0, Xinapse Systems Ltd., Thorpe Waterville, UK.). A typical T2 of 20ms was calculated for the grey matter and 17ms in the white matter. Poor signal at the TE of 60ms and a resultant T2 map with reduced SNR and standard deviations for the mean T2 grey matter ROI (20ms) were 11.7 – 15.0%. With adjusted TEs of 10, 22, 34 and 46ms, the T2 maps were improved with ROI standard deviations of 10.5-11.2%.

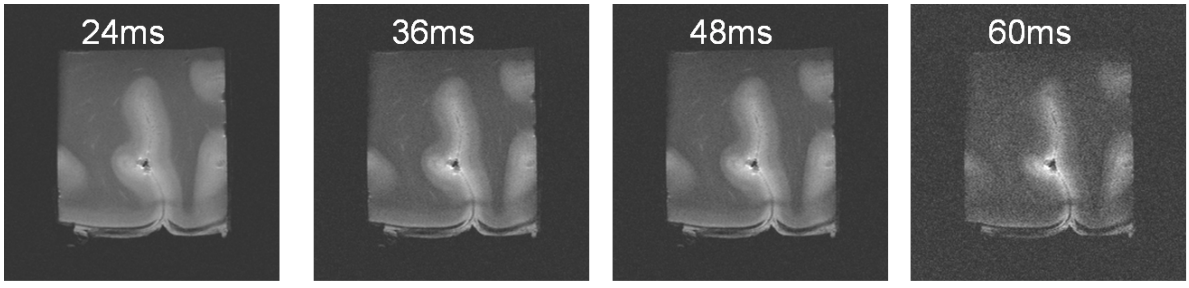

Figure 5.2: Initial T2 experiment: TE of 24, 36, 48 and 60ms demonstrating change in tissue contrast and poor signal at TE of 60ms.

5.2.4.2 T1 pilot experiment

A progressive saturation technique was used for the determination of T1 with a series of successive SE sequences with progressively longer TRs. Compared to low-field *in vivo* work, a shorter TE and longer TRs were used: TE 15ms and TR 450, 600, 800, 1000, 2000, 4000ms (Figure 5.3). Model fitting using the equation $S(TR) = \rho(1 - \exp(-TR/T1))$ where $S(TR)$ is the SI acquired at each successive TR, again using JIM software, revealed a T1 of 959ms for grey matter and 767ms for white matter with standard deviations for ROI measurements ranging between 8.2-9.0%.

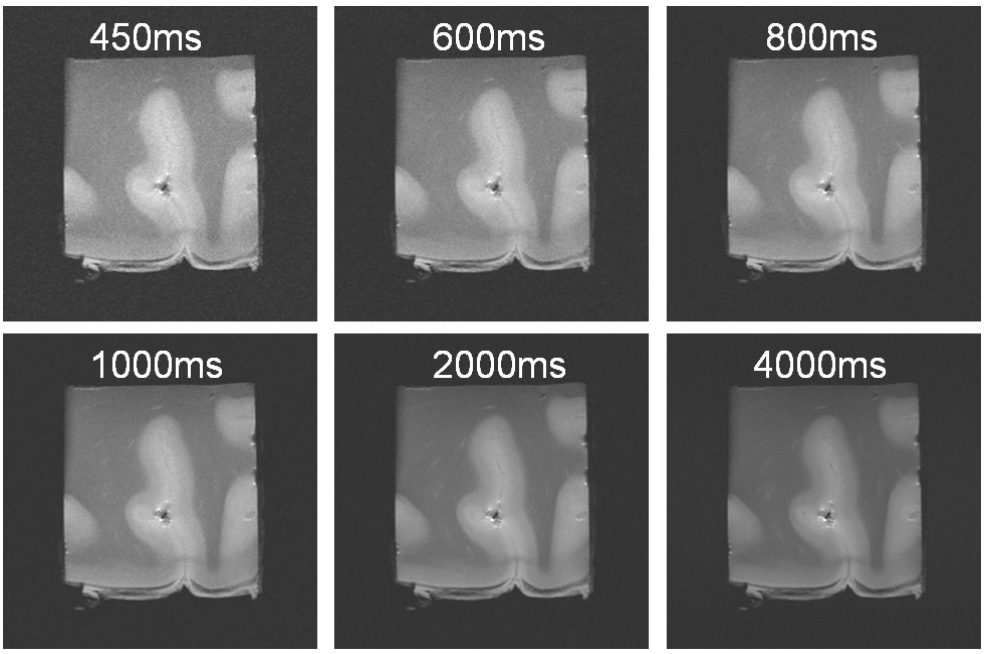

Figure 5.3: T1 experiment with TR of 450, 600, 800, 1000, 2000 and 4000ms, demonstrating change in tissue contrast at successive TRs.

5.2.4.3 High resolution T2W images

Finally, for the high resolution imaging, the TEs were adjusted for optimal visualization of the grey matter by choosing a TE as close to the measured grey matter T2 (20ms) as possible and a TR of approximately 3 x the measured T1 for grey matter (959ms). The initial parameters used were TE24ms, TR2000ms and TE60ms, TR 3000ms (Figure 5.4).

Figure 5.4: Optimisation of MRI parameters for visualization of the cortex.

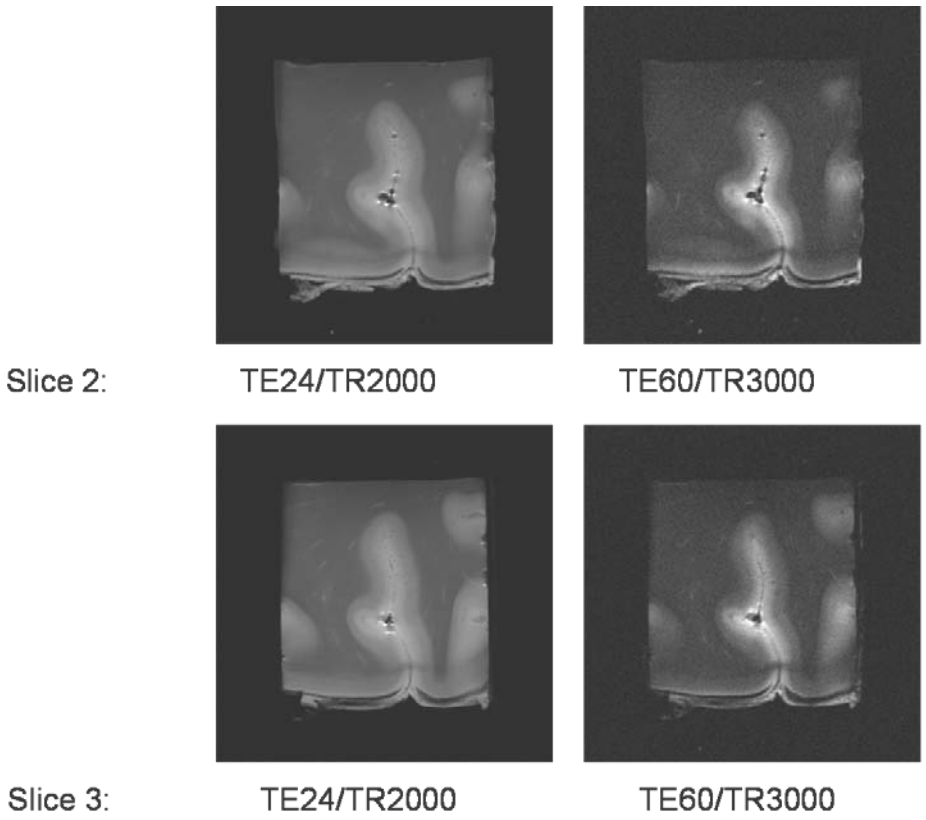

As can be seen above, the images produced with the longer TE and TR are heavily T2W and are ideal for viewing the white matter. However, a more intermediate weighted sequence with a shorter TE and TR, revealed more detail within the grey matter (frontal cortex). The matrix size was increased to 512 x 512 and 20 averages were performed to increase signal with an acquisition time of approximately 7 hours.

5.2.4.4 Image artefacts

On the initial image acquisition, a low SI line parallel to the edge of the cortical surface was noted (Figure 5.5). In order to investigate whether this was a magnetic susceptibility or imaging sampling artefact from the MRI acquisition, the phase and frequency encoding directions were reversed for a further acquisition but the artefact was still present. In order to determine whether the artefact was due to RF inhomogeneity from the surface coil, the specimen was pushed further into the coil and turned around but the artefact remained in the same location. Finally the sample was cut into a smaller piece so that the specimen was not in such close proximity to the plastic histopathology cassette to avoid possible chemical shift artefact from the plastic/air interface, but again the artefact was in the same location.

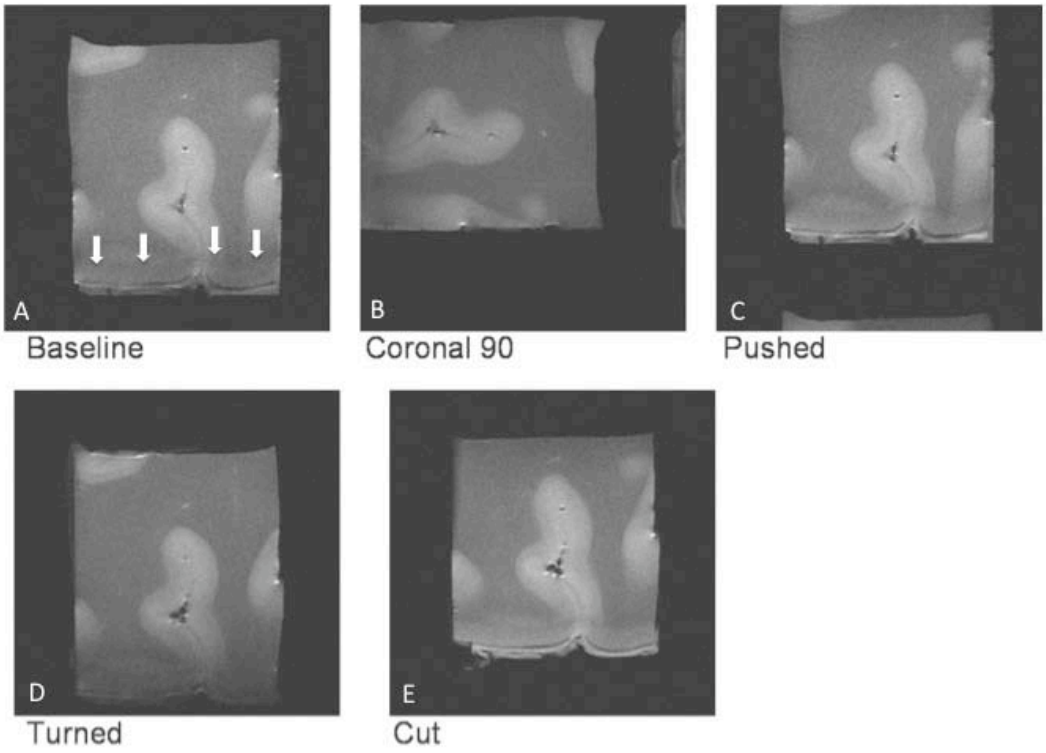

Figure 5.5: Fixation artefact in the cortex. (A) Baseline image demonstrating a low signal intensity line parallel to the outer surface of the specimen (arrows). In order to ascertain whether this was an acquisition artefact or intrinsic to the specimen, the phase and frequency encoding directions reversed (B), the sample was pushed further into the coil (C), the specimen was turned in the coil (D) and finally the sample was cut into a smaller piece. The artefact was present on all images and concluded to be intrinsic to the specimen.

On histological processing, no abnormality was observed in that location to correlate with the MRI abnormality. It was therefore proposed that the artefact could represent the leading edge of formalin fixation which could occur when the formol-saline, in which the sample is immersed, is changed. The artefact could represent a concentration of unknown ions which are then dissolved by histological processing. There are no reports of similar artefacts in the literature and the exact cause of this is being currently investigated. I therefore remained alert to this artefact during the course of our experiments. Fortunately, when the T1, T2 and FA and MD maps were calculated, the artefact was no longer visualised and therefore not thought to affect the quantitative measurements obtained (Figure 5.6).

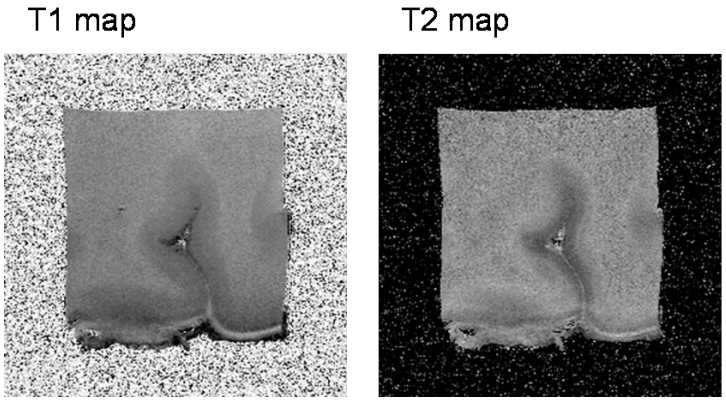

Figure 5.6: T1 and T2 maps of the same specimen as that shown in Figure 5.5 demonstrating absence of the fixation artefact.

5.2.5 Final MRI protocol

For T1 measurement, successive SE images were acquired with TRs of 450, 600, 800, 1000, 2000, 4000 ms; TE 15 ms; 2 averages; acquisition matrix size 256x128; slice thickness 2 mm. T2 measurements were obtained using a SE sequence to acquire successive images with TEs of 10, 22, 34 and 46 ms; TR 2000 ms; 2 averages; matrix size 256x128; slice thickness 1 mm. To investigate tissue-water diffusion, successive images were acquired with diffusion weighting applied along 6 non-colinear directions (G_x, G_y, G_z = [(1,1,0), (0,1,1), (1,0,1), (-1,1,0), (0,-1,1), (1,0,-1)]) with a diffusion weighting (*b* factor) of 1000 s/mm^2, and with no diffusion gradients (i.e. with a *b* factor of 0 s/mm^2) and TR 2000 ms; TE 22 ms; matrix size 256x256, 2 averages and slice thickness 1 mm. Finally, a high-resolution T2W coronal image (TE 24 ms; TR 2400 ms; matrix size 512x512; 20 averages, slice thickness 1 mm; in-plane resolution 78 µm) was acquired providing good anatomical contrast for qualitative assessment. For all acquisitions the FOV was 40x40mm and 7 contiguous coronal slices were obtained. The total measurement time per specimen was approximately 10 hours.

5.2.6 Image analysis

All image processing was performed off-line, on a dedicated workstation (Sun Microsystems, Mountain View, CA, USA), using commercially available software (JIM Version 4.0; Xinapse Systems Ltd, Thorpe Waterville, UK.).

5.2.6.1 Qualitative

The high-resolution intermediate-weighted images for each pulvinar and cortical specimen were assessed by a single neuroradiologist in a non-blinded manner for visible artefacts and any differences in signal intensities between the control and diseased specimens. For the cortical specimens, T2W SI profiles were generated perpendicular to the cortical surface, from deep (subcortical U fibres) to superficial (pial surface), to objectively depict the differences between vCJD and control specimens.

5.2.6.2 Quantitative

All quantitative image processing was performed off-line on a dedicated workstation (Sun Microsystems, Mountain View, CA, USA). The process was fully automated taking ~20 mins. Using commercially available software (JIM Version 4.0; Xinapse Systems Ltd, Thorpe Waterville, UK.), T1 and T2 maps were computed by performing pixel-by-pixel non-linear fitting to the equations $S(TR) = \rho(1 - \exp(-TR/T1))$ and $S(TE) = \rho(\exp(-TE/T2))$, respectively. $S(TR)$ and $S(TE)$ are the signal intensities of the T1- and T2W images acquired at the respective TR or TE, and ρ is the proton density in arbitrary units. DTI data were calculated using Camino (http://www.cs.ucl.ac.uk/research/medic/camino/) (Cook *et al*., 2006) to provide FA and MD maps.

5.2.7 Region of Interest (ROI)

To assess differences between the control and vCJD specimens ROIs were defined in the FC and FWM for each frontal lobe specimen and in the Pu for the pulvinar specimen (Figure 5.7). The ROIs (size 40 - 170 mm^2) were defined on the SE images providing optimal grey-white matter contrast (TE 10 ms; TR 2000 ms), saved and then re-loaded for each of the T1, T2, MD and FA maps. One ROI in each area was determined per specimen.

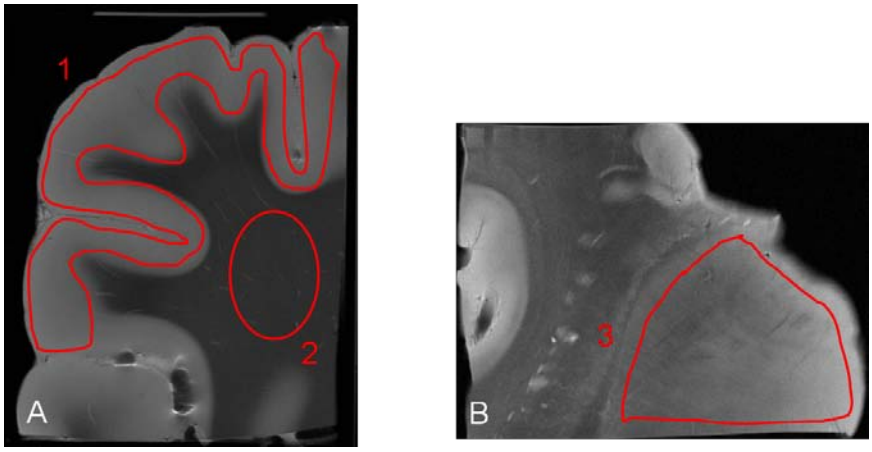

Figure 5.7: High resolution T2W images (TE=24, TR=2400) of the (A) frontal cortex and (B) pulvinar specimens, demonstrating manually drawn ROIs in the FC (1), WM (2) and Pu (3)

5.2.8 Histological analysis

Following the MRI measurements, samples were re-immersed in 10% buffered formal saline for one week (Pioneer Research Chemicals, Ltd., Colchester, UK.) followed by incubation in 98% formic acid for 1 h. Following further washing for 24 h in 10 % buffered formal saline, tissue samples were processed and paraffin wax embedded. Sections were cut at a nominal thickness of 4 µm and mounted on Superfrost UltraPlus charged glass slides. Following dewaxing in xylene and an alcohol gradient, the sections were stained with haematoxylin (Harris' haematoxylin) and eosin (0.5%, Merck) (H&E). For immunohistochemical staining, dewaxed sections were treated with 98% formic acid for 5 min and then boiled in a low ionic strength buffer (2.1 mM Tris, 1.3 mM EDTA, 1.1 mM sodium citrate, pH 7.8) for 20 min for antigen retrieval. Prion Protein (PrP) deposition was visualized using KG9 as the primary antibody (1:2000) and gliosis was detected with anti GFAP rabbit polyclonal antiserum (DAKO, 1:1000), using an automated immunostaining system (www.ventanamed.com).

Finally, for the cortical samples, Nissl staining was performed for identification of the cortical laminations.

.

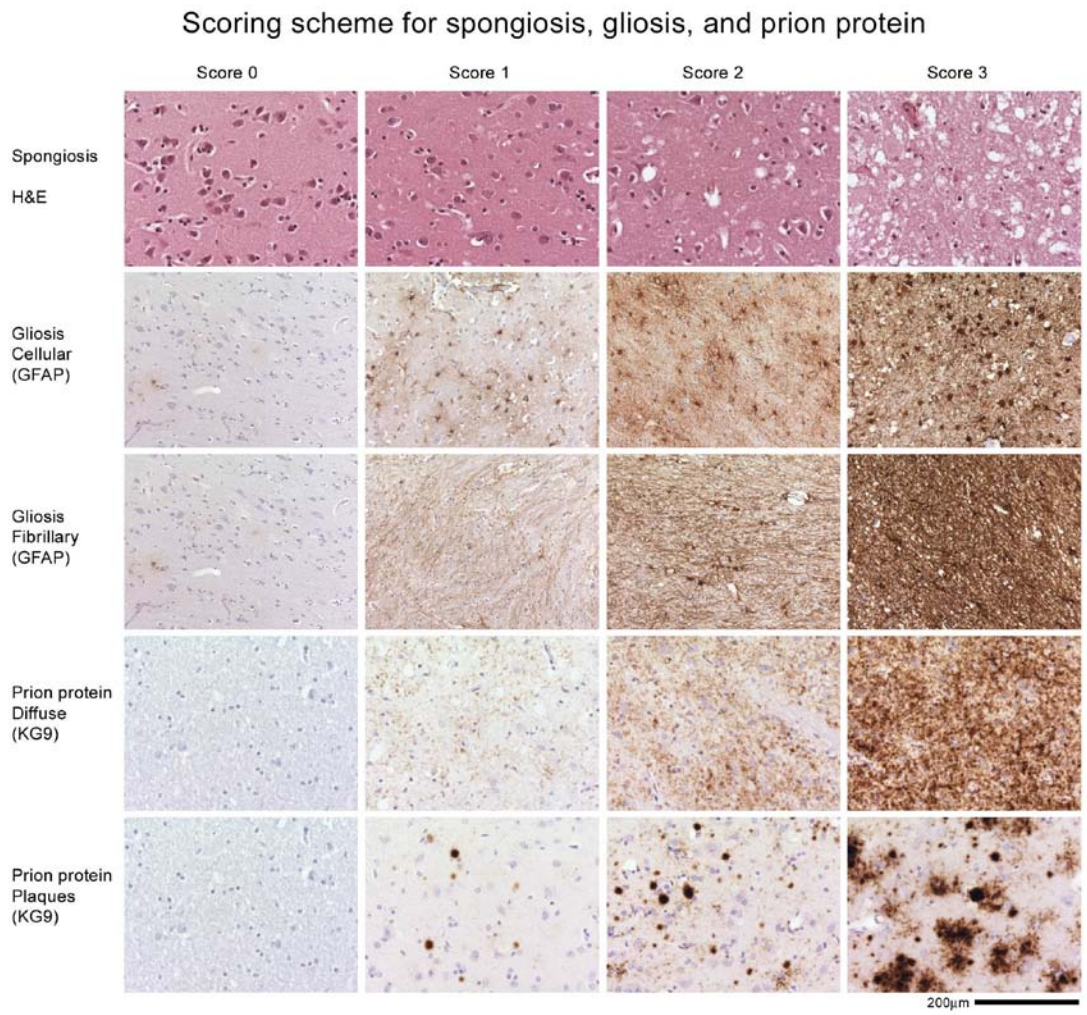

Figure 5.8: Scoring scheme devised in conjunction with the neuropathologist using specimens from the study for spongiosis, gliosis and prion protein deposition: 0=none, 1=mild, 2=moderate, 3=severe; spongiosis was detected using H&E staining, gliosis was detected with GFAP staining and prion protein deposition with KG9 staining

All slides were assessed by a single experienced consultant neuropathologist, who was aware of the diagnoses. Areas corresponding to the ROIs on MRI were scored for the degree of spongiosis, gliosis and prion protein deposition in a semi-quantitative manner from 0 to 3 (0=none, 1=mild, 2=moderate, 3=severe; Figure 6.8). The scoring scheme was devised in conjunction with the neuropathologist using human cortex samples from the study. Photographs were taken on an ImageView digital camera (www.soft-imaging.de) and composed with Adobe Photoshop.

5.2.9 Statistical analysis

The independent t-test was used to assess differences for each of the 4 MRI measures: T1, T2, MD and FA in the FC, FW and Pu ROIs between the prion-diseased and control specimens. The differences in each histology measure: spongiosis, gliosis and prion protein deposition between the diseased and control specimens was assessed using the Mann-Whitney-U test. A one-way ANOVA with post-hoc tests was used to assess differences in measures between the FC, FW and Pu ROIs in each specimen group. The Spearman rank correlation was used to assess the relationship between each MRI measure and each histopathology score for the cortex and pulvinar regions in the diseased specimens only. The relationship between each MRI measure and length of fixation was also assessed to avoid any confounders. A value of $p < 0.05$ was considered statistically significant and all statistical tests were performed using SPSS for Windows (version 11.5, SPSS, Chicago, IL, USA).

5.3 Results

5.3.1 Specimens

All vCJD patients exhibited the pulvinar sign on conventional antemortem MRI and where obtained (n=4), pulvinar hyperintensity on b1000 DWI in vivo. No cortical signal change was detected on any sequence *in vivo*. The control specimens were obtained from patients that had died from a number of conditions which included: AD, Lewy body dementia and vascular dementia. Using the independent t-test, the mean age was borderline higher in the control specimens (68.5years±17.8 in control versus 47.8years±25.2 in diseased specimens, p=0.07) but there were no significant differences in mean length of fixation (46.5 weeks ± 14.7 in control versus 46.2 weeks ± 25.2 in diseased specimens, p=0.98) between the vCJD and control specimen groups.

5.*3.2 Post mortem MRI findings*

5.3.2.1 Differences between diseased and control groups

5.3.2.1.1 Qualitative

Visual inspection of high resolution T2W images of the frontal cortex revealed, in all 6 control specimens, an intracortical laminar structure with a low SI layer (arrow, Fig 5.9A). When directly compared to the corresponding Nissl stain, the low SI band correlated to layer IV of the cortex (Fig 5.9B). However, in 5/6 vCJD specimens, there was apparent loss of the intracortical laminations with homogenous SI across the cortex (see Fig 5.9D). In the remaining vCJD specimen the intracortical structure was attenuated but not completely absent. The cortical SI profiles revealed a focal dip in intensity corresponding to layer IV in all 6 control specimens (Fig 5.9C) while for 5/6 vCJD cases the cortical signal intensities exhibited a smoother profile (Fig 5.9F). The Nissl staining revealed loss of the intracortical structure in vCJD due to neuronal loss where there was spongiosis and prion protein deposition (Fig 5.9E).

Visual inspection of the high resolution T2W images of the pulvinar specimens revealed no differences between the diseased and control specimens.

5.3.2.1.2 Quantitative

I found no significant differences in T1, T2, MD or FA in the frontal cortex, white matter and pulvinar ROIs between the diseased and control specimens (Table 5.1). However, I found differences in MRI measures between the different regions in both the control and vCJD specimens.

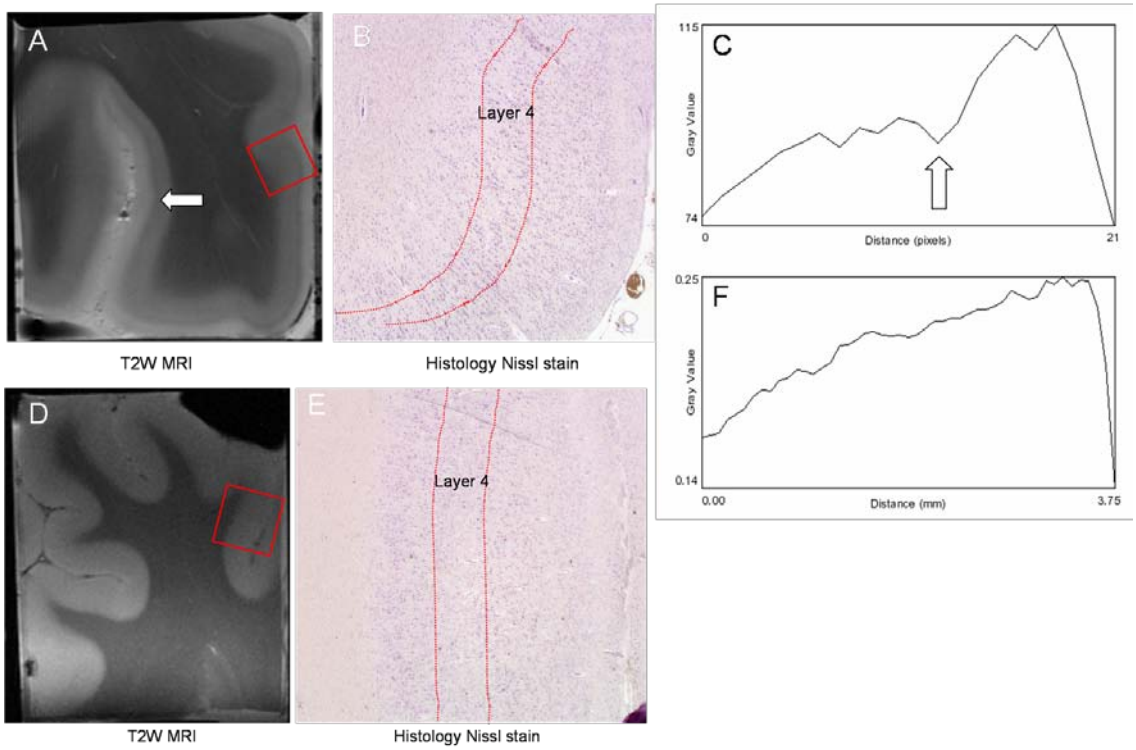

Figure 5.9: High resolution MRI and signal intensity profiles in vCJD and controls. High resolution T2W image of control specimen (A) demonstrating low signal intensity line, (B) corresponding to layer IV in H&E slide and corresponding to the dip in SI on the SI profile (C). (D) High resolution T2W image of vCJD specimen demonstrating more homogenous SI, (E) corresponding to attenuation of layer IV due to spongiosis and neuronal loss and supported by loss of demonstration of layer IV on the SI profile (F).

In the control specimens, significant differences in mean T2, MD and FA were found between the cortex compared to white matter but there were no significant differences between the pulvinar and any region for any of the MRI parameters (mean FW T2 =21.3±3.2ms versus mean FC T2 = 28.9±6.5 ms, p=0.01; mean FW MD = 223.5±56.7 versus mean FC MD=409.8±105.7, p=0.01; mean FW FA = 0.75±0.08 versus mean FC FA=0.41 ± 0.08, p=0.001). In the vCJD specimens, mean T2 was higher in the frontal cortex than in the pulvinar and in the white matter: mean FC T2 =31.7±7.4 ms versus mean Pu T2 = 21.1 ± 4.3 ms (p=0.03); and versus mean FW T2 = 21.78±2.92 ms (p=0.01). As in the control specimens, the mean MD was also higher in the frontal cortex than in the white matter (mean FC MD = 517.0 ± 186.5 s/mm^2 versus mean FW MD = 315.1 ± 85.3 s/mm^2, p=0.02) and FA was higher in the white matter than in the frontal cortex (mean FW FA = 0.75±0.20 versus mean FC FA=0.42±0.19 for cortex, p=0.001; Fig 5.10).

Table 5.1: Summary of quantitative MRI parameters in each ROI in the control and diseased specimen groups.

MRI measure	Region	Controls specimens (n=6) mean	SD	vCJD specimens (n=6) mean	SD	P value
T1 (ms)	Frontal cortex	1159.9	289.1	939.5	194.2	0.15
	White matter	939.7	215.6	807.8	127.6	0.23
	Pulvinar	1075.8	320.8	873.2	220.6	0.23
T2 (ms)	Frontal cortex	28.9	6.5	31.7	7.4	0.50
	White matter	21.3	3.2	21.8	2.9	0.77
	Pulvinar	23.6	6.1	21.1	4.3	0.43
MD (mm^2/s)	Frontal cortex	409.8	105.7	517.0	186.5	0.24
	White matter	223.5	56.7	267.7	98.7	0.36
	Pulvinar	380.3	85.4	315.1	85.4	0.21
FA	Frontal cortex	0.41	0.08	0.42	0.18	0.89
	White matter	0.75	0.13	0.76	0.20	0.94
	Pulvinar	0.63	0.21	0.58	0.16	0.67

5.3.2.2 Semi-quantitative histology findings

Spongiosis and prion protein deposition were detected in the vCJD specimens in the cortex and pulvinar but not in the white matter (median spongiosis in the frontal cortex = 1, (range 0-2) and pulvinar = 2 (range 1-3); median prion protein deposition in the frontal cortex = 2 (range 2-3) and pulvinar = 3 (range 2-3). Gliosis was detected in all three regions in the vCJD specimens. Spongiosis and prion protein deposition were not detected in the non CJD control specimens except for one specimen where the spongiosis was thought to be due to degradation of tissue before fixation rather than intracellular vacuoles. Gliosis was detected in the frontal cortex, pulvinar and white matter (Table 5.2). There was no significant difference in gliosis scores in each region between vCJD and controls.

Table 5.2: Summary of histopathological scores in each region on the vCJD group (A) and control group (B)

(A)

Histology	White matter	Frontal cortex	pulvinar
gliosis	2 (2-3)*	1 (0-2)	2.5 (2-3)*
spongiosis	0	1 (0-2)	2 (1-3)
PrP	0	2 (2-3)	3 (2-3)

(B)

Histology	White matter	Frontal cortex	pulvinar
gliosis	1 (1-3)	1 (0-2)	2 (2-3)
spongiosis	0	1 (0-2)	0
PrP	0	0	0

Note. Median values with range in brackets

* p=0.038, white matter versus frontal cortex; p=0.024, pulvinar versus frontal cortex in vCJD patient group

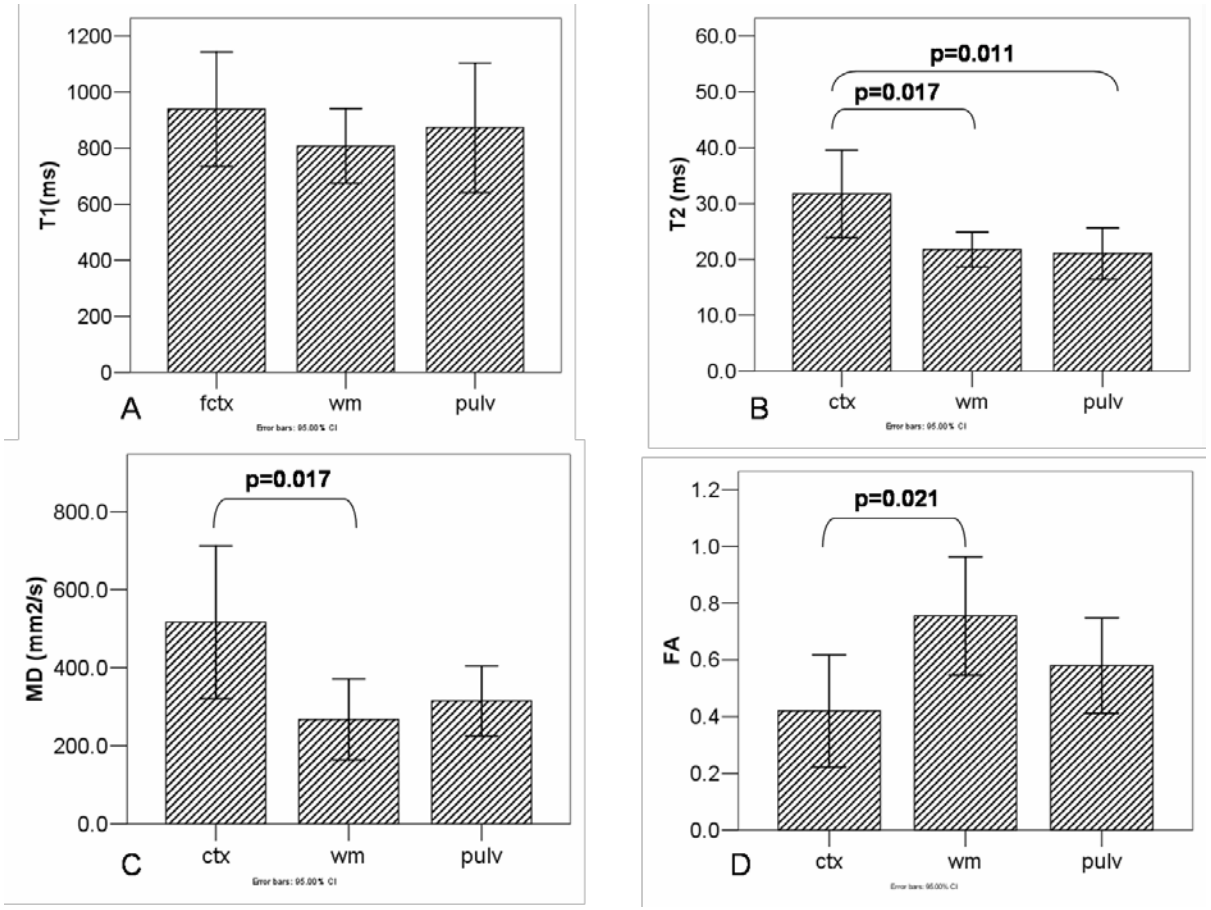

Figure 5.10: Comparison of MRI measures in the frontal cortex, white matter and pulvinar ROIs in vCJD specimens: (A) no significant differences in T1 measurements between regions are demonstrated; (B) increased T2 measurements in cortex compared to the white matter (p=0.017) and cortex compared to the pulvinar (p=0.011) are noted; (C) increased MD is seen in frontal cortex compared to the white matter (p=0.017); (D) FA is lower in the cortex compared to the white matter (p=0.021).

5.3.2.3 Relationship between MRI measures and histology measures

In the vCJD group, correlations between *ex vivo* MRI measures and histopathological scores were significant for FA and spongiosis (r=-0.926, p=0.008) and FA and gliosis (r=0.878, p=0.021) in the pulvinar ROI only (Figure 5.11). No significant associations between MD, T1 and T2 and any of the histological measures were observed *ex vivo* in the pulvinar. In the cortex ROI, I found no significant association between any of the MRI measures and any of the histopathological measures. I found no association between any MRI measure and length of fixation of the specimens.

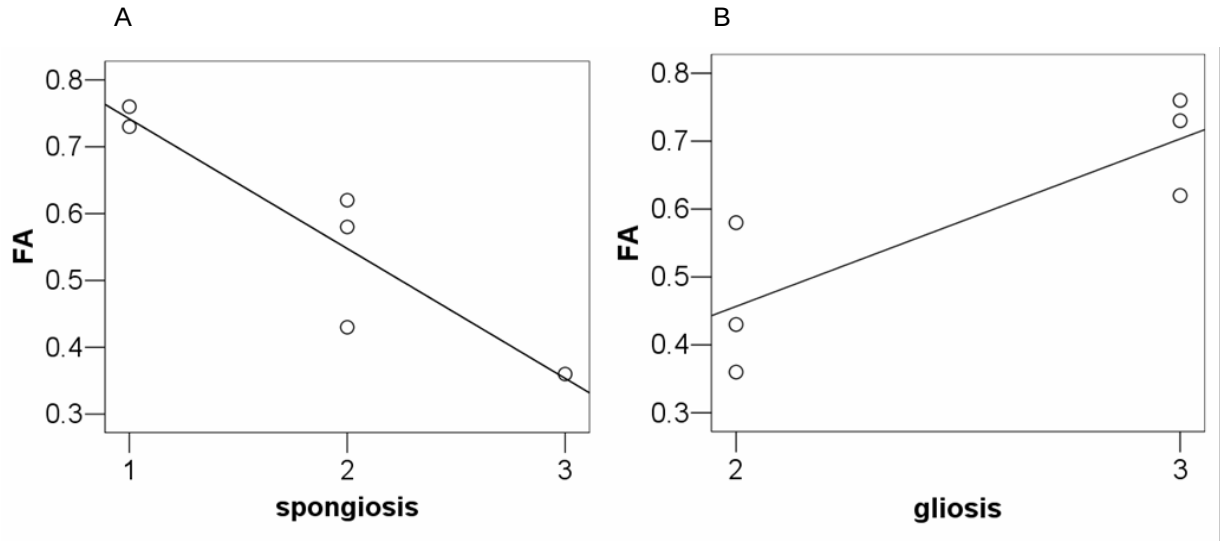

Figure 5.11: Scatterplots demonstrating the relationship between FA and spongiosis (A) and FA and gliosis (B) in the pulvinar ROIs

5.4 Discussion

I have shown that *ex vivo* MRM at 9.4T can depict pathology characteristic of vCJD. I have demonstrated apparent loss of the normal intracortical laminations in vCJD caused by neuronal loss due to a combination of spongiform degeneration and astrocytic gliosis. In this study, I found a significant association of FA, decreasing with the severity of spongiosis but increasing with the severity of gliosis in the pulvinar in vCJD. I found no association of any other MRI measure with histology parameters in this region and no association of MRI and histopathology measures in the cortex. This study is limited by a small sample size but nevertheless, provides novel information on the relationship between quantitative MRI measures and histopathology in human prion diseases.

The triad of spongiform change, neuronal loss and gliosis involving astrocytes and microglia is the neuropathological hallmark of prion diseases [53]. Spongiform change is relatively specific to prion disease and characterised by diffuse or focally clustered, small, round or oval vacuoles in the neuropil of the cerebral cortex (whole thickness or deep layers), the subcortical grey matter and the cerebellar molecular layer, especially head of caudate nucleus and rarely present in the brainstem and spinal cord [54]. In vCJD, this is accompanied by deposition of the abnormal prion protein PrP^{Sc} in the form of multiple rounded amyloid plaques often with a dense eosinophilic core and a pale radiating fibrillary periphery surrounded by a rim or halo of spongiform change and are present in large numbers in the cerebral and cerebellar cortex, particularly in the occipital cortex [53]. Spongiform change is most severe in the basal ganglia, particularly in the caudate nucleus and putamen which contain relatively few amyloid plaques. The thalamus, hypothalamus, brainstem and spinal cord exhibit little spongiform change or amyloid plaque formation [53].

Despite this, cortical signal change or abnormalities have not been described *in vivo* in vCJD. Our findings of loss of intracortical laminations in cortical specimens at 9.4T may prove highly beneficial in the early diagnosis and monitoring of therapy in vCJD. With prelimary reports of *in vivo* 9.4T human MRI studies [199], future *in vivo* assessment of the cerebral cortex, particularly with the generation of SI profiles may help to identify and characterize intracortical disease.

Our findings of intracortical laminations in non-CJD specimens are in keeping with a previous report demonstrating the cytoarchitecture of the human cerebral cortex [200]. Fatterpekar *et al* showed that by the use of Nissl and myelin stains, the low SI horizontal layer in the isocortex corresponded to heavily myelinated laminae such as the intracortical layer IVB (external band of Baillarger), which was thickest in the calcarine cortex [200]. The cortical layers represent horizontal aggregations of neurons with common connections. Variations in the cellular composition and packing of each layer give cortical regions a specific cytoarchitecture that subserves the function of that region [201;202]. I have shown that spongiform degeneration which is characteristic of prion diseases accompanied by neuronal loss causes destruction of the normal cytoarchitecture of the cortex which can be detected by high field MRI. It is possible a sampling error may have affected our results, although I was careful to excise specimens from the same part of the frontal cortex between specimens.

Unfortunately, in our study, I could not obtain quantitative MRI correlates of the visual differences in the cortex. In the cortex, I found no significant differences in any of our MRI measures between our patient and control samples. In fact, I also found no significant differences in any of our MRI measures between our patient and control samples in the pulvinar or the white matter. In particular, the T2 measurements in the pulvinar were not higher than those measured in the control samples. It is well established in the literature that both T1 and T2 decrease with time after death and formalin fixation with one study demonstrating a decrease in T1 of 39% after 760 hours fixation and a decrease in T2 of 38% in 1110 hours after fixation in human grey matter [198] while the ADC of grey and white matter remained constant. ADC is also significantly reduced in post-mortem tissue compared to *in vivo*. Therefore the use of formalin fixation may have masked any differences in MRI measurements between patients and controls, highlighting the limitations of formalin fixation in the interpretation of MRI measurements *ex vivo*. The use of fresh tissue samples may have solved this problem but unfortunately was not an option in this particular high risk disease. In addition, our control samples, although non-CJD controls, demonstrated a variety of other pathologies including Lewy body dementia and AD. The presence of gliosis in all regions within these non-CJD diseases controls possibly masked any differences in MRI measures.

Symmetrical hyperintensity in the pulvinar thalami (relative to the cortex and especially the anterior putamen) is characteristic of vCJD and is known as the pulvinar sign. The pulvinar sign has a sensitivity of 78-90% and a specificity of 100% for vCJD and was originally described on T2W, PD and FLAIR images [36;37]. Through studies which correlate antemortem MRI findings with post-mortem histopathology findings in vCJD, it has been suggested that the histopathological basis of the pulvinar sign (T2 prolongation in the pulvinar nucleus) is astrocytic proliferation.
As yet, there is no evidence that the pulvinar sign should be used for pre-symptomatic testing of vCJD as all reports have been is symptomatic patients at the end-stage of disease. In one report of a blood transfusion acquired case of vCJD, imaging at the time of initial clinical presentation was negative for the pulvinar sign and was only positive only when the patient was severely affected, suggesting that the pulvinar sign is a late feature of vCJD [3].

Few studies have investigated measures of water diffusion *in vivo* in vCJD. Two case reports in vCJD have demonstrated decreased ADC in the caudate and putamen but elevated ADC in the thalami [174;175] which in one of the cases was correlated at post-mortem with the detection of predominantly spongiform cellular changes in the caudate and putamen and predominantly astrocytic changes with neuronal loss in the pulvinar nuclei. In our study of formalin fixed specimens, I found no association of MD with any histology measure.

There is a considerable reduction of MD and FA *ex vivo* compared to *in vivo*, with even further reductions in MD post-fixation [196]. It has been postulated that post-fixation, the combination of dehydration of tissue, lower temperature than in vivo and failure of energy dependent ion transport mechanisms [203] may all contribute to decreased MD, possibly reducing the sensitivity to the histopathological changes with the loss of any *in vivo* relationship to histology measures. FA however, is preserved during the fixation process and provides a robust index of the underlying histology.

In our study, I found that FA decreases with the severity of spongiosis and increases with the severity of gliosis in the pulvinar. Very few studies have investigated DTI in the grey matter in neurological diseases. One study of DTI in Huntingdon's Disease (HD) where FA was specifically investigated in the basal ganglia, demonstrated significant increases in FA in the putamen and globus pallidus in patients compared to

controls [204] The authors speculated that the increases in FA could result from pathological processes that modify tissue integrity, such as neuronal remodelling and loss and secondary astrocytosis, particularly in the light of post-mortem studies demonstrating fibrillary astrocytosis in the caudate, putamen and globus pallidus in HD [205]. Our finding of increased FA with gliosis is also supported by a DTI study in the developing mouse brain where high anisotropy was observed in the cortical plate in the embryonic and post-natal stage. As axonal fibres are not predominant in this region, the authors concluded that the high anisotropy was due to the highly organized radial glia [206]. It is likely that the proportion of the different histological changes that are present in the target tissue determines the FA. Whilst astrocytic proliferation may cause organization of the neuropil causing increased anisotropy, it appears that severe spongiform change with areas of confluent vacuolation in the extracellular space may allow water to diffuse more radially with decreased anisotropy.

I found no association between length of fixation and any of our MRI measures. Our samples had been formalin-fixed for much longer than any of the published reports and it is possible that the reduction in T1 and T2 had reached a plateau phase. Although I argue that the relationship of FA with histology measures is not an effect of formalin fixation, it could be argued that small sample size and multiple statistical tests may have limited our findings.

DTI *in vivo* is evolving as a potent tool in the examination of the central nervous system, improving detection of microstructural changes with clinical applications in a wide variety of neurological diseases including neurodegenerative disease [91 207]. In AD, several studies have found a specific pattern of regional abnormalities that involve the fibre tracts of the corpus callosum, and the white matter of the frontal, temporal and parietal lobes which showed strong correlations with neuropsychological measures [99;100]. Studies of the grey matter in AD, have shown increased diffusivity in the right temporal cortex [101]. To our knowledge, there are no reports of the use of DTI *in vivo* in vCJD but our findings suggest that DTI, with specifically measures of FA in the pulvinar, could offer potential for the detection of early histopathological changes and for monitoring disease severity in human prion diseases. vCJD remains an important public health issue, particularly with recent identification of blood-transfusion acquired cases [3;13;14]and DTI could offer great potential in the identification of patients in the early stages of the disease where therapeutic intervention would be most important.

5.5 Conclusion

I have demonstrated that *ex vivo* MRM at 9.4T can depict pathology characteristic of vCJD through apparent loss of the normal intracortical laminations. We have also shown that FA decreases with the severity of spongiosis and increases with severity of astrocytic proliferation in the pulvinar nucleus. Our findings suggest that in the grey matter, astrocytic proliferation in the extracellular space causes directional organization of the neuropil. Measurements of FA in the cerebral cortex and pulvinar, could offer potential for the detection of early histopathological changes and for monitoring disease severity in human prion diseases.

6 Discussion

6.1 Summary of findings in thesis

In this work I aimed to evaluate the potential of quantitative MRI measurements in providing neuroimaging biomarkers of disease activity and in understanding the pathophysiology of prion diseases. We chose to address these aims through a dual strategy of both *in vivo* and *ex vivo* quantitative MRI experiments. The results presented in this thesis demonstrate that I have achieved these aims. At the start of this thesis our aims were:

1. *To detect regional differences in cerebral ADC in variant, sporadic and inherited forms of prion disease when compared to controls.*

I achieved this in chapters 2 and 3 by ROI measurement in the caudate, putamen and thalamus demonstrating different patterns of regional ADC changes in vCJD, sCJD and inhPrD which reflected the different distribution of histopathology in these diseases. I also showed that by probing slower diffusion compartments with high *b* value DWI, there was improved confidence in the detection of pathological signal change in sCJD. Our results suggest that high *b* value DWI could be a useful additional sequence in the radiological diagnosis of prion diseases especially as there have been no previous reports of high-*b*-value DWI in prion diseases.

2. *To establish whether regional and global cerebral ADC in inhPrD correlate with clinical disease severity.*

The results presented in chapter 2 demonstrate an association of whole brain, regional and mean GM ADC with clinical scales of disease severity. In particular the marked association between mean GM ADC and clinical neurological status suggests this measure may provide a promising quantitative biomarker.

3. *To demonstrate whether regional differences in short TE ^{1}H-MRS in inhPrD can be detected compared with controls, can be correlated with disease severity and can be demonstrated to evolve in serial MRS examinations.*

In Chapter 4, I showed that in a small subgroup of inhPrD patients, there was an association of MI with clinical scales of disease activity and an increase in *myo*-inositol with time. Although there have been previous reports of differences in ^{1}H-MRS measurements in patients with prion diseases compared to controls, to our knowledge

there have hitherto been no reported attempts to correlate these differences with clinical scores in order to assess their potential as biomarkers.

4. *To determine whether quantitative MRI measurements of T1- and T2 relaxation times, FA and MD in fixed post-mortem brain tissue at 9.4T can be correlated with histopathological measures to better understand the pathophysiological changes underlying the early disease course.*

In chapter 5, I demonstrated that MRI at high magnetic field strengths can demonstrate the microstructural changes that affect quantitative MRI measurements. In this chapter, I showed a positive association of FA with gliosis and a negative association of FA with spongiosis in the pulvinar in vCJD. It is likely that the proportion of the different histological changes that are present in the target tissue determines the FA. These results also suggest that DTI, with specifically measures of FA in the pulvinar, could offer potential for monitoring disease activity in human prion diseases.

5. *To evaluate whether high resolution MRI images of fixed post-mortem tissue at 9.4T can detect the histopathological changes characteristic of human prion diseases.*

Finally, also in Chapter 5, I showed that high resolution MRI images of fixed post-mortem tissue at 9.4T can detect the histopathological changes characteristic of human prion diseases through loss of intracortical laminations. As high field scanners become more routine in clinical diagnosis, these observations may help distinguish prion diseases from other dementias.

Altogether, our findings show that DWI and ^{1}H-MRS offer potential as neuroimaging biomarkers in future prion disease therapeutic trials. Important insights into the histopathological basis for the MRI changes are observed. Although our results are limited by small numbers and need to be confirmed in larger studies, they confirm the potential of quantitative MRI in understanding the pathophysiology of this disease.

6.2 Potential future directions

6.2.1 MRI as an objective measure in future trials

As the clinical application of emerging neuroimaging techniques expands, the combination of neuroimaging studies with other investigations that provide data on genetic risk and biomarkers from other tissues (such as serum or CSF) might increase the combined diagnostic sensitivity and specificity as well as the predictive value of the information. As a relevant comparison, already in the AD Neuroimaging Initiative, a large multi-centre study is performing structural MRI scans and FDG- PET scans, in addition to other biomarkers to improve diagnostic accuracy and treatment monitoring of this disease [208].

A biomarker is defined as an indicator of disease activity whereas a surrogate marker can substitute as a clinically meaningful end-point in a clinical trial [209]. A useful neuroimaging biomarker would not only be an indirect measure of neurodegeneration but could be used to monitor a relevant aspect of disease pathophysiology, correlate with treatment-induced changes and assist in identifying responders to a specific treatment [210].

Currently in AD, volumetric MRI is the method of choice to monitor drug effects in neurodegenerative disease, especially in Phase II and III registration trials, mainly because the relationship between neuron loss and atrophy has been well-established in many studies [121 211] and also because of the availability of volumetric sequences on most clinical MRI scanners [212]. However, an important application of neuroimaging is in the detection of neuronal dysfunction before neuronal loss, particularly in the context of the administration of neuroprotective drugs. It is likely that quantitative imaging techniques, although only in the research stages at present, are likely to be more helpful.

6.2.2 MRI as a biomarker in future prion disease trials

The National Prion Monitoring Cohort (NPMC) study launched in October 2008 aims to build on the work of PRION-1 by gathering information on clinical care and therapeutic interventions in as many people diagnosed with or at risk of human prion disease as possible. The objectives are to:

- Characterise the natural history of human prion disease
- Develop a staging system to mark disease progression
- Identify surrogate markers of disease progression

- Monitor any treatments received
- Determine clinical onset in at-risk individuals

As no drug is being trialled, a further opportunity to describe the clinical and MRI features in prion diseases will be provided with the aim of identifying and validating neuroimaging and other biomarkers such that when a therapeutic agent becomes available, measures will already be in place to evaluate treatment efficacy.

6.2.2.1 MRI sequences for the NPMC

6.2.2.1.1 DTI

DTI provides measures theoretically independent of the experimental implementation, reflecting aspects of tissue microstructure size, orientation and organization. From this sequence, it is possible to obtain multiple measures characteristic of water self-diffusion which may be more or less sensitive to disease severity. Based on our post-mortem study findings, I would expect increased FA in the grey matter in patients with prion disease, perhaps as a more sensitive marker of disease activity than MD.

6.2.2.1.2 Chemical shift Imaging

Chemical shift imaging allows the acquisition of spectra from multiple voxels during the same acquisition. This technique will significantly shorten the time taken to acquire multiple spectra such that the entire brain can be imaged in approximately 12 minutes. In addition, imaging at higher magnetic field strengths gives improved signal-to-noise ratio, greater spectral separation and likely improved diagnostic accuracy and better test-retest reproducibility for ^{1}H-MRS. Higher magnetic field strengths will also allow more accurate detection of glutamate and glutamine which may provide additional neuroimaging biomarkers

6.2.3 Other imaging techniques

6.2.3.1 PET-amyloid imaging

Recent developments in PET imaging have enabled the detection of β-amyloid in vivo in AD. A number of radiolabelled agents that bind to β-amyloid have recently been developed which have detected amyloid plaques in mice and in humans with AD [213;214]. The most extensive experience has been with amyloid binding radiotracer [^{11}C]-labelled Pittsburgh compound B (2-[4L'-methylamino)phenyl]-6-hydrobenzothiazole; PiB [215], a thioflavin-T amyloid dye derivative that binds to β-amyloid plaques but not to tangles.

Although the amyloid deposits associated with prion diseases and the amyloid deposits found in AD are composed of different peptides, they share common physical-chemical properties [216], including a high β-sheet secondary structure. As thioflavins bind to β-amyloid plaques associated with AD, it is likely that ^{11}C-PiB PET will also provide an in-vivo marker of prion amyloid deposits. Limitations include the invasive nature of the test, the relative inaccessibility compared to MRI and the relatively high costs [217]

6.2.3.2 Monitoring treatments in development

Animal models of prion disease may be useful in the co-development of neuroimaging measures and treatment. In the future, it may be possible to develop PET and MRI labels that specifically bind to PrP^{Sc}. As anti-aggregation treatments are developed for prion disease initial testing of compounds in animals could be followed by pre-clinical trials in small animals with microPET and MRI microscopy to measure a biomarker for PrP-amyloid and to guide investigators on further testing in humans.

7 Conclusion

The findings in this thesis are a major step forward in the understanding of quantitative MRI in prion diseases. I have shown that quantitative MRI measures of ADC at low and high *b*-value and short TE ^{1}H-MRS are potential neuroimaging biomarkers of disease activity. The use of high field *ex vivo* MRI has provided important insights into the microstructural changes underlying the sensitivity of some of these quantitative MRI methods to prion disease-related changes in the brain. The findings presented here exemplify the potential of quantitative MRI in both increasing our understanding of the pathophysiology of prion diseases and to provide neuroimaging biomarkers which will be of great importance for the future assessment of the efficacy of therapeutic agents.

Publications

This section reviews publications produced as a result of this thesis or work on the Prion-1 Trial.

Siddique D, Hyare H, Wroe S, WebbT, Macfarlane R, Rudge P, Collinge J, Powell C, Brandner S, So P-W, Walker S, Mead S, Yousry T, Thornton JS. Magnetisation transfer ratio may be a surrogate of spongiform change in human prion diseases. Brain. In revision.
I prepared all the samples, performed and analysed all the 1.5T and 9.4T post-mortem imaging data and co-wrote the manuscript.

Hyare H, Wroe S, Mead S, Rudge P, Stevens J, Collinge J, Thornton J, Yousry T, Jager R. High B Value diffusion MR imaging and basal nuclei ADC measurements in variant and sporadic Creutzfeldt-Jakob disease. AJNR 2010; 31(3): 521-6.
I performed all the ADC ROI and histogram analysis, statistical analysis and wrote the manuscript.

Hyare H, Wroe S, Siddique D , Webb T, Fox N, Stevens J, Collinge J, Thornton J, Yousry T, Jager HR. Global and regional measures of apparent diffusion coefficient in inherited prion disease: correlation with disease severity. Neurology 2010; 74(8): 658-65.
I performed all the ADC ROI analysis, statistical analysis and wrote the manuscript.

Kaski D, Mead S, Hyare H, Cooper S, Jampana R, Overell J, Knight R, Collinge J, Rudge P. Variant CJD in an individual heterozygous for PRNP codon 129. Lancet 2009; 374(9707):2128.
I performed the quantitative signal intensity analysis on the MRI images and assisted in the discussion.

Wroe SJ, Pal S, Sodium D, Hyare H, Macfarlane R, Joiner S, Lineman JM, Brander S, Wadsworth JD, Hewitt P, Collinge J. Clinical presentation and pre-mortem diagnosis of variant Creutzfeldt-Jakob disease associated with blood transfusion: a case report. Lancet 2006; 68(9552):2061-2067.
I assisted with the figures and discussion.

Published conference abstracts from thesis:

Hyare H, So P-W, Thornton JS, Powell C, Siddique D, Wroe S, Brandner S, Yousry T. Variant Creutzfeldt-Jakob disease: Ex vivo Cytoarchitecture of Frontal Cerebral Cortex at 9.4T. Proceedings of Annual Meeting of ISMRM, Toronto; May 2008: p460

Hyare H, Thornton JS, Powell C, Siddique D, Mancini L, R Jager, Wroe S, Brandner S, So P-W, Yousry T Variant Creutzfeldt-Jakob disease: quantitative diffusion-weighted imaging in vivo at 1.5T and ex vivo at 9.4T with histopathological correlation. Proceedings of Annual Meeting of ISMRM, Toronto; May 2008: p510.

Hyare H, Siddique D, Webb T, Wroe S, Collinge J, Thornton J, Yousry T. Proton magnetic Resonance Spectroscopy as a biomarker in Inherited Prion Disease. Proceedings of Joint Annual Meeting of ISMRM-ESMRMB, Berlin, April 2007; p610.

APPENDICES

Appendix A: Clinical assessment performed.

Appendix B: Prion-1 Trial Neurological exam proforma.

Appendix C: MMSE (Mini Mental State Examination).

Appendix D: CDR (Clinician's Dementia Rating Scale).

Appendix E: ADAS-COG (Alzheimer's Disease Assessment Scale).

Appendix F: BARTHEL (Modified Barthel Score of Activities of Daily Living).

Appendix G: GIC (Global Impression of Change).

Appendix H: Bland Altman Analysis of intra- and inter-observer variability.

Appendix I: Patient Information Sheet for MRI.

Appendix J: Standard Operating Procedures for MRI under General Anaesthetic.

Appendix K: Risk assessment and transportation of tissue specimens to Imperial.

Appendix L: Experiment to determine the effect of perfluoropolyethers (PFPE) on quantitative MRI and corroborative histology.

Appendix M: CJD specimen trail proforma.

APPENDIX A

Clinical assessment

All neurological assessments were performed by a qualified neurologist: either the Consultant Neurologist at the National Prion Clinic or by the two neurology Research Fellows. In addition, the following neurological rating scale scores were calculated at each time point in order to assess disease severity:

- Mini Mental State Examination (MMSE) [138]: used as an overall severity score for cognitive function. A maximum score of 30 indicates no deficit of memory or language and a minimum score of 0 indicates severe deficit of memory and language.
- Clinician's Dementia Rating Scale (CDR) [139]: a measure widely used in clinical studies of dementia. Using a semi-structured interview with the patient or a caregiver, it measures a patient's function in areas of memory, orientation, judgement and problem solving, community affairs, home and hobbies, and personal care, providing a score ranging from 0 to18. Each component is scored from 0 to 3 (0=no impairment, 1=mild impairment, 2=moderate impairment, 3=severe impairment).
- Rankin scale [140]: a global assessment of the impact of disease on activities of daily living, providing a score ranging from 0 to 5 (0=no symptoms, 1=no significant disability despite symptoms, 2=slight disability, 3=moderate disability, 4=moderately severe disability, 5=severe disability).
- Alzheimer's Disease Assessment Scale (ADAS-COG) [141]: performed in those with a MMSE of 10 or greater. This is a more detailed assessment of cognition, validated in Alzheimer's disease. Score ranges from 0 to 75. It assesses 12 items covering word recall, naming objects and fingers, performing simple commands, constructional praxis, ideational praxis, orientation, word recognition, remembering test instructions, spoken language ability, word-finding difficulty, comprehension and concentration.
- Barthel Activities of Daily Living scale (ADL) [142]: measures ability to perform activities of daily living on a scale of 0 (unable to perform any ADL) to 20 (can perform all ADSL).
- A clinician's global impression of disease severity (CGIS) [143]: A scoring system completed by both doctors and nurses to assess change in severity of disease

(0=normal, not ill, 1=borderline mentally ill, 3=mildly ill, 4=moderately ill, 5=markedly ill, 6=severely ill, 7=amongst the most ill).

- Brief Psychiatric Rating Scale (BPRS) [144]: Psychiatric status was assessed by using a series of standardised structured questions, providing a final score ranging from 24 to 168. It scored 24 items on a qualitative scale from 1 to 7 (according to whether the symptom was absent, very mild, mild, moderate, moderately severe, severe or extremely severe). Components included somatic concern, anxiety, depression, sociality, guilt, hostility, elated mood, grandiosity, suspiciousness, hallucinations, unusual thought content, bizarre behaviour, self-neglect, disorientation, conceptual disorganisation, blunted affect, emotional withdrawal, motor retardation, tension, uncooperativeness, excitement distractibility, motor hyperactivity, mannerisms and posturing, anxiety, depression, hostility, disorientation and blunted affect.

APPENDIX B

FORM 7	PRION-1 TRIAL **NEUROLOGICAL EXAMINATION**

MRC PRION-1

Date form completed: Day ☐☐ Month ☐☐ Year 2 0 0 ☐ Male ○ Female ○ Initials ☐☐☐ Soundex ☐☐☐☐

Date of birth: ☐☐ ☐☐ 1 9 ☐☐ Hospital Number ☐☐☐☐☐☐☐

PRION-1 Study Number ☐☐☐☐☐☐ Video ID number ☐☐☐ Visit week number 0 4 8 16 24 36 48 60 72 84 96 Extra

NEUROLOGICAL EXAMINATION

1. **Is the neurological examination being digitally recorded?** ..... Yes ☐ No ☐ Full video ☐ Severely affected protocol *☐

2. **Cognitive Function** (For all tests: Tick if correct, cross if incorrect, leave blank if not tested, U if unable to quantify)

No.	Task	Standard Question	Workings	Number Correct
1.*	Memory	"What is your name? What is your age? Which month is your birthday in?"	name / age / month	/ 3
2.	Letter cancelling	"Can you show me all the letter A / B / E's?"		/ 12
3.	Line drawings	"Can you tell me what these drawings are?"	scorpion/ tricycle/ spade/ owl/ violin/ hippo/ ladybird/ peg/ squirrel/ padlock beetle/trolley/spanner/cockerel/guitar/camel/butterfly/nail/goat/door handle crab/skateboard/basket/duck/harp/kangaroo/spider/safety pins/sheep/key	/ 10
4.	Reading passage	"Can you read this passage out for me? I will ask you some questions about it later."	dysphasia / poor fluency / neologism	norm/mild/mod/sev
5.	Spelling	"Can you spell the word...as in..."	aunt / eye / build / humour / neighbour / autumn	/ 6
6.	Fragmented letters	"Can you see any letters here?"	E / N / K L / M / P A / C / W	/ 3
7.	Fragmented objects	"Can you see any objects here?"	teapot / shoe / chair / guitar or violin pig / cake / boot / car fish / boat / plane / dog	/ 4
8.	Calculation	"I'd like you to do some sums for me. What is..."	5+4(9), 7+5(12), 13+8(21), 17+25(42)	/ 4
9.	Miming	"Show me how you."	brush teeth / comb hair / use a screwdriver	/ 3
10.	Copying gestures	"Can you copy these shapes for me with your hand?"	'ring' / 'horns' / 'three prongs'	/ 3
11.	Frontal lobe sequencing	"Can you copy this for me?"	-	norm/mild/mod/sev
12.	Words beginning with the letter	"Can you give me as many words beginning with the letter F / A / S as possible?" (Choose one only)		
13.	Proverbs	"Can you tell me what these sayings mean?"	strike while the iron / too many cooks	/ 2
14.	Digit span	"Can you repeat these numbers after me?"	5-8-2, 6-4-3-9, 4-2-7-3-1, 6-1-9-4-7-3, 5-9-1-7-4-2-8	/ 5
15.	Recall	"Tell me everything you can remember about the passage you read out to me"		norm/mild/mod/sev

Motor Function

No.	Task	Standard question	Right	Left	Example
16.*	Eye movements	"Keep your head still and follow my finger with your eyes"	norm / nystagmus / failure of upgaze / other		
17.	Finger-nose testing	Put your index finger on your nose....then on my finger...and keep going backwards and forwards between the two" ...and now with the other hand"	norm / mild / mod / sev	norm / mild / mod / sev	
18.	Rapid alternating hand movements	"Can you copy this for me?...and with the other hand"	norm / mild / mod / sev	norm / mild / mod / sev	
19.	Sequential index finger tapping	"Can you do this for me?" "And with the other hand"	norm / mild / mod / sev	norm / mild / mod / sev	
20.	Sequential opposition	"Can you do this for me?" "And with the other hand"	norm / mild / mod / sev	norm / mild / mod / sev	
21.*	Primitive reflexes	"Could you look straight ahead for me? I am just going to tap on your forehead...and now on your lip...and look at the camera while I stroke your hands...and now I'm going to touch your hand"	norm / glabellar / pout / palmomental / grasp present		
22.*	One minute hand observation	"Could you put your hands on your knees and relax for a minute while we watch your hands?"	norm / myoclonus / chorea / tremor / other		
23.	Walking	"Could you walk to....and back again for me?"	gait: norm / ataxic / apraxic / cerebellar impairment: norm / mild / mod / sev / wheelchair / bedbound scale: 0 / 1 / 2 / 3 / 4 / 5 / 6		
24.	Heel toe walking	"Can you put one foot in front of the other like this?"	norm / mild / mod / sev / wheelchair / bedbound		
25.	Rombergs	"Can you stand with your feet together....and now shut your eyes"	norm / abnormal		
26.*	Neurological exam	Tone/ Power/ Reflexes (esp plantar)	norm tone / pow / ref abnormal tone / pow / ref	norm tone / pow / ref abnormal tone / pow / ref	

Overall assessment

	Yes	No	Fluctuates
Is patient able to cope with task demands?			
Is overall level of attention and concentration satisfactory?			
Is the patient cooperative?			

Overall impression of impairment in this patient was:

	None	Mild	Moderate	Severe	Cannot assess
Cognitive Impairment					
Extrapyramidal Impairment					
Pyramidal Impairment					
Cerebellar Impairment					

Signature		Print name		Date		Video Identification Number	

APPENDIX C

FORM 6

PRION-1 TRIAL

MMSE

MRC PRION-1

Date test performed: Day ☐☐ Month ☐☐ Year 2 0 0 ☐ Male ○ Female ○ Initials ☐☐☐ Soundex ☐☐☐☐

Date of birth: ☐☐ ☐☐ 1 9 ☐☐ Inpatient ☐ Outpatient ☐ Home ☐ Hospital Number ☐☐☐☐☐☐☐

PRION-1 Study Number ☐☐☐☐☐☐ Visit month number **0** ☐ **1** ☐ **2** ☐ **4** ☐ **6** ☐ **9** ☐ **12** ☐ **15** ☐ **18** ☐ **21** ☐ **24** ☐ **Extra** ☐

MINI MENTAL STATE EXAMINATION (MMSE)

Score each **correct** answer or action as shown in italics. Approach the patient with respect and encouragement. Ask

Do you have any trouble with your memory? ..... Yes ☐ No ☐

May I ask you some questions about your memory? ..... Yes ☐ No ☐

Time orientation	What is the	year?	_____	*(1)*	**Score**
		season?	_____	*(1)*	
		month of the year?		*(1)*	
		date?		*(1)*	
		day of the week?	_____	*(1)*	Total ☐
Place orientation	Where are we now? What is the	country?	_____	*(1)*	
		county?	_____	*(1)*	
		town or city?		*(1)*	
		building?		*(1)*	
		floor of the building?		*(1)*	Total ☐
Word registration	Listen carefully. I am going to say 3 words. You say them back to me after I stop. Ready? Here they are … LEMON (wait 1 second), KEY (wait 1 second), BALL (wait 1 second). What were those words?		_____	*(1)*	
			_____	*(1)*	
				(1)	Total ☐
	(Repeat the words until the patient learns all three)				
Attention and calculation	Subtract 7 from 100 and continue to subtract 7 from each subsequent remainder until I tell you to stop. What is	100 take away 7?	_____	*(1)*	
	Keep going		_____	*(1)*	
				(1)	
				(1)	
				(1)	
	Please spell WORLD for me? Then ask him/her to spell it backwards:			*(1)*	
				(1)	
				(1)	
				(1)	
			_____	*(1)*	Total ☐ (for the best performed task)
Word recall	What were those 3 words I asked you to remember?		_____	*(1)*	
			_____	*(1)*	
				(1)	Total ☐
Naming	What is this	*(show pencil)*?	_____	*(1)*	
		(show watch)?		*(1)*	Total ☐
Repetition	Now I am going to ask you to repeat what I say. Ready … ? No ifs, ands, or buts. Now you say that.		_____	*(1)*	Total ☐
Comprehension	Listen carefully because I am going to ask you to do something. Take this paper	in your right hand	No ☐ Yes ☐	*(1)*	
		fold it in half	No ☐ Yes ☐	*(1)*	
		and put it on the floor	No ☐ Yes ☐	*(1)*	Total ☐
Reading	Please read the following and do what it says, but do not say it aloud *(Give the patient the sheet with "Close your eyes" on it)*		No ☐ Yes ☐	*(1)*	Total ☐
Writing	Please write a sentence. *(If the patient does not respond say* Write about the weather*)*		No ☐ Yes ☐	*(1)*	Total ☐
Drawing	Please copy this design. *(Hand the sheet with the design to the patient)*		No ☐ Yes ☐	*(1)*	Total ☐
					Total Score (sum) = ☐

Doctor's signature	Print name	Date

APPENDIX D

FORM 11

PRION-1 TRIAL

CDR

MRC PRION-1

Date test performed — Day / Month / Year (2 0 0) — Male ○ Female ○ — Initials — Soundex

Date of birth — (1 9) — Inpatient ☐ Outpatient ☐ Home ☐ — Hospital Number

PRION-1 Study Number

Visit month number: **0** ☐ **1** ☐ **2** ☐ **4** ☐ **6** ☐ **9** ☐ **12** ☐ **15** ☐ **18** ☐ **21** ☐ **24** ☐ **Extra** ☐

CLINICIAN'S DEMENTIA RATING (CDR)

Each of the 6 domains should be rated by circling the number by the term that best describes the patient's current capabilities. Rate each domain as independently as possible, as it is not unusual for patients to have varying degrees of impairment across domains. Only assign scores greater than 0 if impairment is due to cognitive loss.

			Score
Memory	No memory loss or slight inconstant forgetfulness	0	
	Mild consistent forgetfulness; partial recollection of events; "benign" forgetfulness	0.5	
	Moderate memory loss; more marked for recent events; defect interferes with everyday activities	1	
	Severe memory loss; only highly learned material retained; newly material rapidly lost	2	
	Severe memory loss; only fragments remain	3	☐
Orientation	Fully orientated	0	
	Fully orientated except for slight difficulty with time relationships	0.5	
	Moderate difficulty with time relationships; orientated for place at examination, but may have geography disassociation elsewhere	1	
	Severe difficulty with time relationships; usually disorientated in time, often in place	2	
	Orientated to person only	3	☐
Judgement and problem solving	Solves everyday problems well; judgement good in relation to past performance	0	
	Only slight impairment in solving problems, similarities, differences	0.5	
	Moderate difficulty in handling problems, similarities, differences; social judgement usually maintained	1	
	Severely impaired in handling problems, similarities, differences; social judgement usually impaired	2	
	Unable to make judgements or solve problems	3	☐
Community affairs	Independently functions at usual level in job, shopping, business and financial affairs, volunteer and social groups	0	
	Slight impairment in these activities	0.5	
	Unable to function independently at these activities although may still be engaged in some; appears normal to casual inspection	1	
	No pretence of independent function outside home; appears well enough to be taken to functions outside family home	2	
	No pretence of independent function outside home; appears too ill to be taken outside family home	3	☐
Home and hobbies	Life at home, hobbies, intellectual interests well maintained	0	
	Life at home, hobbies, intellectual interests well slightly impaired	0.5	
	Mild but definite impairment of function at home; more difficult chores abandoned; more complicated hobbies and interests abandoned	1	
	Only simple chores preserved; very restricted interests, poorly sustained	2	
	No significant function at home	3	☐
Personal care	Fully capable of self care	0	
	Needs prompting	1	
	Requires assistance in dressing, hygiene, keeping of personal effects	2	
	Requires substantial help with personal care; frequently incontinent	3	☐

Total Score (sum) = ☐

Doctor's signature	Print name	Date

APPENDIX E

FORM 10

PRION-1 TRIAL
ADAS-COG

MRC PRION-1

Date test performed: Day ☐☐ Month ☐☐ Year 2 0 0 ☐ | Male ❍ Female ❍ | Initials ☐☐☐ | Soundex ☐☐☐☐

Date of birth: Day ☐☐ Month ☐☐ Year 1 9 ☐☐ | Inpatient ☐ Outpatient ☐ | Home ☐ | Hospital Number ☐☐☐☐☐☐☐

PRION-1 Study Number ☐☐☐☐☐☐

Visit month number: 0 ☐ 1 ☐ 2 ☐ 4 ☐ 6 ☐ 9 ☐ 12 ☐ 15 ☐ 18 ☐ 21 ☐ 24 ☐ Extra ☐

ALZHEIMER'S DISEASE ASSESSMENT SCALE (ADAS-COG)

Score each **incorrect** answer or action in each of the 11 domains below.

1. Word recall

I am going to show you some words, one at a time. Please read each word out loud and try to remember it, because later I will ask you to try to remember all of the words I have shown you. *(The patient reads aloud 10 words exposed for 2 seconds each. The patient then recalls the words aloud. Three trials of reading and recalling are given.)*

Trial 1	Recalled	Not recalled
Butter	☐	☐
Arm	☐	☐
Shore	☐	☐
Letter	☐	☐
Queen	☐	☐
Cabin	☐	☐
Pole	☐	☐
Ticket	☐	☐
Grass	☐	☐
Engine	☐	☐
Total not recalled		

Trial 2	Recalled	Not recalled
Pole	☐	☐
Letter	☐	☐
Butter	☐	☐
Queen	☐	☐
Arm	☐	☐
Shore	☐	☐
Grass	☐	☐
Cabin	☐	☐
Ticket	☐	☐
Engine	☐	☐
Total not recalled		

Trial 3	Recalled	Not recalled
Shore	☐	☐
Letter	☐	☐
Arm	☐	☐
Cabin	☐	☐
Pole	☐	☐
Ticket	☐	☐
Engine	☐	☐
Grass	☐	☐
Butter	☐	☐
Queen	☐	☐
Total not recalled		

Score = mean number of words not recalled on 3 trials (maximum = 10) = ☐

2. Naming objects and fingers

I am going to show you some objects. What is this called? *or* What is the name of this thing? *(If the patient does not respond, give the cue listed below. If the patient still does not respond or makes an error go onto the next object).*

Objects	Standard clue that can be used to assist those patients having difficulties	Correct	Incorrect (or not named)
Flower	- grows in the garden	☐	☐
Bed	- used for sleeping	☐	☐
Whistle	- makes a sound when you blow it	☐	☐
Pencil	- used for writing	☐	☐
Rattle	- a baby's toy	☐	☐
Mask	- hides your face	☐	☐
Scissors	- cuts paper	☐	☐
Comb	- used on hair	☐	☐
Wallet	- holds your money	☐	☐
Harmonica	- a musical instrument	☐	☐
Stethoscope	- doctor uses it to listen to your heart	☐	☐
Tweezers	- used to pick up things	☐	☐
Now can you name the fingers on your left/right *(dominant)* hand?		☐	☐
Thumb		☐	☐
Index		☐	☐
Middle		☐	☐
Ring		☐	☐
Little		☐	☐
		Total incorrect	

Score (**0**=0-2 incorrect; **1**=3-5 incorrect; **2**=6-8 incorrect; **3**=9-11 incorrect; **4**=12-14 incorrect; **5**=15-17 incorrect) = ☐

3. Commands

I am going to ask you to do some actions. *(Each command should be read once. If the patient does not respond, or makes an error, give the command one more time. Then go onto the next command. All commands should be given.)*

Command *(Each underlined element represents a single step. Each command is scored as a whole)*	Correct	Incorrect (or not performed)
Make a fist	☐	☐
Point to the ceiling and then to the floor	☐	☐
Line up a pencil, watch, and card, in that order, on a table in front of the patient		
Put the pencil on top of the card and then put it back	☐	☐
Put the watch on the other side of the pencil and then turn over the card	☐	☐
Tap each shoulder twice, with two fingers, keeping your eyes shut	☐	☐

Score = number of incorrectly performed commands (minimum 0, maximum 5) = ☐

4. Constructional praxis

On this paper is a shape. Try to draw another one that looks just like this, somewhere on the page.
(Allow 2 attempts for each shape, then go onto the next shape. A drawing should be scored as correct if the patient has reproduced all the essential geometric features of the original. Changes in size do not count as errors. Small gaps between lines do not indicate an error, as long as the shape has been reproduced.)

Shape	Correct	Incorrect (or not drawn)
Circle *(a closed curved figure)*	☐	☐
Two overlapping rectangles	☐	☐

(forms must be 4-sided, and overlap must be similar to presented form. Changes in size are not scored.)

Correct Incorrect

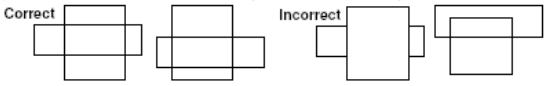

Diamond *(Figure must be 4-sided, oriented with points at the top and bottom, and the sides are approximately equal length.)*	☐	☐

Correct Incorrect

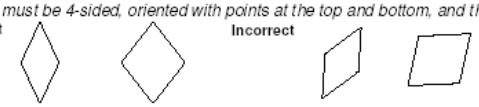

Cube *(The form is 3-dimensional, with front face in the correct orientation, internal lines drawn correctly between corners. Opposite sides of faces should be approximately parallel.)*	☐	☐

Correct Incorrect

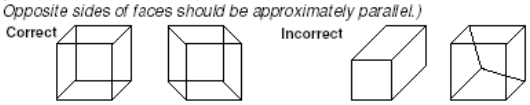

Total ☐ **correct**

Score = number of incorrectly drawn figures (score=**5** if only scribbles, parts of shapes, or words) = ☐

5. Ideational praxis

I want you to pretend that you have written yourself a letter. Take this piece of paper, fold it so that it will fit into the envelope, and then put it into the envelope. Then seal the envelope, address the envelope to yourself, and show me where the stamp goes. *(If the patient forgets part of the task, or is having difficulty, repeat the instruction for the component of the task where the patient is having difficulty.)*

Command	Correct	Incorrect (or not performed)
Fold a letter	☐	☐
Put the letter in an envelope	☐	☐
Seal the envelope	☐	☐
Address the envelope	☐	☐
Indicate where the stamp goes	☐	☐

Score = number of incorrectly performed commands = ☐

6. Orientation

Ensure that no clocks, watches, or calendars are visible.

	Correct	Incorrect (or not answered)		Correct	Incorrect (or not answered)
Full name *(first and last)*	☐	☐	Year	☐	☐
Day	☐	☐	Season *(within 1 week of upcoming or 2 weeks of previous season)*	☐	☐
Date *(± 1 day)*	☐	☐	Time of day *(± 1 hour)*	☐	☐
Month	☐	☐	Place *(partial or full name of site)*	☐	☐

Score = number of incorrect answers = ☐

7. Word recognition

FORM 10	PRION-1 TRIAL **ADAS-COG**

MRC PRION-1

I am going to show you some words printed on cards. I want you to read each word out loud and try to remember it. *(If the patient cannot read a word, say the word out loud. However, it is important for the patient to actually look at each word and try to read it.)* Now I'm going to show you another set of words. Some of the words were on the list I just showed you, and others are new. For each word, I want you to tell me whether it is one of the words I just showed you. Is this one of the words I showed you before, yes or no? *(or* Did I show you this word before?*) (The same instruction is given before the second test word. For the remaining test words say* How about this one?*) (If the patient does not remember the task (eg reads the word rather than responding "Yes" or "No"), then repeat or rephrase the entire question and make a note that the patient had to be reminded.)*

Trial 1	Yes/ Shown	No/ New	Remind
Nurse	○	☐	☐
Magazine	☐	○	☐
Wizard	☐	○	☐
Van	☐	○	☐
Leopard	☐	○	☐
Sale	○	☐	☐
Sea	☐	○	☐
Train	☐	○	☐
Coin	☐	○	☐
Ship	○	☐	☐
Institution	☐	○	☐
Map	○	☐	☐
Axe	○	☐	☐
Board	☐	○	☐
Carrot	○	☐	☐
Milk	○	☐	☐
Volume	○	☐	☐
Forest	○	☐	☐
Anchor	☐	○	☐
Gem	☐	○	☐
Cat	○	☐	☐
Fund	☐	○	☐
Edge	○	☐	☐
Cake	○	☐	☐
Total circles ticked (incorrect response)			☐

Trial 2	Yes/ Shown	No/ New	Remind
Board	☐	○	☐
Turnip	○	☐	☐
Gem	☐	○	☐
Institution	☐	○	☐
Coin	☐	○	☐
Master	○	☐	☐
Magazine	☐	○	☐
Van	☐	○	☐
Anchor	☐	○	☐
Lumber	○	☐	☐
Servant	○	☐	☐
Pond	○	☐	☐
Military	○	☐	☐
Hospital	○	☐	☐
Sea	☐	○	☐
Jungle	○	☐	☐
Nail	○	☐	☐
Wizard	☐	○	☐
Leopard	☐	○	☐
Train	☐	○	☐
Editorial	○	☐	☐
Bread	○	☐	☐
Fund	☐	○	☐
Trade	○	☐	☐
Total circles ticked (incorrect response)			☐

Trial 3	Yes/ Shown	No/ New	Remind
Coin	☐	○	☐
Plank	○	☐	☐
War	○	☐	☐
Porch	○	☐	☐
Toast	○	☐	☐
Rope	○	☐	☐
Anchor	☐	○	☐
Board	☐	○	☐
Leopard	☐	○	☐
Judge	○	☐	☐
Magazine	☐	○	☐
Camp	○	☐	☐
Sea	☐	○	☐
Institution	☐	○	☐
Tack	○	☐	☐
Emerald	○	☐	☐
Van	☐	○	☐
Globe	○	☐	☐
Train	☐	○	☐
Fund	☐	○	☐
Coast	○	☐	☐
Gem	☐	○	☐
Wizard	☐	○	☐
Kitten	○	☐	☐
Total circles ticked (incorrect response)			☐

Score = mean number of incorrect words on 3 trials (max=12; score 12 if average more than 12 incorrect responses) = ☐

8. Remembering test instructions

Evaluate the patient's ability to remember the requirements of the word recognition task above.

0 did not need any extra reminders of instructions
1 very mild – forgot once
2 mild – reminded twice
3 moderate – reminded 3 or 4 times
4 moderately severe – reminded 5 or 6 times
5 severe – reminded 7 or more times

Score = ☐

9. Spoken language ability

Provide a global rating of the quality of speech, ie clarity, difficulty in making oneself understood.

0 no instance where it is difficult to understand the patient
1 very mild – one instance of lack of understandability
2 mild – patient has difficulty less than 25% of time
3 moderate – patient has difficulty 25-50% of time
4 moderately severe – patient has difficulty more than 50% of time
5 severe – one or two word utterance; fluent, but empty speech; mute

Score = ☐

10. Word-finding difficulty in spontaneous speech

Rate the patient's difficulty in finding desired words, e.g., circumlocutions.

0 no evidence of word-finding difficulty in spontaneous speech

1 very mild – 1 or 2 instances, not clinically significant

2 mild – noticeable circumlocution or synonym substitution

3 moderate – loss of words without compensation on occasion

4 moderately severe – frequent loss of words without compensation

5 severe – nearly total loss of content words; speech sounds empty; 1-2 words utterances

Score = ☐

11. Comprehension

Rate the patient's ability to understand speech. Do not include responses to commands.

0 no evidence of poor comprehension

1 very mild – 1-2 instances of misunderstanding

2 mild – 3-5 instances of misunderstanding

3 moderate – requires several repetitions and rephrasing

4 moderately severe – patient only occasionally responds correctly; e.g., yes/no questions

5 severe – patient rarely responds to questions appropriately, not due to poverty of speech

Score = ☐

12. Concentration/distractibility

Rate the frequency with which the patient is distracted by irrelevant stimuli and/or must be reoriented to the ongoing task because the patient has lost his/her train of thought or appears to be caught up in his/her own thoughts.

0 no evidence of poor concentration or distractibility

1 very mild – one instance of poor concentration

2 mild – 2-3 instances of poor concentration/distractibility; signs of restlessness and inattentiveness

3 moderate – 4-5 instances during interview

4 moderately severe – poor concentration/distractibility throughout much of interview

5 severe – extreme difficulty in concentration and extremely distractible, unable to complete tasks

Score = ☐

SCORE SUMMARY

Copy the scores in each domain from the grey boxes, then total.

1 Word recall *(max 10)* ☐	**5** Ideational praxis *(max 5)* ☐	**9** Spoken language ability *(max 5)* ☐
2 Naming objects and fingers *(max 5)* ☐	**6** Orientation *(max 8)* ☐	**10** Word-finding difficulty in spontaneous speech *(max 5)* ☐
3 Commands *(max 5)* ☐	**7** Word recognition *(max 12)* ☐	**11** Comprehension *(max 5)* ☐
4 Constructional praxis *(max 5)* ☐	**8** Remembering test instructions *(max 5)* ☐	**12** Concentration/ distractability *(max 5)* ☐

Total score ***(max 75)*** ☐

Doctor's signature	Print name	Date

APPENDIX F

FORM 9

PRION-1 TRIAL

BARTHEL ADL

MRC PRION-1

Date test performed: Day ☐☐ Month ☐☐ Year 2 0 0 ☐ Male ○ Female ○ Initials ☐☐☐ Soundex ☐☐☐☐

Date of birth: ☐☐ ☐☐ 1 9 ☐☐ Inpatient ☐ Outpatient ☐ Home ☐ Hospital Number ☐☐☐☐☐☐☐

PRION-1 Study Number ☐☐☐☐☐☐

Visit month number 0 ☐ 1 ☐ 2 ☐ 4 ☐ 6 ☐ 9 ☐ 12 ☐ 15 ☐ 18 ☐ 21 ☐ 24 ☐ Extra ☐

MODIFIED BARTHEL ACTIVITIES OF DAILY LIVING (ADL)

A) Bowels Score = ☐
- 0: Incontinent or needs enema
- 1: Occasional accident
- 2: Continent

B) Bladder Score = ☐
- 0: Incontinent or catheterised
- 1: Occasional accident
- 2: Continent for > 7 days

C) Grooming Score = ☐
- 0: Needs help with personal care
- 1: Independent with aids if necessary

D) Toilet use Score = ☐
- 0: Dependent
- 1: Needs some help
- 2: Fully independent

E) Feeding Score = ☐
- 0: Unable
- 1: Needs help
- 2: Independent

F) Transfers Score = ☐
- 0: Unable, no sitting balance
- 1: Major help (one or two people, physical), can sit
- 2: Minor help (verbal or physical)
- 3: Independent

G) Mobility Score = ☐
- 0: Immobile
- 1: Wheelchair – independent
- 2: Walk with help of one person
- 3: Independent

H) Dressing Score = ☐
- 0: Dependent
- 1: Needs help
- 2: Independent

I) Stairs Score = ☐
- 0: Unable
- 1: Needs help
- 2: Independent

J) Bathing Score = ☐
- 0: Dependent
- 1: Independent

Total Score (sum, max 20) = ☐

APPENDIX G

FORM 12

PRION-1 TRIAL

GLOBAL IMPRESSION OF CHANGE

MRC PRION-1

Date test performed: Day | Month | Year 2 0 0 | Male ❍ Female ❍ | Initials | Soundex

Date of birth: 1 9 | Inpatient ☐ Outpatient ☐ Home ☐ | Hospital Number

PRION-1 Study Number | Visit month number: 0 ☐ 1 ☐ 2 ☐ 4 ☐ 6 ☐ 9 ☐ 12 ☐ 15 ☐ 18 ☐ 21 ☐ 24 ☐ Extra ☐

RATING OF GLOBAL SEVERITY

Each rater should select the **one** descriptor which best characterises your global impression of the patient's **current** condition. Your rating should be carried out independently, but be based on information derived from review of patient records and other study assessments and may note information elicited from other study personnel (CIBIC-plus).

1 Normal, not ill at all
2 Borderline mentally ill
3 Mildly ill
4 Moderately ill
5 Markedly ill
6 Severely ill
7 Amongst the most ill

	Day	Month	Year		
Doctor	Date of Rating			2 0 0	Rating ☐	Rater's Initials
Nurse	Date of Rating			2 0 0	Rating ☐	Rater's Initials

RATING of CHANGE from BASELINE

Select the **one** descriptor which best characterises your global impression of the patient's **current** condition relative to the patient's condition at **baseline** (trial/study entry). Your rating should be carried out independently, and be based **only** on information derived from your **interviews with both the patient and the caregiver**, with reference to your notes from the baseline interview (CIBIC-plus).

1 Markedly improved
2 Moderately improved
3 Minimally improved
4 Unchanged
5 Minimally worse
6 Moderately worse
7 Markedly worse

Note: **mild** means there should be a "**detectable**" change in the patient; **moderate** that the degree of change should be "**clearly apparent**"; and **marked** that the degree of change should be considered "**dramatic**".

	Day	Month	Year		
Doctor	Date of Rating			2 0 0	Rating ☐	Rater's Initials
Nurse	Date of Rating			2 0 0	Rating ☐	Rater's Initials

RATING of CHANGE from LAST ASSESSMENT

This following section should be completed by the doctor completing the sections above

Using the same scale, select the **one** descriptor which best characterises the composite global impression of all the clinical and nursing staff of the patient's **current** condition relative to the patient's condition at **the last assessment**.

	Day	Month	Year		
Overall	Date of Rating			2 0 0	Rating ☐	Rater's Initials
Cognitive Performance	Date of Rating			2 0 0	Rating ☐	Rater's Initials
Motor skills	Date of Rating			2 0 0	Rating ☐	Rater's Initials
Psychiatric Status	Date of Rating			2 0 0	Rating ☐	Rater's Initials

Doctor's signature	Print name	Date

Nurse's signature	Print name	Date

APPENDIX H

Intra-observer and inter-observer variability:

To assess intraobserver variability, the ROI analysis in all 6 regions was repeated for 4 patient data-sets in 2 sessions separated by 10 days. Bland-Altman analysis demonstrated a mean difference of -5.1 mm^2/s, (95% CI = -13.75 to 3.55), p=0.235.

Output:

```
. Biography time1 time2

Number of measurement pairs: 24

difference derived: time1-time2
Mean difference (relative bias) = -5.1000036, 95% CI = [-13.755958, 3.5559507]
SD of difference = 20.498966 SE of difference= 4.184334

Test (t-test) that mean difference is zero: t= -1.2188328 do= 23 P= .2352616

95% of differences are predicted to lie within the 95% limits of agreement: -
46.097936, 35.897929

These limits of agreement are of course estimates, and have the following
confidence intervals:
95% CI for LOWER limit of agreement = [-61.090489, -31.105383]
95% CI for UPPER limit of agreement = [20.905376, 50.890481]

SD of time1: 43.668542
SD of time2: 49.441602

Pitman test of equality of paired variances: P=.17214367

The mean difference and the 95% limits of agreement are indicated on the
Bland-Altman graph...
```

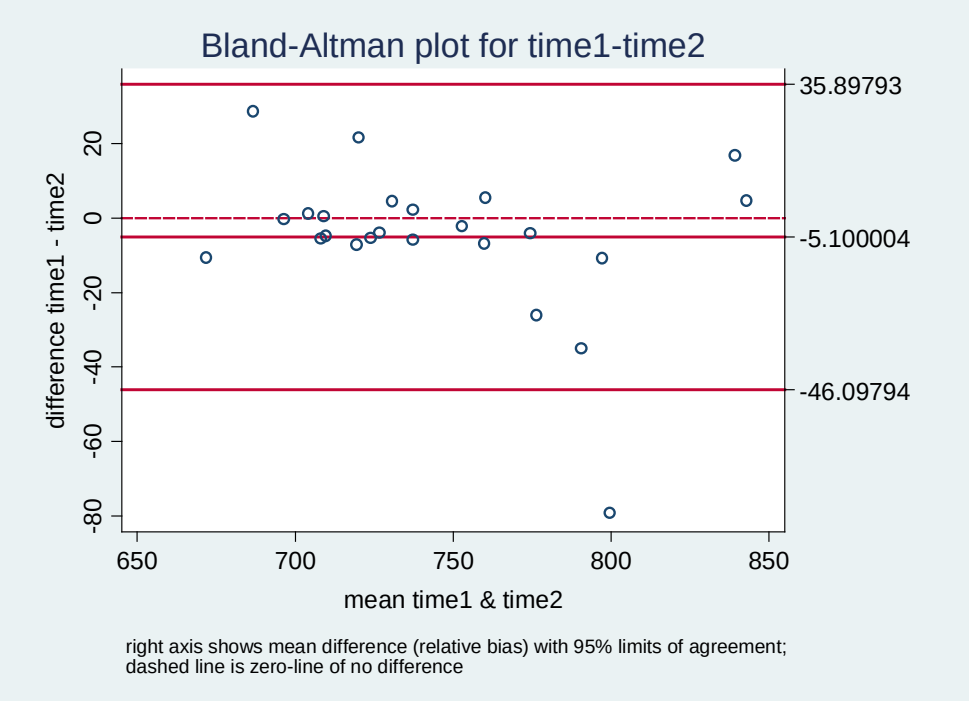

Inter-observer variability:

To assess inter-observer variability, a second observer placed ROIs on the same four patients and Bland-Altman analysis demonstrated a mean difference of 3.81 mm^2/s, (95% CI = -5.47 to 13.08), p=0.40.

Output:

```
. Biography observer1 observer2

Number of measurement pairs: 24

difference derived: observer1-observer2
Mean difference (relative bias) = 3.808342, 95% CI = [-5.4670195, 13.083703]
SD of difference = 21.965842 SE of difference= 4.4837587

Test (t-test) that mean difference is zero: t= .84936373 do= 23 P= .40443343

95% of differences are predicted to lie within the 95% limits of agreement: -
40.123342, 47.740026

These limits of agreement are of course estimates, and have the following
confidence intervals:
95% CI for LOWER limit of agreement = [-56.188739, -24.057944]
95% CI for UPPER limit of agreement = [31.674628, 63.805423]

SD of observer1: 65.470005
SD of observer2: 60.284534

Pitman test of equality of paired variances: P=.25957636

The mean difference and the 95% limits of agreement are indicated on the
Bland-Altman graph...
```

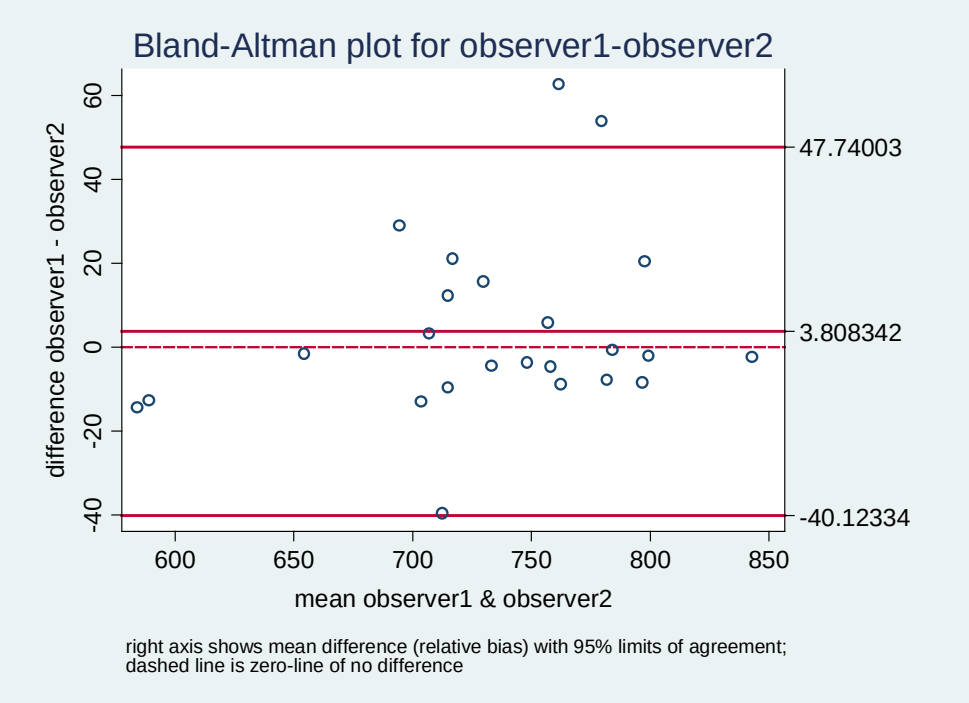

APPENDIX I

Patient Information Sheets: PRION-1: Clinical investigations

(*Form to be on local headed paper)*

Version: 2.0 Date: 12 January 2006

PRION-1: MRI

What is MRI?

MRI stands for Magnetic Resonance Imaging. This is a scanning procedure that uses a combination of a strong magnet, radio waves and a computer to produce very detailed pictures of your body. The scan will not hurt and has no long-term effect on your body once it is over.

What does an MRI scan show?

An MRI scan provides pictures of the inside of your body. Whereas an ordinary x-ray produces very good pictures of the bones, an MRI scan can show details of the brain, muscles, nerves, cartilage and other internal organs.

Preparation for an MRI scan

As the MRI scanner uses a very strong magnet, there are some safety guidelines that must be followed. Let the staff in the scanning department know as soon as possible if any of the following applies to you:

- you have a pacemaker
- you have an artificial heart valve
- you have ever had surgery on your head or spine
- you have any metallic implants, for example joint replacement
- you have ever had metal in your eyes, for example from welding or metalwork
- you may be pregnant

In some of these cases you may need to have an X-ray to make sure that it is safe for you to have an MRI scan. The staff in the MRI Department will discuss this with you. You will also be asked to remove personal belongings such as your watch, jewellery, keys, credit cards and coins. This is because if you go into the scan room with loose metal objects in your pockets they may be pulled out by the strong magnetic field and fly into the scanner. If you wear your watch into the scanner it may not work when you come out and if you have credit cards in your pocket the information held on the magnetic strip will be wiped off. Metal fastenings on your clothes are all right because the magnetic field is not strong enough to pull them off. However, if they are close to the part of your body you are having scanned they may interfere with the pictures and you may be asked to change into a gown.

Involuntary movements such as muscle jerking, which is common in prion disease, can interfere with the MRI scan. If this is likely to be a problem with your scan, the study doctor will discuss with you about having sedation before the scan. This sedation may either be taken in tablet form or as a general anaesthetic. If the MRI scan were to be performed under a general anaesthetic it carries the usual risks associated with receiving general anaesthetic.

What happens during the scan?

You will be asked to lie on the scanner couch where you will be made as comfortable as possible. The position will vary depending on the part of the body that is being scanned. For example, for a scan of the

head you will be asked to lie with your neck or head in a specially shaped support. You should tell the staff if you are not comfortable as you will need to keep very still during the scan which may take up to 45 minutes to complete. There will be an intercom in the scanning room or some other means of communicating with the staff during the scan. Once you are ready to start you will be moved into the scanner. The scanner is a long tube, and the part of your body being scanned must be completely inside this tube. Although the staff will be able to reassure you during the scan, some people do find this unpleasant and slightly frightening.

Each set of pictures takes about five minutes and while the pictures are being taken you will hear a knocking sound. This noise means the scanner is collecting information to produce the pictures and therefore you must keep very still. If you move while the pictures are being taken they will be blurred and the scan may need to be repeated. Several sets of pictures may be taken during each examination and there will be a short pause between them. The scanner will go quiet between pictures; during this time the staff will be setting up ready to start the next set.

Will I need an injection?

When certain areas of the body are scanned, you may need an injection of a special dye known as a contrast agent that helps to see more detail on the pictures. If you need an injection it will be given into a vein in your arm by a radiologist or one of the radiographers trained to give injections. Sometimes several scans will be taken before the dye is injected and then further scans are taken after the injection. If your scan is being performed under general anaesthetic, you would be assessed by an anaesthetist who would give you an injection as part of this procedure.

Can anyone be with me during the scan?

As there are no harmful rays, a friend or relative can stay in the room with you during the scan. Anyone coming into the scan will also be asked questions about pacemakers and metal objects in their body, and will be asked to remove all metallic objects such as watches and jewellery.

What happens after the scan?

There are no after effects from the scan so you can carry on with your normal activities immediately.

When will I receive the results of the scan?

For each scan as many as 50 images may be produced which need to be carefully studied by the radiologists? The radiologists will produce a detailed report that will be sent to your specialist, usually within 7 to 14 days. More complicated analyses comparing information from different scans over long periods of time will only be carried out at the end of the trial, so the results will not be available to you for example, at your routine clinic visits.

This information sheet has been adapted from an information sheet prepared by the Brain and Spine Foundation. Their permission to reproduce this is gratefully acknowledged.
www.brainandspine.org

APPENDIX J

STANDARD OPERATING PROCEDURE FOR MRI SCANS DONE UNDER GENERAL ANAESTHESIA (GA) AT THE NATIONAL HOSPITAL FOR NEUROLOGY AND NEUROSURGERY (NHNN) FOR THE NATIONAL PRION CLINIC (NPC)

1. Patients with different forms of prion disease will be scanned under general anaesthetic, where patient movement would otherwise prevent scans of adequate quality being obtained.

2. The procedure will be discussed with patients, or their next of kin (in cases where patients are cognitively impaired and lack capacity to consent), as far as possible in advance by one of the trial fellows or the trial nurse. Information about the procedure will be provided and intended benefits and risks explained. In addition, in cognitively impaired patients, written assent will be obtained from next of kin in advance of the scan appointment. This procedure will be repeated at follow-up trial visits. The next of kin may be referred to Dr. Sally Wilson, consultant anaesthetist, NHNN (email: sally.wilson@uclh.org or extension 8711 at NHNN) if they request a detailed discussion directly with the anaesthetist.

3. Dr. Sally Wilson (email: sally.wilson@uclh.org or extension 8711 at NHNN or air call through NHNN switchboard) and Caroline Andrews, superintendent radiographer, MRI Department, NHNN (email: caroline.andrews@uclh.org or extension 3638 at NHNN) will be informed (where possible) two weeks in advance by one of the trial nurses (Christopher Rhymes, email: christopher.rhymes@uclh.org or Suzanne Walker, email: suzanne.walker@uclh.org or phone 02074052882).

4. MRI scans will be done under GA on Wednesday afternoons at 2:30 pm. Patients will usually be admitted for planned assessments on Tuesday to the Nuffield Ward at NHNN and stay for 2 nights. Dr. Sally Wilson will consent those patients on the ward who are able to give consent themselves. She will be assisted by one of the trial or clinical research fellows (Dr. D. Sodium, email: d.siddique@prion.ucl.ac.uk, Dr Tom Webb, email: t.webb@prion.ucl.ac.uk, Dr. H. Hyare, email: harpreet.hyare@uclh.org or phone: 02074052882) or by one of the trial nurses (see above).

5. Patients will be kept overnight after MRI scan under GA has been performed. Out of hours neurology cover will be provided by the on-call neurology SHO and Spry, and anaesthetic cover will be provided by the on-call anaesthetic Spry (bleep 8131). Dr Sally Wilson will be available out of hours through switchboard in case of an emergency.

6. All patients having MRI scan under GA will be resuscitated in the event of a cardio respiratory arrest during or after the procedure.

APPENDIX K

Risk assessment

In accordance with the Health and Safety Department at Imperial College a risk assessment was performed for handling of Category 3 substances and an application was made to the Health and Safety Executive (HSE), UK. Approval from the HSE was obtained for the project on 01/03/07.

To control possible exposure during transportation brain samples were double-sealed by placing in a screw-top histopathology pot and then inside a plastic grip bag. The double-sealed samples were placed inside a Bio jar and then within an UN-approved transport container with a biohazard sticker and the names of 2 people to contact in case of emergency (see below). The histopathology pot and plastic grip bag would not be opened in the laboratory and therefore a spillage should not occur.

If when the transport boxes were opened, there was evidence of a leak, then the samples were not removed but taken immediately back to the MRC Prion Unit, Institute of Neurology, UCL. In the unlikely event of a spillage, the area was to be wiped with a

paper towel dampened with 2M sodium hydroxide and then re-wiped with a paper towel dampened with water. Paper towels would be contained in a sharps box and returned to the MRC Prion Unit for autoclaving at 134 degrees Celsius.

All samples were transported to the Biological Imaging Centre (BIC), Imaging Sciences Department, MRC Sciences Centre, Hammersmith Hospital, Imperial College, London. In accordance with the Human Tissue Act 2004, the tissue specimens of prion disease and controls to use in the project were stored in the Department of Neuropathology at the Institute of Neurology under a storage licence held by UCLH. In section 30, subsection (2)(a) of the Act, a licence is not required for possession of an anatomical specimen away from licensed premises "where the specimen has come from premises in respect of which a storage licence is in force" and (b)(i) is "authorised in writing by the designated individual to have possession of the specimen". In section 16 subsection (7)(a) the Act states that "references to storage do not include storage which is incidental to transportation". Therefore, in accordance with the Act, samples were transported to the BIC with a letter of authorisation and with a documented specimen trail (Appendix L) and were returned to the Institute of Neurology the next working day.

APPENDIX L

Experiment to determine the effect of perfluoropolyethers (PFPE) on quantitative MRI and corroborative histology of brain tissue.

Purpose

To establish whether the immersion of fixed tissue samples in PFPE either alters their qualitative and quantitative MRI properties, or influences subsequent histological findings.

Methods

Specimen preparation

All studies were performed in accordance with the Animals (Scientific Procedures) Act 1986 (UK). To assess effect of prolonged PFPE exposure on quantitative MRI, 8 male *CD1* mice (12-15 weeks old) were culled by carbon dioxide asphyxiation. Their brains were excised from skull and dura and immersed in 10% formol-saline (Pioneer Research Chemicals, Ltd., Colchester, UK). After 10 days of fixation, 4 brains were immersed in Fomblin® Perfluorosolv PFS-1 (Solvay Solexis, Milan, Italy) while the remaining 4 were kept in the 10% formol-saline. After 48 hours, each brain was positioned within a 2.5 ml plastic syringe filled with Fomblin®, wedged between cotton-wool plugs to minimize sample motion, and MRI acquisitions performed the same day. All specimens were immersed in Fomblin® during the actual MRM acquisitions.

A second experiment was performed to compare histological findings in a group of specimens exposed to PFPE for 48 hours with a group with no such exposure: a further 8 adult *CD1* mice were culled by carbon dioxide asphyxiation and the excised brains immersed into 10% buffered formol saline. After 2 days of fixation, 4 were immersed in Fomblin® for 48 hours before being returned to 10% formol-saline for one week before processing. The remaining 4 brains remained in 10% formol-saline throughout.

MRI

MRI was performed with a horizontal bore 9.4T/21cm Varian Inova MRI system (Varian Inc, Palo Alto, CA) using a 43 mm internal diameter quadrature volume coil (Magnetic Resonance Laboratories, Oxford) at room temperature (bore temperature was 22 ºC). For T1 measurement, successive SE images were acquired with TRs of 450,

600, 800, 1000, 2000, 4000 ms; TE 15 ms; 2 averages; acquisition matrix size 256x128; slice thickness 2 mm. T2 measurements were obtained using a SE sequence to acquire successive images with TEs of 10, 22, 34 and 46 ms; TR 2000 ms; 2 averages; matrix size 256x128; slice thickness 2 mm. To investigate tissue-water diffusion, successive images were acquired with diffusion weighting applied along 6 non-colinear directions ($G_{x,}$ $G_{y,}$ G_z = [(1,1,0), (0,1,1), (1,0,1), (-1,1,0), (0,-1,1), (1,0,-1)]) with a diffusion weighting (*b* factor) of 1000 s/mm^2, and with no diffusion gradients (i.e. with a *b* factor of 0 s/mm^2) and TR 2000 ms; TE 22 ms; matrix size 256x256, 2 averages and slice thickness 2 mm. MTR was measured using a gradient-echo sequence with TE 5 ms; TR 186ms; matrix size 256x256; 16 averages; slice thickness 2 mm acquired with and without an effective off-resonance saturation pulse (offset frequencies 6 and 100 kHz respectively). Finally, a high-resolution T2W coronal image (TE 20 ms; TR 2400 ms; FOV 50x50 mm; matrix size 256x256; 20 averages, slice thickness 1 mm; in-plane resolution 158 µm) was acquired providing good anatomical contrast for qualitative assessment. For all acquisitions the FOV was 50x50mm and 7 contiguous coronal slices were obtained. The total measurement time per specimen was approximately 10 hours.

Image analysis

Qualitative analysis

The high-resolution T2W images were assessed by a single neuroradiologist, blinded to the grouping of the mouse brains, for visible artefacts or variations in SI.

Quantitative analysis

All quantitative image processing was performed off-line on a dedicated workstation (Sun Microsystems, Mountain View, CA, USA), being fully automated taking ~20 mins. Using commercially available software (JIM Version 4.0; Xinapse Systems Ltd, Thorpe Waterville, UK.), T1 and T2 maps were computed by performing pixel-by-pixel non-linear fitting to the equations S(TR) = ρ(1 – exp(-TR/T1)) and S(TE) = ρ(exp(-TE/T2)), respectively. S(TR) and S(TE) are the signal intensities of the T1- and T2W images acquired at the respective TR or TE, and ρ is the proton density in arbitrary units. MTR maps were generated pixel-by-pixel according to the formula: MTR = [(M_o – M_s)/M_o] x 100, where M_o and M_s, are the SI without and with the off-resonance saturation pulse. DTI data were calculated using Camino (http://www.cs.ucl.ac.uk/research/medic/camino/) [218] to provide FA and MD maps.

For each specimen, ROIs in the right thalamus (Figure A, ROI 1) and right cerebral cortex (Figure A, ROI 2) were defined manually by a single experienced observer according to a published mouse brain atlas [219]. The cortical ROI was chosen specifically to investigate quantitative MRM changes close to the edge of the specimen. The ROIs (size 1.8 – 2.4 mm^2) were defined on the SE images providing optimal grey-white matter contrast (TE 10 ms; TR 2000ms), saved and then re-loaded for each of the T1, T2, MT, MD and FA maps.

Statistics

The effect of Fomblin® on MRI measures was analyzed using a repeated measures ANOVA with ROI location as the within-subjects factor and group (control versus pre-treatment with Fomblin®) as the between-subjects factor. Where an effect was detected, post-hoc comparison tests were performed. Parametric tests were used despite the small number of specimens, to provide increased power to detect a significant difference compared to the equivalent non-parametric test. A value of $p < 0.05$ was considered statistically significant and all statistical tests were performed using SPSS for Windows (version 11.5, SPSS, Chicago, IL, USA).

Histological Analysis

For both experiments, following re-immersion in 10% buffered formal saline for one week (Pioneer Research Chemicals, Ltd., Colchester, UK.), tissue samples were processed and embedded in paraffin wax. Wax sections were cut at a nominal thickness of 3 µm and mounted on Superfrost UltraPlus charged glass slides. Following dewaxing in xylene and an alcohol gradient, the sections were stained with H&E. For immunohistochemical staining, dewaxed sections were boiled (microwaved) in a low ionic strength buffer (2.1 mM Tris, 1.3 mM EDTA, 1.1 mM sodium citrate, pH 7.8) for 20 minutes. Immunoreactivity of astrocytes and neurones were tested using rabbit anti-glial fibrillary acidic protein (GFAP) antiserum (DAKO) and mouse monoclonal anti-neurofilament antibodies (NF200, Sigma-Aldrich Co. Ltd, Poole), respectively. A biotinylated-anti IgG secondary antibody (*i*View SA-HRP, Ventana Medical Systems, Tuscon, AZ, USA) was applied before development with 3,3'-diaminobenzidine tetrachloride as the chromogen (iView DAB, Ventana Medical Systems, Tuscon, AZ, USA). H&E was used as the counterstain and appropriate controls were used throughout.

All slides were assessed by a single consultant neuropathologist. Fine nuclear detail, in particular the chromatin and nucleoli were assessed within neurons, astrocytes and oligodendrocytes. The synaptic structure of the neuropil and the integrity of myelinated fibre tracts were assessed throughout the mouse brain. Specific structures assessed included the hippocampus, thalamus and cerebellum.

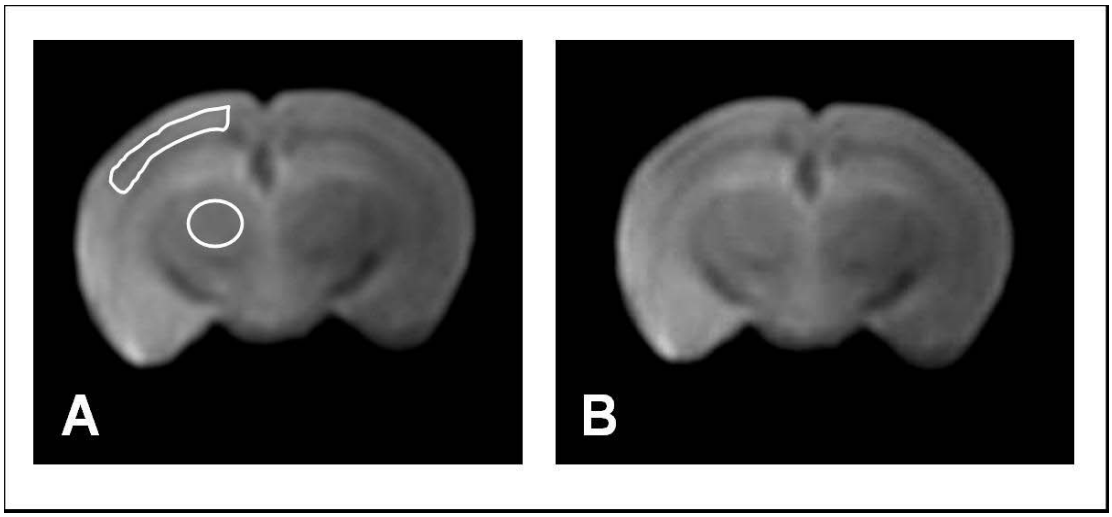

Figure A: High resolution T2W images (TR/TE 2400/24 ms, 20 averages, FOV 50x50mm, 256 x 256 matrix, in plane resolution 158µm, slice thickness 1 mm) of (A) control and (B) Fomblin® pre-treated mouse brain; no differences were apparent on visual inspection. The location of the right thalamic (1) and right cortical (2) ROIs from which quantitative MRI values were obtained is shown in (A)

Results

Qualitative MRI

Visual inspection of high resolution T2W MRI images of control and PFPE-immersed mouse brains revealed no detectable differences between the two groups (see Figure A).

Quantitative MRI

I detected an effect of ROI location for MTR at the 5% level (mean MTR = 61.6 ± 6.0 for right thalamus ROI versus 58.6 ± 4.7 for right cortex ROI; p=0.005) and MD at the 10% level (mean MD = 324.0 ± 74.4 for right thalamus ROI versus 361.4 ± 89.3 for right cortex ROI; p=0.058). When adjusted for Fomblin treatment®, the differences in MTR and MD between the cortical and thalamic ROIs no longer reached significance (Table). I did not detect an effect of Fomblin® in any of the MRI measures.

Table: Mean regional quantitative MRI values for control (n = 4) and PFPE pre-treated specimens (n = 4)

	Right thalamus ROI		*Right cerebral cortex ROI*		*F*	*P**
	Control	PFPE pre-treated	Control	PFPE Pre-treated		
T1(ms)	1499.7	1505.3	1535.9	1503.2	0.065	0.808
	(85.1)	(3.0)	(79.6)	(71.0)		
T2(ms)	34.8	33.6	36.3	39.3	0.046	0.837
	(4.4)	(3.1)	(4.6)	(11.2)		
MTR	62.6	60.6	59.7	57.4	0.298	0.605
	(5.4)	(7.2)	(4.4)	(5.3)		
MD(mm^2/s)	339.3	308.7	383.3	339.5	0.402	0.550
	(59.8)	(93.4)	(84.6)	(100.8)		
FA	0.35	0.41	0.36	0.35	0.583	0.583
	(0.06)	(0.11)	(0.10)	(0.05)		

Note. T1 = spin-lattice and T2 = spin-spin relaxation time constants respectively, MTR = magnetisation transfer ratio, MD = mean diffusivity, FA = fractional anisotropy. Values are mean (standard deviation). *test of between subjects effects in repeated measures ANOVA

Histopathology

For both experiments, H & E staining revealed fine nuclear detail with well discernible chromatin and nucleoli in neurons, identical structure of astrocytic and oligodendroglial nuclei. The neuropil had the same fine granular synaptic structure in both experimental and control groups. Myelinated fibre tracts were also identical in both groups. In particular, no vacuolisation or other artefacts were observed. Specific structures, such as the stratum radiatum in the hippocampus, showed delicate processes that were unaltered by extended PFPE immersion. Immunoreactivity in the treated group was no different from that in the control group with respect to intensity and immunostaining. GFAP which labels astrocytes and neurofilament (NF200) which labels axons throughout the brain, were identical in both groups. For both experiments, there was no discernable histological difference between formalin-fixed brains immersed in PFPE for extended periods of time compared those remaining in formalin (Figure B).

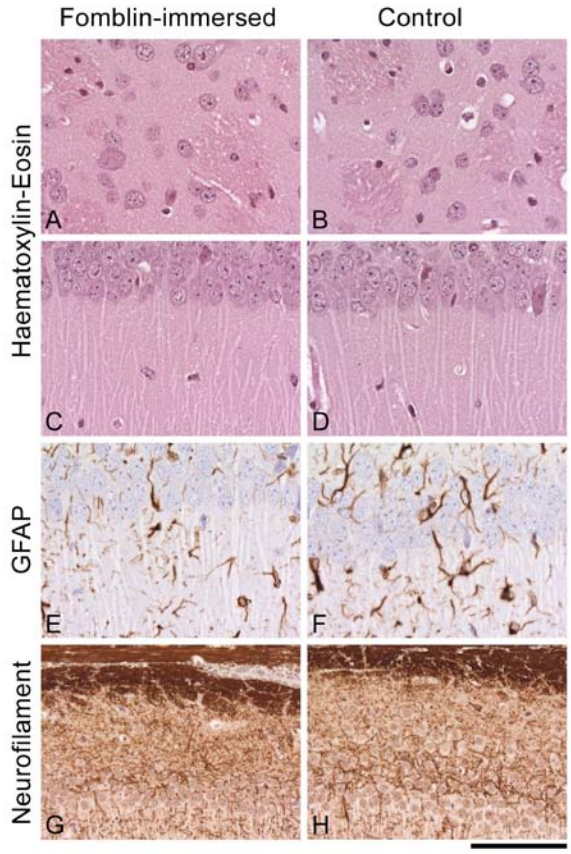

Figure B: ***Left column*** Fomblin®-immersed brain, ***right column*** control brain. **A, B**: H&E stained sections from the striatum. Nuclear detail, grey matter and white matter structures are well preserved and are identical in control and Fomblin® exposed specimens. **C, D**: high-power magnification from the neuronal ribbon of the hippocampus. Well preserved nuclear detail in both groups, including equal visualisation of delicate processes in the stratum radiatum. **E, F**: GFAP immunohistochemical staining for detection of astrocytes. In both controls and Fomblin®-immersed brains GFAP immunoreactivity is the same with delicate processes and contrast. **G, H**: Neurofilament immunohistochemistry, which labels delicate processes in the hippocampus as well as thick fibre bundles in the corpus callosum (in the upper edge of both images). No difference in staining contrast, intensity and visualisation of delicate processes is seen.
Scale bar 50µm (A-F), 100µm(G-H)

Conclusion

In conclusion, I have confirmed that prolonged immersion of fixed cerebral tissue in a PFPE for the purpose of MRM does not significantly modify quantitative magnetic resonance findings and does not compromise detection of histopathological features.

APPENDIX M

UCL INSTITUTE OF NEUROLOGY
QUEEN SQUARE

THE NATIONAL HOSPITAL FOR NEUROLOGY AND
NEUROSURGERY
QUEEN SQUARE
LONDON WC1N 3BG

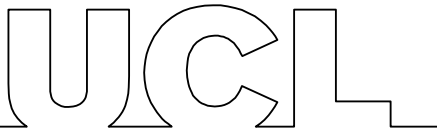

DEPARTMENT OF NEURODEGENERATIVE DISEASES
HEAD OF DEPARTMENT: Professor J. Collinge BSc, MB, ChB, MD, FRCP, FRS

DIVISION OF NEUROPATHOLOGY
HEAD OF DIVISION: Professor S. Brander MD, Micah

INSTITUTE OF NEUROLOGY (ION) / BIOLOGICAL IMAGING CENTRE, HAMMERSMITH HOSPITAL (BIC) SPECIMEN TRAIL DOCUMENTATION SHEET

1	**Specimen identification number (NP code)**	
2	**Person collecting specimen (ION)**	
3	**Time and Date of collection (ION)**	
4	**Time and Date of Arrival (BIC, Hammersmith Hospital)**	
5	**Person assuming responsibility for specimen (BIC, Hammersmith Hospital)**	
6	**Expected Time and Date of specimen collection**	
7	**Person, witnessing the removal of specimen (BIC, Hammersmith Hospital)**	
8	**Person collecting specimen (BIC, Hammersmith Hospital)**	
9	**Time and Date of Collection (BIC, Hammersmith Hospital)**	
10	**Time and Date of return of specimen (ION)**	
11	**Person returning specimen (ION)**	
12	**Contact Details (for use in the event of any unforeseen eventualities):** **1. Clinical Research Fellow: Harpreet Hyare 07939061494** **2. ION histopathology's: Caroline Powell 07970931026** **3. Pathologist: Professor S Brander**	

Acknowledgements

I would like to thank my supervisors Tarek Yousry, John Thornton and Stephen Wroe for their help and advice throughout my PhD. I am also indebted in the latter stages to Rolf Jager, Simon Mead and Peter Rudge for their support. I would also like to thank John Collinge without whom I would never have undertaken this research and to the MRC for funding this Clinical Research Fellowship.

I am indebted to the team working on the PRION-1 trial for their encouragement and advice with neurological and nursing issues. Special thanks to Durre, Tom, Suvankar, Chris, Suzanne, Michele and Clare.

I would also like to thank the histopathology department for all the histology support on the high field study, especially to Caroline Powell and Catherine O'Malley for their efficient processing and finally to Sebastian Brandner for his enthusiasm and histological analysis.

For the 9.4T scanning at Imperial College, I thank Po-Wah So for all the time that she took to scan my samples and for her teaching and advice. I also thank Harry Parkes for advice on post-processing of samples.

To Ray, for his wonderful visual input, not only for the thesis but for all the posters and presentations throughout the three years. Essential statistical support was provided by Sarah Walker and in the latter stages by Costas Kallides.

I would like to thank all the patients and relatives who participated in the Prion-1 Trial.

Finally my love and thanks to all those who kept me going: my family, friends and especially to Carl.

I dedicate this thesis to the memory of my beloved late father Harminder Singh Hyare.

Reference List

1. Collinge J, Palmer MS. Prion diseases. *Current Opinion in Genetics and Development* 1992;2:448-54

2. Mallucci G, Collinge J. Update on Creutzfeldt-Jakob disease. *Current Opinion in Neurobiology* 2004;17:641-47

3. Wroe SJ, Pal S, Siddique D, et al. Clinical presentation and pre-mortem diagnosis of variant Creutzfeldt-Jakob disease associated with blood transfusion: a case report. *Lancet* 2006;368:2061-67

4. Prusiner SB. Molecular Biology of Prion Diseases. *Science* 1991;252:1515-22

5. Borchelt DR, Scott M, Taraboulos A, et al. Scrapie and cellular prion proteins differ in their kinetics of synthesis and topology in cultured cells. *J Cell Biol* 1990;110:743-52

6. Caughey B, Raymond GJ. The scrapie-associated form of PrP is made from a cell surface precursor that is both protease- and phospholipase-sensitive. *J Biol Chem* 1991;266 No 27:18217-23

7. Collinge J. Molecular neurology of prion disease. *Journal of Neurology Neurosurgery and Psychiatry* 2005;76:906-19

8. Riek R, Hornemann S, Wider G, et al. NMR structure of the mouse prion protein domain PrP (121-231). *Nature* 1996;382:180-82

9. Collinge J, Sidle KCL, Meads J, et al. Molecular analysis of prion strain variation and the aetiology of 'new variant' CJD. *Nature* 1996;383:685-90

10. Parchi P, Castellani R, Capellari S, et al. Molecular Basis of Phenotypic Variability in Sporadic Creutzfeldt-Jakob Disease. *Annals of Neurology* 1996;39:669-80

11. Fraser H, Bruce ME, Davies D, et al. The Lymphoreticular system in the Pathogenesis of Scrapie. In:Prusiner SB, Collinge J, Powell J, Anderton B, eds. *Prion Diseases of Humans and Animals*. London: Ellis Horwood; 1992

12. Prinz M, Montrasio F, Klein MA, et al. Lymph nodal prion replication and neuroinvasion in mice devoid of follicular dendritic cells. *Proc Natl Acad Sci U S A* 2002;99:919-24

13. Llewelyn CA, Hewitt PE, Knight RS, et al. Possible transmission of variant Creutzfeldt-Jakob disease by blood transfusion. *Lancet* 2004;363:417-21

14. Peden AH, Head MW, Ritchie DL, et al. Preclinical vCJD after blood transfusion in a PRNP codon 129 heterozygous patient. *Lancet* 2004;364:527-29

15. Collinge J, Clarke A. A general model of prion strains and their pathogenicity. *Science* 2007;318:930-36

16. Palmer MS, Dryden AJ, Hughes JT, et al. Homozygous prion protein genotype predisposes to sporadic Creutzfeldt-Jakob disease. *Nature* 1991;352:340-42

17. Brown P, Preece MA, Will RG. "Friendly fire" in medicine: hormones, homografts, and Creutzfeldt-Jakob disease. *Lancet* 1992;340:24-27

18. Hill AF, Desbruslais M, Joiner S, et al. The same prion strain causes vCJD and BSE. *Nature* 1997;389:448-50, 526

19. Brown P, Rodgers-Johnson P, Cathala F, et al. Creutzfeldt-Jakob disease of long duration: clinicopathological characteristics, transmissibility, and differential diagnosis. *Annals of Neurology* 1984;16:295-304

20. Gomori AJ, Partnow MJ, Horoupian DS, et al. The ataxic form of Creutzfeldt-Jakob disease. *Arch Neurol* 1973;29:318-23

21. Zerr I, Kallenberg K, Summers DM, et al. Updated clinical diagnostic criteria for sporadic Creutzfeldt-Jakob disease. *Brain* 2009;132:2659-68

22. Zerr I, Bodemer M, Räcker S, et al. Cerebrospinal fluid concentration of neuron-specific enolase in diagnosis of Creutzfeldt-Jakob disease. *Lancet* 1995;345:1609-10

23. Hsich G, Kenney K, Gibbs CJ, Jr., et al. The 14-3-3 brain protein in cerebrospinal fluid as a marker for transmissible spongiform encephalopathies. *N Engl J Med* 1996;335:924-30

24. Steinhoff BJ, Racker S, Herrendorf G, et al. Accuracy and reliability of periodic sharp wave complexes in Creutzfeldt-Jakob disease. *Arch Neurol* 1996;53:162-66

25. Zerr I, Pocchiari M, Collins S, et al. Analysis of EEG and CSF 14-3-3 protein as aids to the diagnosis of Creutzfeldt-Jakob disease. *Neurology* 2000;55:811-15

26. Young GS, Geschwind MD, Fischbein NJ, et al. Diffusion-weighted and fluid-attenuated inversion recovery imaging in Creutzfeldt-Jakob disease: high sensitivity and specificity for diagnosis. *AJNR Am J Neuroradiol* 2005;26:1551-62

27. Tschampa HJ, Neumann M, Zerr I, et al. Patients with Alzheimer's disease and dementia with Lewy bodies mistaken for Creutzfeldt-Jakob disease. *J Neurol Neurosurg Psychiatry* 2001;71:33-39

28. Poser S, Mollenhauer B, Krauss A, et al. How to improve the clinical diagnosis of Creutzfeldt-Jakob disease. *Brain* 1999;122:2345-51

29. Steinhoff BJ, Zerr I, Glatting M, et al. Diagnostic value of periodic complexes in Creutzfeldt-Jakob disease. *Ann Neurol* 2004; 56(5):702-8

30. Tschampa HJ, Zerr I, Urbach H. Radiological assessment of Creutzfeldt-Jakob disease. *Eur Radiol* 2006; 17(5): 1200-11

31. Bateman D, Hilton D, Love S, et al. Sporadic Creutzfeldt-Jakob disease in a 18-year old in the UK. *Lancet* 1995;346:1155-56

32. Britton TC, Al-Sarraj S, Shaw C, et al. Sporadic Creutzfeldt-Jakob disease in a 16-year-old in the UK. *Lancet* 1995;346:1155

33. Will RG, Zeidler M, Stewart GE, et al. Diagnosis of new variant Creutzfeldt-Jakob disease. *Annals of Neurology* 2000;47:575-82

34. Henry C, Knight R. Clinical features of variant Creutzfeldt-Jakob disease. *Rev Med Virol* 2002;12:143-50

35. Heath CA, Cooper SA, Murray K, et al. Validation of diagnostic criteria for variant Creutzfeldt-Jakob disease. *Ann Neurol* 2010;67:761-70

36. Zeidler M, Sellar RJ, Collie DA, et al. The pulvinar sign on magnetic resonance imaging in variant Creutzfeldt-Jakob disease. *Lancet* 2000;355:1412-18

37. Collie DA, Summers DM, Sellar RJ, et al. Diagnosing Variant Creutzfeldt-Jakob Disease with the Pulvinar Sign: MR Imaging Findings in 86 Neuropathologically Confirmed Cases. *AJNR Am J Neuroradiol* 2003;24:1560-69

38. Mead S, Poulter M, Uphill J, et al. Genetic risk factors for variant Creutzfeldt-Jakob disease: a genome-wide association study. *Lancet Neurol* 2009;8:57-66

39. Kaski D, Mead S, Hyare H, et al. Variant CJD in an individual heterozygous for PRNP codon 129. *Lancet* 2009;374:2128

40. Mead S. Prion disease genetics. *European Journal of Human Genetics* 2006;14:273-81

41. Windl O, Giese A, Schulz-Schaeffer W, et al. Molecular genetics of human prion diseases in Germany. *Hum Genet* 1999;105:244-52

42. Pocchiari M, Ladogana A, Petraroli R, et al. Recent Italian FFI cases. *Brain Pathol* 1998;8:564-66

43. Kovacs GG, Puopolo M, Ladogana A, et al. Genetic prion disease: the EUROCJD experience. *Hum Genet* 2005;1-9

44. Dagvadorj A, Petersen RB, Lee HS, et al. Spontaneous mutations in the prion protein gene causing transmissible spongiform encephalopathy. *Ann Neurol* 2002;52:355-59

45. Mitrova E, Lowenthal A, Appeal B. Familial Creutzfeldt-Jakob disease with temporal and spatial separation of affected members. *Eur J Epidemiol* 1990;6:233-38

46. Goldfarb LG, Brown P, Mitrova E, et al. Creutzfeldt-Jacob disease associated with the PRNP codon 200Lys mutation: an analysis of 45 families. *Eur J Epidemiol* 1991;7:477-86

47. Collinge J, Palmer MS, Campbell TA, et al. Inherited prion disease (PrP lysine 200) in Britain: two case reports. *BMJ* 1993;306:301-2

48. Goldfarb LG, Brown P, McCombie WR, et al. Transmissible familial Creutzfeldt-Jakob disease associated with five, seven, and eight extra octapeptide coding repeats in the *PRNP* gene. *Proc Natl Acad Sci USA* 1991;88:10926-30

49. Poulter M, Baker HF, Frith CD, et al. Inherited prion disease with 144 base pair gene insertion: I: Genealogical and molecular studies. *Brain* 1992;115:675-85

50. Barbanti P, Fabbrini G, Salvatore M, et al. Polymorphism at codon 129 or codon 219 of *PRNP* and clinical heterogeneity in a previously unreported family with Gerstmann- Straussler-Scheinker disease (PrP-P102L mutation). *Neurology* 1996;47:734-41

51. Webb TE, Poulter M, Beck J, et al. Phenotypic heterogeneity and genetic modification of P102L inherited prion disease in an international series. *Brain* 2008;131:2632-46

52. Kretzschmar HA, Kufer P, Riethmuller G, et al. Prion protein mutation at codon 102 in an Italian family with Gerstmann-Straussler-Scheinker syndrome. *Neurology* 1992;42:809-10

53. Aguzzi A, Weissmann C. Prion diseases. *Haemophilia* 1998;4:619-27

54. Bonduelle M, Escoureolle R, Bouygues P, et al. (Anatomo-clinical findings in a case of Creutzfeldt-Jakob disease). *Neurol Neurochir Pol* 1973;7:182-83

55. Mizutani T, Okumura A, Oda M, et al. Panencephalopathic type of Creutzfeldt-Jakob disease: primary involvement of the cerebral white matter. *J Neurol Neurosurg Psychiatry* 1981;44:103-15

56. Gray F, Chrétien F, Adle-Biassette H, et al. Neuronal apoptosis in Creutzfeldt-Jakob disease. *Journal of Neuropathology and Experimental Neurology* 1999;58:321-28

57. Collinge J. Human prion diseases: aetiology and clinical features. In:Growdon JH, Rossor M, eds. *The Dementias* . Newton, MA: Butterworth-Heinemann; 1998; 113-148

58. Parchi P, Giese A, Capellari S, et al. Classification of sporadic Creutzfeldt-Jakob Disease based on molecular and phenotypic analysis of 300 subjects. *Annals of Neurology* 1999;46:224-33

59. Parchi P, Chen SG, Brown P, et al. Different patterns of truncated prion protein fragments correlate with distinct phenotypes in P102L Gerstmann-Sträussler-Scheinker disease. *Proc Natl Acad Sci USA* 1998;95:8322-27

60. Tschampa HJ, Kallenberg K, Kretzschmar HA, et al. Pattern of Cortical Changes in Sporadic Creutzfeldt-Jakob Disease. *AJNR Am J Neuroradiol* 2007;28:1114-18

61. Meissner B, Kallenberg K, Sanchez-Juan P, et al. Isolated Cortical Signal Increase on MR Imaging as a Frequent Lesion Pattern in Sporadic Creutzfeldt-Jakob Disease. *AJNR Am J Neuroradiol* 2008; 29(8):1519-24

62. Meissner B, Kallenberg K, Sanchez-Juan P, et al. MRI lesion profiles in sporadic Creutzfeldt-Jakob disease. *Neurology* 2009;72:1994-2001

63. Yee AS, Simon JH, Anderson CA, et al. Diffusion-weighted MRI of right-hemisphere dysfunction in Creutzfeldt-Jakob disease. *Neurology* 1999;52:1514-15

64. Gertz HJ, Henkes H, Cervos Navarro J. Creutzfeldt-Jakob disease: correlation of MRI and neuropathologic findings. *Neurology* 1988;38:1481-82

65. Finkenstaedt M, Szudra A, Zerr I, et al. MR imaging of Creutzfeldt-Jakob disease. *Radiology* 1996;199:793-98

66. Barboriak D, Provenzale JM, Boyko OB. MR diagnosis of Creutzfeldt-Jakob disease: significance of high signal intensity of the basal ganglia. *AJR* 1994;162:137-40

67. Milton WJ, Atlas SW, Lavi E, et al. Magnetic resonance imaging of Creutzfeldt-Jacob disease. *Am Neurol Assoc* 1991;438-40

68. Tartaro A, Fulgente T, Delli Pizzi C, et al. MRI alterations as an early finding in Creutzfeld-Jakob disease. *Eur J Radiol* 1993;17:155-58

69. Rother KI, Clay OK, Bourquin JP, et al. Long non-stop reading frames on the antisense strand of heat shock protein 70 genes and prion protein (PrP) genes are conserved between species [see comments]. *Biol Chem* 1997;378:1521-30

70. Pearl GS, Anderson RE. Creutzfeldt-Jakob disease: high caudate signal on magnetic resonance imaging. *South Med J* 1989;82:1177-80

71. Meissner B, Kortner K, Bartl M, et al. Sporadic Creutzfeldt-Jakob disease: magnetic resonance imaging and clinical findings. *Neurology* 2004;63:450-56

72. Tschampa HJ, Kallenberg K, Urbach H, et al. MRI in the diagnosis of sporadic Creutzfeldt-Jakob disease: a study on inter-observer agreement. *Brain* 2005;128:2026-33

73. Kropp S, Finkenstaedt M, Zerr I, et al. [Diffusion-weighted MRI in patients with Creutzfeldt-Jakob disease]. *Nervenarzt* 2000;71:91-95

74. Shiga Y, Miyazawa K, Sato S, et al. Diffusion-weighted MRI abnormalities as an early diagnostic marker for Creutzfeldt-Jakob disease. *Neurology* 2004;63:443-49

75. Matoba M, Tonami H, Miyaji H, et al. Creutzfeldt-Jakob disease: Serial changes on diffusion-weighted MRI. *J Comp Ass Tomog* 2001;25:274-77

76. Ukisu R, Kushihashi T, Kitanosono T, et al. Serial diffusion-weighted MRI of creutzfeldt-jakob disease. *AJR Am J Roentgenol* 2005;184:560-66

77. Tribl GG, Strasser G, Zeitlhofer J, et al. Sequential MRI in a case of Creutzfeldt-Jakob disease 229. *Neuroradiology* 2002;44:223-26

78. Tschampa HJ, Murtz P, Flacke S, et al. Thalamic Involvement in Sporadic Creutzfeldt-Jakob Disease: A Diffusion-Weighted MR Imaging Study. *AJNR Am J Neuroradiol* 2003;24:908-15

79. Schroter A, Zerr I, Henkel K, et al. Magnetic resonance imaging in the clinical diagnosis of Creutzfeldt-Jakob disease. *Arch Neurol* 2000;57:1751-57

80. Matsusue E, Kinoshita T, Sugihara S, et al. White Matter Lesions in Panencephalopathic Type of Creutzfeldt-Jakob Disease: MR Imaging and Pathologic Correlations. *AJNR Am J Neuroradiol* 2004;25:910-18

81. de Priester JA, Jansen GH, de Kruijk JR, et al. New MRI findings in Creutzfeldt-Jakob disease: high signal in the globus pallidus on T1-weighted images. *Neuroradiology* 1999;41:265-68

82. Kovanen J, Erkinjuntti T, Iivanainen M, et al. Cerebral MR and CT imaging in Creutzfeldt-Jakob disease. *J Comput Assist Tomogr* 1985;9:125-28

83. Fulbright RK, Kingsley PB, Guo XD, et al. The imaging appearance of Creutzfeldt-Jakob disease caused by the E200K mutation. *Magn Reson Imaging* 2006;24:1121-29

84. Fulbright RK, Hoffmann C, Lee H, et al. MR Imaging of Familial Creutzfeldt-Jakob Disease: A Blinded and Controlled Study. *AJNR Am J Neuroradiol* 2008; 29(9):1638-43

85. Mittal S, Farmer P, Kalina P, et al. Correlation of diffusion-weighted magnetic resonance imaging with neuropathology in Creutzfeldt-Jakob disease. *Arch Neurol* 2002;59:128-34

86. Bahn MM, Parchi P. Abnormal diffusion-weighted magnetic resonance images in Creutzfeldt-Jakob disease. *Arch Neurol* 1999;56:577-83

87. Lim CC, Tan K, Verma KK, et al. Combined diffusion-weighted and spectroscopic MR imaging in Creutzfeldt-Jakob disease. *Magn Reson Imaging* 2004;22:625-29

88. Manners DN, Parchi P, Tonon C, et al. Pathologic correlates of diffusion MRI changes in Creutzfeldt-Jakob disease. *Neurology* 2009;72:1425-31

89. Russmann H, Vingerhoets F, Miklossy J, et al. Sporadic Creutzfeldt-Jakob disease A comparison of pathological findings and diffusion weighted imaging. *J Neurol* 2005; 252(3):338-42

90. Zeidler M, Collie DA, Macleod MA, et al. FLAIR MRI in sporadic Creutzfeldt-Jakob disease. *Neurology* 2001;56:282

91. Bozzali M, Cherubini A. Diffusion tensor MRI to investigate the dementias: a brief review. Magn Reson.Imaging 2007; 25: 969-977

92. Le Bihan DL. Diffusion MR imaging: clinical applications. Turner, R. S., Douek, P., and Patronas, N. AJR 1999; 159: 969-977

93. Patterson DM, Padhani AR, Collins DJ. Technology insight: water diffusion MRI - a potential new biomarker of response to cancer therapy. Nature Reviews Clinical Oncology 2008; 5: 220-223

94. McRobbie DW, Moore EA, Graves MJ, et al. *To BOLDly go: new frontiers. MRI from picture to proton*, 3rd ed. Cambridge: Cambridge University Press; 2005; 317-342

95. Stejskal EO, Tanner J.E. Spin diffusion measurements: spin echoes in the presence of a time dependent field gradient. *Journal of Chemical Physics* 1965;42:288-92

96. Beaulieu C. The basis of anisotropic water diffusion in the nervous system - a technical review. *NMR in Biomedicine* 2002;15:435-55

97. Sundgren PC, Dong Q, Gomez-Hassan D, et al. Diffusion tensor imaging of the brain: review of clinical applications. *Neuroradiology* 2004;46:339-50

98. Horsfield MA, Jones DK. Applications of diffusion-weighted and diffusion tensor MRI to white matter diseases - a review. *NMR Biomed* 2002;15:570-77

99. Bozzali M, Falini A, Franceschi M, et al. White matter damage in Alzheimer's disease assessed in vivo using diffusion tensor magnetic resonance imaging. *J Neurol Neurosurg Psychiatry* 2002;72:742-46

100. Rose SE, Chen F, Chalk JB, et al. Loss of connectivity in Alzheimer's disease: an evaluation of white matter tract integrity with colour coded MR diffusion tensor imaging. *J Neurol Neurosurg Psychiatry* 2000;69:528-30

101. Bozzali M, Franceschi M, Falini A, et al. Quantification of tissue damage in AD using diffusion tensor and magnetization transfer MRI. *Neurology* 2001;57:1135-37

102. Kantarci K, Petersen RC, Boeve BF, et al. DWI predicts future progression to Alzheimer disease in amnestic mild cognitive impairment. *Neurology* 2005;64:902-04

103. Kantarci K, Jack CR, Jr. Neuroimaging in Alzheimer disease: an evidence-based review. *Neuroimaging Clin N Am* 2003;13:197-209

104. Sehy JV, Ackerman JJH, Neil JJ. Evidence that both the fast and slow water ADC components arise from intracellular space. *Magn Reson Med* 2002;48:765-70

105. Clark CA, Le Bihan D. Water diffusion compartmentation and anisotropy at high b values in the human brain. *Magn Reson Med* 2000;44:852-59

106. Clark CA, Hedehus M, Moseley ME. In vivo mapping of the fast and slow diffusion tensors in human brain. *Magn Reson Med* 2002;47:623-28

107. Tha KK, Terae S, Kudo K, et al. Early detection of subacute sclerosing panencephalitis by high b-value diffusion-weighted imaging: a case report. *J Comput Assist Tomogr* 2006;30:126-30

108. Kim HJ, Choi CG, Lee DH, et al. High-b-value diffusion-weighted MR imaging of hyperacute ischemic stroke at 1.5T. *AJNR Am J Neuroradiol* 2005;26:208-15

109. Yoshiura T, Mihara F, Tanaka A, et al. High b value diffusion-weighted imaging is more sensitive to white matter degeneration in Alzheimer's disease. *Neuroimage* 2003;20:413-19

110. Yoshiura T, Wu O, Zaheer A, et al. Highly diffusion-sensitized MRI of brain: dissociation of gray and white matter. *Magn Reson Med* 2001;45:734-40

111. DeLano MC, Cooper TG, Siebert JE, et al. High-b-value diffusion-weighted MR imaging of adult brain: image contrast and apparent diffusion coefficient map features. *AJNR Am J Neuroradiol* 2000;21:1830-36

112. Govindaraju V, Young K, Maudsley AA. Proton NMR chemical shifts and coupling constants for brain metabolites. *NMR Biomed* 2000;13:129-53

113. McRobbie DW, Moore EA, Graves MJ, et al. It's not just squiggles: in vivo spectroscopy. *MRI from picture to proton.* 3rd ed. Cambridge: Cambridge University Press; 2005; 300-316

114. Baslow MH. N-acetylaspartate in the vertebrate brain: metabolism and function. *Neurochem Res* 2003;28:941-53

115. Miller BL. A review of chemical issues in 1H NMR spectroscopy: N-acetyl-L-aspartate, creatine and choline. *NMR Biomed* 1991;4:47-52

116. Rudkin TM, Arnold DL. Proton magnetic resonance spectroscopy for the diagnosis and management of cerebral disorders. *Arch Neurol* 1999;56:919-26

117. Kantarci K, Weigand SD, Petersen RC, et al. Longitudinal 1H MRS changes in mild cognitive impairment and Alzheimer's disease. *Neurobiol Aging* 2007;28:1330-39

118. Kantarci K, Jack CR, Jr., Xu YC, et al. Regional metabolic patterns in mild cognitive impairment and Alzheimer's disease: A 1H MRS study. *Neurology* 2000;55:210-17

119. Soher BJ, Vermathen P, Schuff N, et al. Short TE in vivo (1)H MR spectroscopic imaging at 1.5 T: acquisition and automated spectral analysis. *Magn Reson Imaging* 2000;18:1159-65

120. Grafe MR, Press GA, Berthoty DP, et al. Abnormalities of the brain in AIDS patients: correlation of postmortem MR findings with neuropathology. *AJNR Am J Neuroradiol* 1990;11:905-11

121. Bobinski M, de Leon MJ, Wegiel J, et al. The histological validation of post mortem magnetic resonance imaging-determined hippocampal volume in Alzheimer's disease. *Neuroscience* 2000;95:721-25

122. Schmierer K, Parkes HG, So PW, et al. High field (9.4 Tesla) magnetic resonance imaging of cortical grey matter lesions in multiple sclerosis. *Brain* 2010;133:858-67

123. Schmierer K, Wheeler-Kingshott CA, Boulby PA, et al. Diffusion tensor imaging of post mortem multiple sclerosis brain. *Neuroimage* 2007;35:467-77

124. van der WL, Thomas DL, Thornton JS, et al. MRI of animal models of brain disease. *Methods Enzymol* 2004;386:149-77

125. Johnson GA, Benveniste H, Engelhardt RT, et al. Magnetic resonance microscopy in basic studies of brain structure and function. *Ann N Y Acad Sci* 1997;820:139-47

126. Johnson GA, Benveniste H, Black RD, et al. Histology by magnetic resonance microscopy. *Magn Reson Q* 1993;9:1-30

127. Bilgili Y, Unal B. Effect of region of interest on interobserver variance in apparent diffusion coefficient measures. *AJNR Am J Neuroradiol* 2004;25:108-11

128. Jones DK, Symms MR, Cercignani M, et al. The effect of filter size on VBM analyses of DT-MRI data. *Neuroimage* 2005;26:546-54

129. Hosszu LLP, Baxter NJ, Jackson GS, et al. Structural mobility of the human prion protein probed by backbone hydrogen exchange. *Nature Struct Biol* 1999;6:740-43

130. Enari M, Flechsig E, Weissmann C. Scrapie prion protein accumulation by scrapie-infected neuroblastoma cells abrogated by exposure to a prion protein antibody. *Proc Natl Acad Sci USA* 2001;98:9295-99

131. Peretz D, Williamson RA, Kaneko K, et al. Antibodies inhibit prion propagation and clear cell cultures of prion infectivity. *Nature* 2001;412:739-43

132. Hannon GJ. RNA interference. *Nature* 2002;418:244-51

133. Collinge J, Gorham M, Hudson F, et al. Safety and efficacy of quinacrine in human prion disease (PRION-1 study): a patient-preference trial. *Lancet Neurology* 2009;2009:334-44

134. Mueller SG, Schuff N, Weiner MW. Evaluation of treatment effects in Alzheimer's and other neurodegenerative diseases by MRI and MRS. NMR Biomed. 2006; 19: 655-668

135. Murata T, Shiga Y, Higano S, et al. Conspicuity and evolution of lesions in Creutzfeldt-Jakob disease at diffusion-weighted imaging. *AJNR Am J Neuroradiol* 2002;23:1164-72

136. Lin YR, Young GS, Chen NK, et al. Creutzfeldt-jakob disease involvement of rolandic cortex: a quantitative apparent diffusion coefficient evaluation. *AJNR Am J Neuroradiol* 2006;27:1755-59

137. Haik S, Galanaud D, Linguraru MG, et al. In Vivo Detection of Thalamic Gliosis: A Pathoradiologic Demonstration in Familial Fatal Insomnia. *Arch Neurol* 2008;65:545-49

138. Folstein MF, Folstein SE, McHugh PR. "Mini-mental state". A practical method for grading the cognitive state of patients for the clinician. *J Psychiatr Res* 1975;12:189-98

139. Morris JC. Clinical dementia rating: a reliable and valid diagnostic and staging measure for dementia of the Alzheimer type. *Int Psychogeriatr* 1997;9 Suppl 1:173-76

140. RANKIN J. Cerebral vascular accidents in patients over the age of 60. I. General considerations. *Scott Med J* 1957;2:127-36

141. Rosen WG, Mohs RC, Davis KL. A new rating scale for Alzheimer's disease. *Am J Psychiatry* 1984;141:1356-64

142. Collin C, Wade DT, Davies S, et al. The Barthel ADL Index: a reliability study. *Int Disabil Stud* 1988;10:61-63

143. Guy W. Clinical Global Impressions (CGI). In:US Department of Health and Human Services PHSADAaMHANPRB, ed. *ECDEU Assessment Manual for Psychopharmacology.* Rockville, MD: 1976; 218-222

144. Overall JE, Gorham DR. The Brief Psychiatric Rating Scale. *Psychol Rep* 1962;10:799-812

145. Smith SM. Fast robust automated brain extraction. *Hum Brain Mapp* 2002;17:143-55

146. Evans A, Kambewr M, Collines D, et al. *Magnetic resonance scanning and epilepsy.* New York: Plenum; 1994

147. Smith SM, Zhang Y, Jenkinson M, et al. Accurate, robust, and automated longitudinal and cross-sectional brain change analysis. *Neuroimage* 2002;17:479-89

148. Smith SM, De Stefano N, Jenkinson M, et al. Normalized accurate measurement of longitudinal brain change. *J Comput Assist Tomogr* 2001;25:466-75

149. Jenkinson M, Bannister P, Brady M, et al. Improved optimization for the robust and accurate linear registration and motion correction of brain images. *Neuroimage* 2002;17:825-41

150. Jenkinson M, Smith S. A global optimisation method for robust affine registration of brain images. *Med Image Anal* 2001;5:143-56

151. Zhang Y, Brady M, Smith S. Segmentation of brain MR images through a hidden Markov random field model and the expectation-maximization algorithm. *IEEE Trans Med Imaging* 2001;20:45-57

152. Plummer D. DispImage: A display and analysis toll for medical images. *Rivista di Neurologica* 1992;5:489-95

153. Tatu U, Braakman I, Helenius A. Membrane Glycoprotein Folding, Oligomerization and Intracellular-Transport - Effects of Dithiothreitol in Living Cells. *EMBO J* 1993;12:2151-57

154. Helenius J, Soinne L, Perkio J, et al. Diffusion-weighted MR imaging in normal human brains in various age groups. *AJNR Am J Neuroradiol* 2002;23:194-99

155. Rovaris M, Iannucci G, Cercignani M, et al. Age-related changes in conventional, magnetization transfer, and diffusion-tensor MR imaging findings: study with whole-brain tissue histogram analysis. *Radiology* 2003;227:731-38

156. Wimberger D, Uranitsch K, Schindler E, et al. Gerstmann-Sträussler-Scheinker Syndrome: MR findings. *J Comp Ass Tomog* 1993;17 (2):326-27

157. Montagna P, Cortelli P, Avoni P, et al. Clinical features of Fatal Familial Insomnia: phenotypic variability in relation to a polymorphism at codon 129 of the prion protein gene. *Brain pathol* 1998;8:515-20

158. Rashid W, Hadjiprocopis A, Griffin CM, et al. Diffusion tensor imaging of early relapsing-remitting multiple sclerosis with histogram analysis using automated segmentation and brain volume correction. *Mult Scler* 2004;10:9-15

159. Lee H, Rosenmann H, Chapman J, et al. Thalamo-striatal diffusion reductions precede disease onset in prion mutation carriers. *Brain* 2009; 132:2680-7

160. Mascalchi M, Lolli F, Della NR, et al. Huntington disease: volumetric, diffusion-weighted, and magnetization transfer MR imaging of brain. *Radiology* 2004;232:867-73

161. Barajas RF, Jr., Rubenstein JL, Chang JS, et al. Diffusion-weighted MR imaging derived apparent diffusion coefficient is predictive of clinical outcome in primary central nervous system lymphoma. *AJNR Am J Neuroradiol* 2010;31:60-66

162. Arvinda HR, Kesavadas C, Sarma PS, et al. Glioma grading: sensitivity, specificity, positive and negative predictive values of diffusion and perfusion imaging. *J Neurooncol* 2009;94:87-96

163. Jain R, Scarpace LM, Ellika S, et al. Imaging response criteria for recurrent gliomas treated with bevacizumab: role of diffusion weighted imaging as an imaging biomarker. *J Neurooncol* 2010;96:423-31

164. DeArmond S, Kretschmar V, Prusiner DB. Prion Diseases. In:Graham D, Lantos P, eds. *Greenfield's Neuropathology*. Hodder Arnold; 2002; 273-323

165. Brandner S, Isenmann S, Kühne G, et al. Identification of the end stage of scrapie using infected neural grafts. *Brain Pathol* 1998;8:19-27

166. Zerr I, Giese A, Windl O, et al. Phenotypic variability in fatal familial insomnia (D178N-129M) genotype. *Neurology* 1998;51:1398-405

167. Almer G, Hainfellner HA, Jellinger K, et al. Fatal familial insomnia: a new Austrian family. *Brain* 1999;122:5-16

168. Nitrini R, Mendonca RA, Huang N, et al. Diffusion-weighted MRI in two cases of familial Creutzfeldt--Jakob disease. *J Neurol Sci* 2001;184:163-67

169. Seo HS, Chang KH, Na DG, et al. High b-value diffusion (b = 3000 s/mm2) MR imaging in cerebral gliomas at 3T: visual and quantitative comparisons with b = 1000 s/mm2. *AJNR Am J Neuroradiol* 2008;29:458-63

170. Cambier DM, Kantarci K, Worrell GA, et al. Lateralized and focal clinical, EEG, and FLAIR MRI abnormalities in Creutzfeldt-Jakob disease. *Clin Neurophysiol* 2003;114:1724-28

171. Fukushima R, Shiga Y, Nakamura M, et al. MRI characteristics of sporadic CJD with valine homozygosity at codon 129 of the prion protein gene and PrP(Sc) type 2 in Japan. *J Neurol Neurosurg Psychiatry* 2004;75:485-87

172. Hamaguchi T, Kitamoto T, Sato T, et al. Clinical diagnosis of MM2-type sporadic Creutzfeldt-Jakob disease. *Neurology* 2005;64:643-48

173. Hirose K, Iwasaki Y, Izumi M, et al. MM2-thalamic-type sporadic Creutzfeldt-Jakob disease with widespread neocortical pathology. *Acta Neuropathol (Berl)* 2006; 112(4):503-11

174. Waldman AD, Jarman P, Merry RT. Rapid echoplanar diffusion imaging in a case of variant Creutzfeldt-Jakob disease; where speed is of the essence. *Neuroradiology* 2003; 45(8):528-31

175. Oppenheim C, Brandel JP, Hauw JJ, et al. MRI and the second French case of vCJD. *Lancet* 2000;356:253-54

176. Sharma HJ, Multani AS, Dutta AK, et al. Safety and immunogenicity of an indigenously developed Haemophilus influenzae type b conjugate vaccine through various phases of clinical trials. *Hum Vaccin* 2009;5: 483-7

177. Haik S, Dormont D, Faucheux BA, et al. Prion protein deposits match magnetic resonance imaging signal abnormalities in Creutzfeldt-Jakob disease
4. *Ann Neurol* 2002;51:797-99

178. Garcia Santos JM, Ordonez C, Torres dR. ADC measurements at low and high b values: insight into normal brain structure with clinical DWI. *Magn Reson Imaging* 2008;26:35-44

179. Niendorf T, Dijkhuizen RM, Norris DG, et al. Biexponential diffusion attenuation in various states of brain tissue: implications for diffusion-weighted imaging. *Magn Reson Med* 1996;36:847-57

180. Cordery RJ, Macmanus D, Godbolt A, et al. Short TE Quantitative Proton Magnetic Resonance Spectroscopy in Variant Creutzfeldt-Jakob Disease. *Eur Radiol* 2006;1-7

181. Konaka K, Kaido M, Okuda Y, et al. Proton magnetic resonance spectroscopy of a patient with Gerstmann-Straussler-Scheinker disease. *Neuroradiology* 2000;42:662-65

182. Montagna P, Cortelli P, Gobbi G, et al. Proton magnetic resonance spectroscopy (MRS) of the thalamus in fatal familial insomnia (FFI). *Neurology* 1997;A296

183. Oppenheim C, Zuber M, Galanaud D, et al. Spectroscopy and serial diffusion MR findings in hGH-Creutzfeldt-Jakob disease. *J Neurol Neurosurg Psychiatry* 2004;75:1066-69

184. Shyu WC, Lee CC, Hsu YD, et al. Panencephalitic Creutzfeldt-Jakob disease: unusual presentation of magnetic resonance imaging and proton magnetic resonance spectroscopy. *J Neurol Sci* 1996;138:157-60

185. Pandya HG, Coley SC, Wilkinson ID, et al. Magnetic resonance spectroscopic abnormalities in sporadic and variant creutzfeldt--jakob disease. *Clin Radiol* 2003;58:148-53

186. Waldman AD, Cordery RJ, MacManus DG, et al. Regional brain metabolite abnormalities in inherited prion disease and asymptomatic gene carriers demonstrated in vivo by quantitative proton magnetic resonance spectroscopy. *Neuroradiology* 2006;48:428-33

187. Lodi R, Parchi P, Tonon C, et al. Magnetic resonance diagnostic markers in clinically sporadic prion disease: a combined brain magnetic resonance imaging and spectroscopy study. *Brain* 2009;

188. Provencher SW. Estimation of metabolite concentrations from localized in vivo proton NMR spectra. *Magn Reson Med* 1993;30:672-79

189. Vidal C, Meric P, Provost F, et al. Preclinical metabolic changes in mouse prion diseases detected by 1H-nuclear magnetic resonance spectroscopy. *Neuroreport* 2006;17:89-93

190. Behar KL, Boucher R, Fritch W, et al. Changes in *N*-acetylaspartate and myo-inositol detected in the cerebral cortex of hamsters with Creutzfeldt-Jakob disease. *Magn Reson Imaging* 1998;16:963-68

191. Urenjak J, Williams SR, Gadian DG, et al. Proton nuclear magnetic resonance spectroscopy unambiguously identifies different neural cell types. *J Neurosci* 1993;13:981-89

192. Collinge J, Brown J, Hardy J, et al. Inherited prion disease with 144 base pair gene insertion: II: Clinical and pathological features. *Brain* 1992;115:687-710

193. Pfeuffer J, Juchem C, Merkle H, et al. High-field localized 1H NMR spectroscopy in the anesthetized and in the awake monkey. *Magn Reson Imaging* 2004;22:1361-72

194. Yung L, Huang Y, Lessard P, et al. Pharmacokinetics of quinacrine in the treatment of prion disease. *BMC Infect Dis* 2004;4:53

195. Godbolt AK, Waldman AD, MacManus DG, et al. MRS shows abnormalities before symptoms in familial Alzheimer disease. *Neurology* 2006;66:718-22

196. Schmierer K, Wheeler-Kingshott CA, Tozer DJ, et al. Quantitative magnetic resonance of postmortem multiple sclerosis brain before and after fixation. *Magn Reson Med* 2008;59:268-77

197. Pfefferbaum A, Sullivan EV, Adalsteinsson E, et al. Postmortem MR imaging of formalin-fixed human brain. *Neuroimage* 2004;21:1585-95

198. Yong-Hing CJ, Obenaus A, Stryker R, et al. Magnetic resonance imaging and mathematical modeling of progressive formalin fixation of the human brain. *Magn Reson Med* 2005;54:324-32

199. Vaughan T, DelaBarre L, Snyder C, et al. 9.4T human MRI: preliminary results. *Magn Reson Med* 2006;56:1274-82

200. Fatterpekar GM, Naidich TP, Delman BN, et al. Cytoarchitecture of the human cerebral cortex: MR microscopy of excised specimens at 9.4 Tesla. *AJNR Am J Neuroradiol* 2002;23:1313-21

201. Carpenter MB, Sutin J. The cerebral cortex. *Human Neuroranatomy.* Baltimore: William and Wilkins; 1983; 643-705

202. Berry M, Bannister LH, Standing SM. Nervous System. In:Williams PL, Bannister L H, Standing S M, eds. *Gray's Anatomy.* Edinburgh: Churchill Livingstone; 1995; 643-705

203. Le Bihan D, Turner R, Douek P, et al. Diffusion MR imaging: clinical applications. *AJR Am J Roentgenol* 1992;159:591-99

204. Rosas HD, Tuch DS, Hevelone ND, et al. Diffusion tensor imaging in presymptomatic and early Huntington's disease: Selective white matter pathology and its relationship to clinical measures. *Mov Disord* 2006;21:1317-25

205. Vonsattel JP, Myers RH, Stevens TJ, et al. Neuropathological classification of Huntington's disease. *J Neuropathol Exp Neurol* 1985;44:559-77

206. Mori S, Itoh R, Zhang J, et al. Diffusion tensor imaging of the developing mouse brain. *Magn Reson Med* 2001;46:18-23

207. Nucifora PG, Verma R, Lee SK, et al. Diffusion-tensor MR imaging and tractography: exploring brain microstructure and connectivity. *Radiology* 2007;245:367-84

208. Mueller SG, Weiner MW, Thal LJ, et al. Ways toward an early diagnosis in Alzheimer's disease: the Alzheimer's Disease Neuroimaging Initiative (ADNI). *Alzheimers Dement* 2005;1:55-66

209. Katz R. Biomarkers and surrogate markers: an FDA perspective. *NeuroRx* 2004;1:189-95

210. Small GW, Bookheimer SY, Thompson PM, et al. Current and future uses of neuroimaging for cognitively impaired patients. *Lancet Neurol* 2008;7:161-72

211. Jack CR, Jr., Dickson DW, Parisi JE, et al. Antemortem MRI findings correlate with hippocampal neuropathology in typical aging and dementia. *Neurology* 2002;58:750-57

212. Mueller SG, Schuff N, Weiner MW. Evaluation of treatment effects in Alzheimer's and other neurodegenerative diseases by MRI and MRS. *NMR Biomed* 2006;19:655-68

213. Klunk WE, Debnath ML, Pettegrew JW. Development of small molecule probes for the beta-amyloid protein of Alzheimer's disease. *Neurobiol Aging* 1994;15:691-98

214. Newberg AB, Wintering NA, Plossl K, et al. Safety, biodistribution, and dosimetry of 123I-IMPY: a novel amyloid plaque-imaging agent for the diagnosis of Alzheimer's disease. *J Nucl Med* 2006;47:748-54

215. Klunk WE, Engler H, Nordberg A, et al. Imaging brain amyloid in Alzheimer's disease with Pittsburgh Compound-B. *Ann Neurol* 2004;55:306-19

216. Merz PA, Wisniewski HM, Somerville RA, et al. Ultrastructural morphology of amyloid fibrils from neuritic and amyloid plaques. *Acta Neuropathol* 1983;60:113-24

217. McMahon PM, Araki SS, Sandberg EA, et al. Cost-effectiveness of PET in the diagnosis of Alzheimer disease. *Radiology* 2003;228:515-22

218. Cook PA, Bai Y, Nedjati-Gilani S, et al. Camino: open-source diffusion-MRI reconstruction and processing. Proceedings of the International Society of Magnetic Resonance in Medicine 2006; 14: 2759

219. Paxinos G, Franklin KBJ. *The mouse brain in stereotaxic coordinates.* San Diego (CA): Academic Press; 2001